WASHINGTON UNIVERSITY
SEVER INSTITUTE OF TECHNOLOGY
DEPARTMENT OF CHEMICAL ENGINEERING

DYNAMICS OF ASYMMETRIC FIXED-BED REACTORS: COUPLING OF EXOTHERMIC AND ENDOTHERMIC REACTIONS

by

Milind S. Kulkarni

Prepared under the direction of Professor Milorad P. Dudukovic′

A Thesis presented to the Sever Institute of Washington University in partial fulfillment of the requirements of the degree of

DOCTOR OF SCIENCE

December, 1996

Saint Louis, Missouri

WASHINGTON UNIVERSITY
SEVER INSTITUTE OF TECHNOLOGY
DEPARTMENT OF CHEMICAL ENGINEERING

ABSTRACT

DYNAMICS OF ASYMMETRIC FIXED-BED REACTORS UNDER FORCED UNSTEADY STATE CONDITIONS: COUPLING OF EXOTHERMIC AND ENDOTHERMIC REACTIONS

by Milind S. Kulkarni

ADVISOR: Professor Milorad P. Dudukovic′

December, 1996
Saint Louis, Missouri

Performance of a bi-directional fixed-bed reactor subject to both flow reversal and switching between exothermic and endothermic reactions is studied. During *odd semi-cycles (blows)* an exothermic reaction heats the bed, during *even semi-cycles* an endothermic reaction cools the bed and produces the desired product in the hot zone. It is shown that such operation is possible and efficient when the inlet gas temperature is lower than the initial bed temperature leading to the *wrong-way behavior* when the temperature front moves with a finite velocity (*creep velocity*) from the feed end to the exit during a semi-cycle. A fixed-bed operated periodically in the above described mode is *asymmetric* as the dynamic nature of the bed changes during each cycle. The front velocity during an exothermic semi-cycle is different from the front velocity during an endothermic semi-cycle and an asymptotic expression is developed for the *differential creep (front) velocity* that quantifies this difference. The asymptotic expression for the creep velocity works very well except in the inlet and outlet region of the fixed-bed reactor. Due to a non zero differential creep velocity the front exhibits an effective displacement after each cycle. A developed expression for energy efficiency indicates that 100% efficiency can be reached only if the differential creep velocity is zero. A relation for the balanced operation of a reactor-regenerator is

developed. Differences in reactor performance caused by reactions occurring in the gas or solid phase are also discussed.

It is shown that to operate such an asymmetric fixed-bed reactor in a periodic steady state, two conditions need to be satisfied—the energy liberated during the exothermic semi-cycle should be equal to or greater than the energy consumed during the endothermic semi-cycle, and the product of the front velocity and semi-cycle period for the endothermic semi-cycle must be equal to or greater than that for the exothermic semi-cycle. The energy efficiency and conversions for both reactions increase with increasing bed length and decreasing semi-cycle periods for a fixed ratio of the exothermic and endothermic semi-cycle periods. The effect on operability and energy efficiency of the heats of reactions, inlet mass fluxes, front velocities during both semi-cycles, and of the ratio as well as the magnitude of individual semi-cycle periods is discussed.

An approach based on the asymmetric bi-directional fixed-bed reactor operated in a cyclic mode to produce synthesis gas by coupling endothermic steam reforming reaction with exothermic methane combustion is simulated and discussed. The processes simulated above exhibit very steep moving fronts.

A robust numerical algorithm is required to simulate the physics of the problem. A spatially and temporally adaptive completely implicit finite difference algorithm, which can accurately capture the moving temperature and reaction fronts in fixed-bed reactors with highly exothermic reactions, is developed for that purpose and presented. The spatial grid adaptation based on the magnitude of the second derivative and manipulation of the time step size based on the characteristic time of the process are the two key features of the developed algorithm. Robustness of the algorithm is demonstrated by simulating stiff problems.

Dedication

to my sisters, father and mother
and
to the laughter and beer, not necessarily in that order
and
to the women who are not feminists although they are rare
and
to those who are brave enough to admit that Rapper is not a Singer

and
to Anheuser Busch without which there would be no Budweiser
and
to Dr. Dudukovic′ who is a darn good advisor

TABLE OF CONTENTS

TABLES

FIGURES

NOTATION

Symbols

A	component A
a_p	surface area/bed volume (m^2/m^3)

B	component *B*
C	component *C*, concentration in Ch. 6 (mol/m^3)
C_p	heat capacity (J/kg.K)
D	component *D*; dispersion coefficient; thermal (J/m.K.s), mass (m^2/s)
d_p	particle diameter (m)
Ea	activation energy (J/mole)
f_{ha}	stagnant film resistence (J/m.K.s) $\frac{\left[\rho_s C_{p,s}(1-\varepsilon)\omega\right]^2}{ha_p}$
$f_{s(ha)}$	intraparticle resistence (J/m.K.s) $\frac{\left[\rho_s C_{p,s}(1-\varepsilon)\omega d_p\right]^2}{60\lambda_s(1-\varepsilon)}$
H	enthalpy (J)
h	heat transfer coefficient (J/m^2.K.s)
i	global spatial node index
j	local spatial node index on an element
k	reaction constant (s^{-1}) for first order reactions (m^3/mol.s) for second order reactions
k_0	frequency factor (s^{-1})
L	total bed length (m)
M_W	molecular weight of the gas
Nr	Order of reaction
Nu	Nusselt number $\frac{hd_p}{\lambda_g}$

n	temporal node index
ni	point interpolation index
nt	point elimination index
N	total number of axial nodes
P	total pressure (N/m^2)
Pe	Peclet number : 1) heat, gas $\frac{\varepsilon\rho_g u_{in} C_{p,g} L}{D_{e,g,h}}$ 2) heat, solids $\frac{(1-\varepsilon)\rho_s u_{in} C_{p,s} L}{D_{e,h,s}}$ 3) mass, gas $\frac{\varepsilon_s u_{in} L}{D_{e,g,ms}}$
Pr	Prandtl number $\frac{C_{p,g}\mu}{\lambda_g}$
p	partial pressure (N/m^2)
Q	total amount of heat produced/semi-cycle (J)
R	universal gas constant (J/mol.K)
Re	Reynold's number $\frac{d_p u \rho}{\mu}$
r	rate of production (mol/$m^3$of bed.s)
St	Stanton number 1) gases $\frac{h a_p L}{\varepsilon\rho_g u_{in} C_{p,g}}$ 2) solids $\frac{h a_p L}{(1-\varepsilon)\rho_s u_{in} C_{p,s}}$
T	local temperature (K)

TD	thermal diffusivity (m^2/s)
t	time (s)
TR	dimensionless group: 1) gases $\frac{1000(-\Delta H)}{M_w C_{p,g} \Delta T_{ad}}$ 2) solids $\frac{P(-\Delta H_{s,B})}{RT_g \rho_s C_{p,s} \Delta T_{ad}}$
U	dimensionless gas velocity $\frac{u}{\varepsilon u_{in}}$
u	local gas velocity (m/s)
$\bar{v}$	a vector of lumped dependent variables
X	average convesion
x	local bed length (m)
y	mole fraction in gas phase; dependent variable
z	dimensionless axial $\frac{x}{L}$; independent variable

Greek Symbols

α	Arrhenius number $\frac{Ea_s}{RT_s}$
β	heat transfer parameter $\frac{(-\Delta H_s) D_{e,pore} C_{p,s}}{\lambda_s T_s}$
ΔH	enthalpy of reaction (J/mol)
ΔT	change in the generic temperature (K)
Δt	time step (s)

Δy	change in variable *y*
δ	tolerance for node placement
ε	void fraction
Φ	Thiele-type modulus $\frac{d_p}{6}\sqrt{\frac{k_s/\rho_s}{D_{e,pore}}}$
ϕ	parameter used to estimate $D_{e,h,s}$ (Kunii and Smith, 1960)
γ	dimensionless group $\frac{Ea}{RT_{g,ad}}$
η	efficiency
κ_1, κ_2	arbitrary coeffcients
λ	thermal conductivity (J/m.s)
μ	viscosity (kg/m.s)
Θ	collision integral
θ	dimensionless temperature: 1) fixed-bed reactor $\frac{T-T_{in}}{\Delta T_{ad}}$ 2) regenerator $\frac{T-T_0}{T_{in}-T_0}$
$\theta_{g,d}$	dimensionless group $\frac{2T_{g,in}-T_{g,in}}{\Delta T_{ad}}$
ρ	density (kg/m^3)
σ_p	hard sphere diameter (Å)
τ	dimensionless time $\frac{t}{L/u_{in}}$

τ_s	space time $\frac{L}{u_{in}}$
$\tau_{s/r}$	dimensionless group $\frac{\tau_s}{\tau_r}$
τ_r	characteristic reaction time $\frac{1}{k_0 \rho_{gm,in}^{Nr-1} / \varepsilon \; e^{\left(\frac{Ea}{RT_{g,ad}}\right)}}$
ω	front velocity in a heat regenerator
ω_r	front velocity in a fixed-bed reactor
Ω	dimensionless density $\frac{\rho}{\rho_{in}}$
Ψ	overall effectiveness factor

Subscripts and Superscripts*

A	species *A*
ad	adiabatic
B	species *B*
CH4	*CH4*, methane
ct	characteristic
cycle	cycle
diff	differential
e	effective, corrected

eddy	related to turbulent eddies
endo	endothermic reaction
eq	equilibrium
even	even or endothermic semi-cycle
exo	exothermic reaction
g	gas
gm	molar
h	heat transfer coefficient
i	global spatial node index
in	inlet conditions
j	local spatial node index in an element
l	spatial element index
m	molar

ms	mass transfer
mx	maximum
min	minimum
N_2	N_2
n	temporal node index
new	new
O_2	O_2
odd	odd or exothermic semi-cycle
old	old
out	outlet conditions

overall	overall
pore	related to pores
r	with reaction
recycle	recycle
s	solid
sn	sensitive
total	total
t	time
utility	utility
0	initial conditions
1	first order derivative for δ
2	second order derivative for δ

ACKNOWLEDGEMENTS

A long time ago when king Solomon lived, when civilized people did not have to eat with forks, when men did not have to wear Calvin Klein underwear to be cool, I started working on this thesis. Many things have happened since I started working on this thesis. Many presidents were elected and broke their promises, over-fed and pampered western athletes who skip their dinners to stay healthy, won many more gold medals in Olympics against the tough competition posed by malnourished athletes from the third world who skip their dinners because they have nothing to eat, rhythmic swimming was declared a sport, rappers were called singers, my father grew bald and I grew older without growing wiser. Well, things could be worse but for quite a few people who helped me finish this thesis before politically correct feminists start

eating men for breakfast and before the 20th Century Fox becomes the previous century's phenomenon. The list of the people who helped me directly and indirectly to finish this thesis is longer than Chile during the hottest day of the summer when objects are at their longest due to high temperatures. However, by now, if I know how to shorten a 190 page thesis into a one and half page abstract, I should know how to reduce such a big list into a few tiny paragraphs.

I thank my advisor Dr. Dudukovic′ who has certainly a lot more ideas in his head than the hair on his head. I thank god (if he exists) for there is no correlation between ideas in a man's head and the hair on his head, otherwise I would be stuck with an advisor who is as dumb as a basketball player who thinks he is white! I thank Dr. Dudukovic′ for his ideas, politically incorrect humor and the patience that he showed with my accented writing! He went through nightmares correcting my personalized English which involves formulation of sentences structured to make the

he is reading Hieroglyphics. Of course, it can be a horrible and demoralizing experience for the reader when he understands every word that is there in a sentence but cannot understand the sentence! I do hope, that Dr. Dudukovic′s hair loss is just an aging phenomenon and not a phenomenon resulting from my writing. Well, in my defense, I did go through nightmares of my own trying to understand his hand writing which can easily pass as a million dollar piece of modern art which I was never able to understand. I thank him for great guidance, good laughs and for not firing me for my jokes.

I thank Dr. Levien and Professor Levenspiel, who introduced me to the world of regenerators. Dr. Levien was my advisor in Oregon State University. He is so smooth and so cool that he should be in Hollywood giving competition to Tom Cruise.

Working under his direction was a very nice experience except that I felt very ugly because he was so... handsome!

Dr. Levenspiel is the genius grand dad of chemical engineering who I cannot thank enough for his academic guidance when I was in Oregon State University, which laid the foundation for my work in Washington University. I think he is "the Grand Old Child" who refuses to forgo his pleasingly childlike nature which makes him the most mature child on the face of this earth. I still remember those days when I used to beat him in the game of ping pong which was hard for the China-bred genius to swallow. I still remember when he went to his optician for an eye check-up to make sure that he was not loosing because he could not see the ball properly! I thank him for teaching me that he is a great man, but I am greater in the game of ping pong! He is a great chemical engineer and even greater person. I will always remember his cynical jokes about the research I was doing in Washington University.

I am grateful to faculty and staff of Chemical Engineering Department for the good times I had here. They were kind enough to grow old with me during the course of my thesis so that I did not feel lonely growing old alone! I am grateful to Dr. Matros for introducing us to the area of symmetric fixed-bed reactors. A brief visit by Dr. Chumakova was very helpful in understanding the Dynamics of asymmetric fixed-bed reactors.

Little things in life can be very important and the little thing I am talking about is Garima. When I was writing this thesis I did not have time to cook and eat. During those Ethiopian times Garima fed me on a constant basis at her place so that I did not have to loose weight and look like her! Most probably she wanted to remain unique in her ultra feather weight category.

I am indebted to all Chinese students in the Chemical Reaction Engineering Laboratory (CREL) for laughing with my jokes although they did not understand them because I spoke English!. I thank everybody indiscriminately who chose or were forced to listen to my jokes, philosophical ramblings and songs which would put rappers to shame.

A man can live without wearing an underwear but he cannot live without money. That is unfortunate but true. I am grateful to Air Products, Amoco, Chevron, Dupont, Eastman Chemicals, Elf Auto-Chem, Exxon, Lummus, Mobil, Monsanto, Statoil, Union Carbide, UOP and other CREL sponsors for their support of this research.

At the cost of appearing sentimental I have to thank my father for his sense of humor which is the best in the world. From him I learnt to derive pleasure by laughing at myself and to derive even greater pleasure by laughing at others! I am grateful to my

mother who thankfully is the only woman in my life. I also thank my two sisters for the reasons unknown to me.

Finally, I am indebted to myself for sticking with me and not running away from me until I finished this thesis because it is not easy to be around a person who talks for 24 hours a day, but then I cannot run away from myself, can I? Also, I thank every body who I forgot to thank but should have thanked. I hope this does not go against me on the day of judgment.

1. INTRODUCTION

1.1 Problem Statement

In ordinary heat recuperators heat transfer takes place through a common wall. If one of the fluids exchanging heat is highly corrosive or generates a lot of heat due to reaction and the rate of heat transfer required is very high, the use of ordinary heat recuperators (heat exchangers), due to the limited heat transfer area and moderate heat transfer coefficients compared to those obtainable in packed beds, is not recommended. Packed bed heat regenerators can be used efficiently in such cases. A packed bed heat regenerator consists of a fixed-bed of solid packing which acts as intermediary in transfer of heat from the hot fluid to the cold fluid. As the hot gas is passed through the cold bed it transfers its thermal energy to the bed before exiting the regenerator as the cooled gas. The temperature of the gas flowing out of the regenerator remains at the initial bed temperature for a long period of time due to the high volumetric thermal capacity of the solids compared to that of the gas and due to the high heat transfer coefficient and heat transfer area. If the heat transfer coefficient between gases and

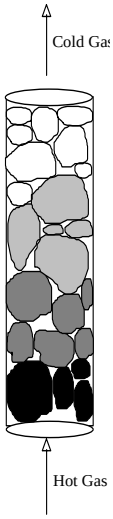

Figure 1.1 Schematic of a heat regenerator.

solids was infinite, we would have an ideal regenerator, and the time required to completely heat (or cool) the bed is then equal to $\rho_s C_{p,s} L (1-\varepsilon)/\varepsilon \rho_g C_{p,g} u$ which is called the characteristic regenerator time (Levenspiel, 1983). Hence, in an ideal regenerator, that was initially cold, the temperature-time history of the exit gas, subject to steady flow of inlet hot gas that started at time zero, looks like a step function. The step from the cold initial bed temperature to the hot gas inlet temperature occurs at the above characteristic regenerator time. In a real heat regenerator, with finite heat transfer coefficients and heat transfer areas, the exit gas temperature curve is S shaped. Hence, in a real heat regenerator the heating process is carried on until the gas coming out of the regenerator shows an appreciable increase in temperature. This part of the regenerator operation is called the 'first blow' or the 'first semi-cycle' and involves heating the regenerator bed. Figure 1.1 shows a typical heat regenerator. In the 'second blow' or 'second semi-cycle' a cold gas is usually introduced at the other end of the regenerator (counter current operation) and is passed through the hot bed. Hence, the cold gas is now heated and exits at the initial hot bed temperature for a long period of time (for an ideal regenerator until the characteristic regenerator time is reached). The second semi-cycle is completed when the exit temperature of the heated cold gas drops considerably. This operation completes 'one cycle' of the heat regenerator process by the end of which heat is transferred to the cold gas stream from hot gases.

In the economic crisis that hit Germany soon after World War I, the Institute of Heat Recovery under the direction of Kurt Rummel was established in Dusseldorf and developed the theory and the design methods for heat regenerators. In 1973 the oil embargo by major oil producing countries in the Middle East made many industrial countries realize their dependence on oil. Research and development towards energy usage and conservation gained momentum again and it became obvious that energy

.

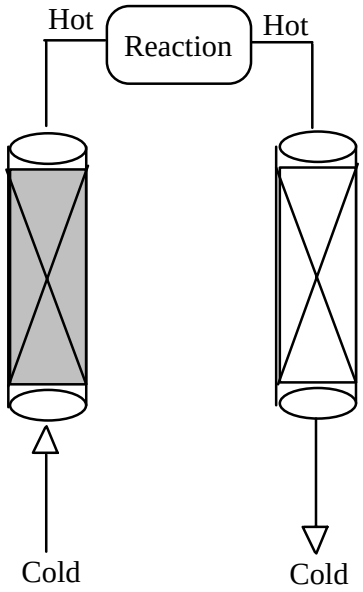

Figure 1.2 Coupling of a heat regenerator through high temperature reaction.

storage devices could greatly assist in improving the overall efficiency of very large plants. In 1975 the Energy Research and Development Corporation (ERDA) of the U.S. government requested the National Research Council (NRC) to undertake a study on the potential of advanced energy storage systems. Thus, the study of heat regenerators gained momentum again.

In the past, most studies of heat regenerators were confined only to investigations of heat transfer in the absence of reaction. Coupling with reaction can be accomplished as shown in Figure 1.2. For example, in the 'Wisconsin Process' where Thermal NO is produced by burning nitrogen in air in the presence of a fuel, heat regenerators were used to preheat the air and to cool the product gas (Ermenc, 1956). More recently, an unsteady state operation with periodic flow reversal of incoming gases, which react in the catalytic packed bed heat regenerator, has been studied and shown to enhance the yield of a thermodynamically limited reaction due to

the shape of the creeping temperature profile in the bed (Matros, 1989). This idea was extensively exploited by Boreskov and coworkers in the regenerative catalytic oxidation of SO_2 to SO_3 (Matros, 1989). The fixed-bed is packed with the vanadium oxide catalyst packing and the reaction occurs in the solid catalyst. This idea of forced flow reversal can also be applied to non catalytic processes involving homogeneous reactions such as NO production from air in presence of a fuel, or synthesis gas production by the REGAS process (Levenspiel, 1988).

Coupling of exothermic and endothermic reactions via heat regenerators can be accomplished in two basic ways: *indirectly* and *directly*. For example, a heat regenerator can be used to *indirectly* produce synthesis gas in the REGAS process. During an *odd* or *exothermic* semi-cycle air+fuel are introduced to the cold heat regenerator and combusted to heat up the bed. During an *even* or *endothermic* semi-cycle, carbonaceous material+steam are passed into the hot regenerator from the opposite direction and the endothermic gasification reaction occurs in the hot bed (Figure 1.3a). The combustion of fuel generates heat which is regeneratively transferred via solids to sustain the endothermic reaction. The endothermic gasification reaction is driven by the hot regenerator-reactor. Since in this case, the exothermic and endothermic reactions do not occur simultaneously at the same place, the endothermic reaction is *indirectly* driven by the exothermic reaction. Direct coupling of the two reactors is illustrated in Figure 1.3b. For example, the homogeneous oxidation of N_2 to NO is an endothermic process which can be driven by exothermic combustion of a fuel via direct coupling. The reaction occurs at very high temperatures (2500-3000 K) and the product gases have to be cooled immediately to freeze the yield of NO. The principle of flow reversal can be used to increase the yield of NO. The feed gases consist of a hydrocarbon fuel and air which flow through a hot heat regenerator. The combustion of fuel and nitrogen occurs

simultaneously and the repeated flow reversal results in a temperature profile with a hot spot sandwiched between two colder regions (Figure 1.3a). The gases are heated at the entrance, nitrogen is oxidized at the hot spot, and the product gases are cooled as they exit the regenerator-reactor. Since in this case, the exothermic and endothermic reactions occur simultaneously at the same location, the endothermic reaction is *directly* driven by the exothermic reaction.

Heat regeneration processes in which no reaction occurs are similar to reactive heat regeneration processes involving one or more reactions in terms of moving temperature fronts. However, the exponential temperature dependence of the rate of reaction causes much steeper moving temperature fronts as well as reaction (concentration) fronts in the reactor regenerator situation. The number of coupled equations to be solved increases with the number of reactions. Thus, global polynomial approximations and traditional finite difference approximations used in the simulation of heat regenerator processes without reaction cannot handle the stiffness and the non-linearity of the reactive regeneration processes.

Some algorithms have been developed to handle catalytic packed bed regenerators with reaction (e.g. Eigenberger and Butt, 1976; Il'in and Luss, 1992). In such beds reaction occurs in the porous solid, and due to the high heat capacity of the solids, the temperature change in the regenerator-reactor is slow. In the case of homogeneous processes, when reaction occurs in the gas phase of the bed, the temperature and the concentration changes are very fast due to rapid temperature changes in the gas phase caused by the low heat capacity of the gas. Thus, the fronts are much steeper and equations are much stiffer to solve in the case of homogeneous reactive-regeneration processes.

This indicates a need for development of a robust numerical algorithm to simulate homogeneous reactive-regeneration processes. The focus of this work is based on development of such an algorithm which can be used to study RE-GAS type

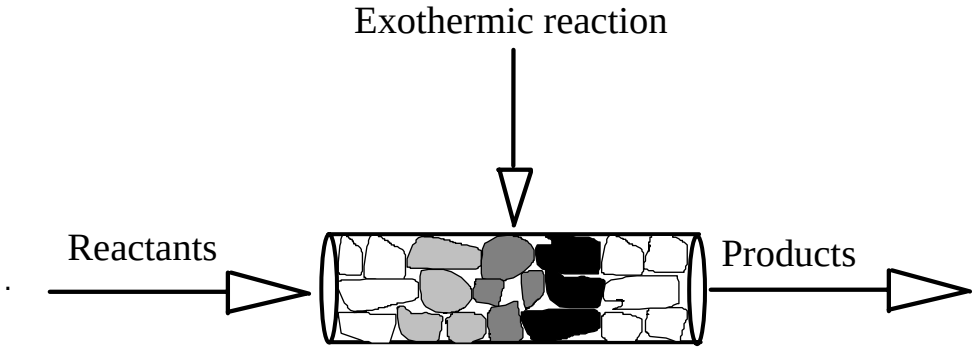

An exothermic reaction occurs in a fixed-bed reactor during an exothermic semi-cycle and heats the solids

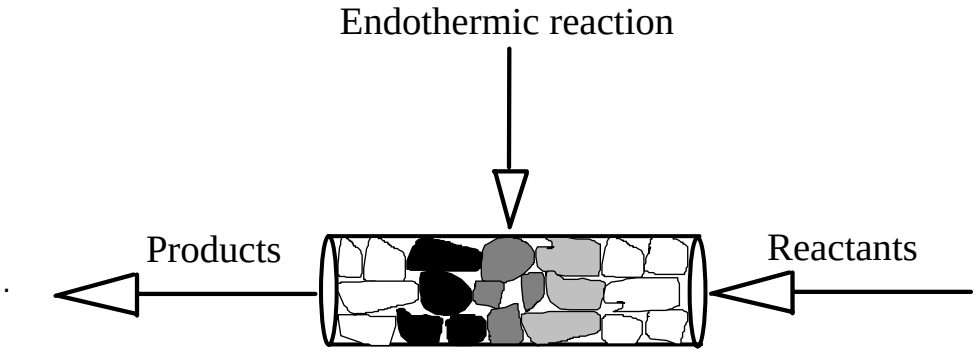

An endothermic reaction is heated by solids and occurs in a fixed-bed reactor during an endothermic semi-cycle with feed from the opposite end. Hence, exothermic and endothermic reaction are indirectly coupled.

Figure 1.3a. A typical operation of an *indirect* fixed-bed reactor.

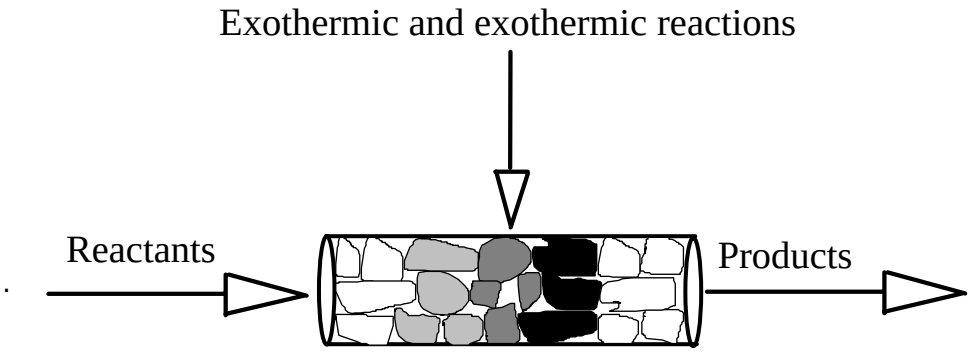

Both exothermic and endothermic reactions occur *directly* in a fixed-bed reactor during an even semi-cycle

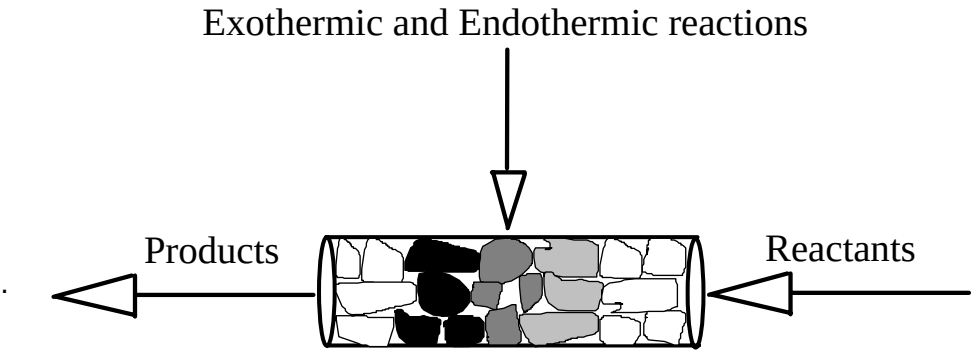

Both exothermic and endothermic reactions occur *directly* from opposite direction in the fixed-bed reactor during an even semi-cycle

Figure 1.3b A typical operation of a *direct* fixed-bed reactor.

processes. This thesis outlines a course of research leading to the development of a numerical algorithm to solve homogeneous reactive-regeneration processes and a study of RE-GAS and RE-GAS type processes.

1.2 Background

This section is divided into three subsections. The first subsection reviews the models for heat regenerators. The solution methods used to solve moving fronts are also discussed. The second subsection addresses the application of heat regenerators as reactors in the chemical and process industry. Possible case studies are discussed in the last subsection.

1.2.1 Heat Regenerators without Reactions

There are basically two classes of heat regenerator models: single blow models and cyclic process models. Usually, one complete cycle of heat regenerator operation includes a heating semi-cycle and a cooling semi-cycle. Each semi-cycle involves a continuous and steady flow of either hot or cold gas into the heat regenerator until there is an appreciable change in the exit gas temperature. The first semi-cycle, which usually involves the first heating period, is often referred to as 'first blow' and the models which describe this operation are referred to as 'single blow models'. The 'cyclic process models' describe the regenerator operation involving repeated heating and cooling semi-cycles. The first blow models essentially describe the step response of the system.

The first attempt to model heat regenerators was based on empirical data used to set up an approximate equation (Jakob, 1957). Jakob (1957) mentions that

Heiligenstaedt (1928-29), Hausen (1931, 1938-39) and Ackermann(1931) were the pioneers in this area. Since modeling of heat regenerators from first principles is the primary focus of this work, details of these early studies will not be discussed here.

Anzelius (1926), Nusselt (1927) and Schumann (1929) were pioneers of single blow (single pass) studies. Hausen (1927, 1929), Nusselt (1928), Schmeidler (1928) and Ackermann (1931) have also treated the cyclic process. Nusselt (1927) performed calculations for five cases with the assumption of constant gas-solid heat transfer coefficient and constant physical properties, such as specific heat and density (Jakob, 1957). The postulated linear model was analytically solved by Anzelius (1926), Nusselt (1927), Hausen (1927, 1929) and finally by Schumann (1929), as reported in Jakob (1957). The Anzelius solution is frequently used to test the accuracy of new numerical algorithms. Hausen (1931) made use of finite differences to solve the cyclic operation. Some simplified models have been proposed by Heiligenstaedt and Rummel (1928-29) and Hausen (1938-39). McAdams (1954) and Kern (1965) cite a linear model which assumes constant thermodynamic gas properties and constant heat transfer coefficient for the heat regenerator process.

Schmidt and Willmott (1981) review many important developments in modeling of heat regenerators in their book, but dedicate only one chapter to packed bed heat regenerators. The heat regenerator with reaction is not treated. The thermal dispersion (Chao and Hoelscher, 1966; Edwards and Richardson, 1968) and intra particle conduction (Babcock, Green and Perry, 1966; Leung and Quon, 1965) are taken into account. Levenspiel (1983) used the dispersion model to account for the spreading of the temperature fronts due to axial dispersion in the gas phase, radial conduction in the solid phase and the film resistance. Ramachandran and Dudukovic′ (1984) developed a moving finite element collocation method for moving fronts. They solved the linear regenerator model using triple collocation, i.e., collocation in space

and time. Dudukovic´ and Ramachandran (1985) also developed design criteria for periodic operation of heat regenerators. Their analysis assumes a constant switching time and they show how to reach the periodic solution to linear equations by using the single blow response.

Khan and Beasley (1989) studied the two dimensional model of a packed bed heat regenerator using finite differences. They used the model developed by Beasley and Clark (1984) which takes into account the variation of void fraction and velocity in the radial direction. Their model includes the effect of radial and axial thermal diffusion, effects of wall heat capacity, longitudinal conduction and losses to the environment. Kulkarni (1992) used orthogonal collocation to solve the non-linear model incorporating the compressibility of the gas, the temperature dependence of the thermodynamic properties of the gas and of the gas-solid heat transfer coefficient. Erk (1993) developed and solved the model for heat regenerators involving phase change of the packing material by a combination of a cell model and orthogonal collocation.

1.2.2 Heat Regenerators with Reactions

A fixed-bed reactor can display creeping reaction and concentration fronts along with temperature fronts (Rhee et al., 1973; Eigenberger, 1976). The reaction, temperature and concentration fronts move very slowly in a fixed-bed due to the high heat capacitance of solids compared to that of gases. The 'wrong-way' behavior of fixed-beds, which refers to the increase in the transient maximum temperature observed along the bed in response to a decrease in inlet temperature or an increase in feed gas velocity has been discussed by Sharma and Hughes (1979), Mehta et al. (1981), Pinjala et al. (1988) and Il'in and Luss (1992).

1.2.2.1 Flow Reversal

The periodic flow reversal has been proven to increase the yield of SO_3 in the thermodynamically limited catalytic reaction between SO_2 and O_2. This principle holds good for any thermodynamically limited exothermic reaction. The gaseous cold reactants are passed through an initially hot catalytic packed bed. The gases get heated, while cooling the hot bed, and due to the released heat of reaction which occurs at high temperature, the gas and the bed temperatures shoot above the initial bed temperature in the reaction zone, only to be brought back to the initial bed temperature as the gas moves along the bed towards the exit. The temperature, reaction and concentration fronts thus move together slowly in the direction of gas flow.

The typical temperature profiles in the fixed-bed reactor during the first semi-cycle are shown in Figure 1.4 (Rhee et al., 1973). The feed gas enters from one side of the bed until the temperature front starts moving out of the bed. Then the feed gases are switched to be fed through what used to be the exit of the bed. The typical temperature profiles in a fixed-bed reactor subject to flow reversal are shown in Figure 1.5 (Matros, 1989). The flow reversal is accomplished by a typical switching arrangement as shown in Figure 1.6. The incoming cold gases get heated and react at the entrance and get cooled along the bed after the hot spot. This inverted U ($\cap$) shaped temperature profile (see Figure 1.5) moves back and forth in the fixed-bed reactor as the direction of the feed is switched every half cycle (Matros, 1989).

The gases get heated in the part of the bed where the temperature is increasing, thus achieving high reaction rates, and after the hot spot the gases get cooled along the cooler part of the bed. Thus, the yield of a thermodynamically limited exothermic

reaction stays high due to a ramp cooling. On the conversion versus temperature diagram (Figure 1.7) it can be seen that close to the optimum path can be followed by

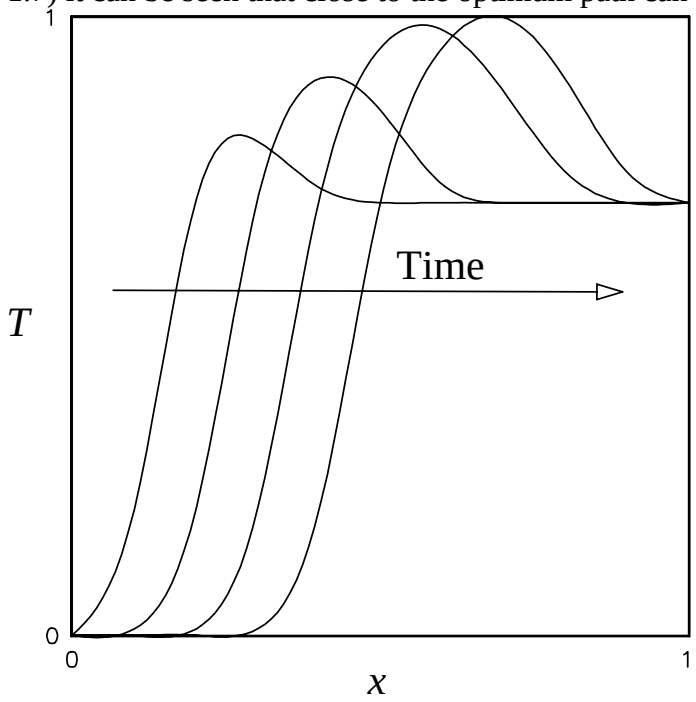

Figure 1.4 Typical temperature fronts in a fixed-bed catalytic reactor during the first semi-cycle.

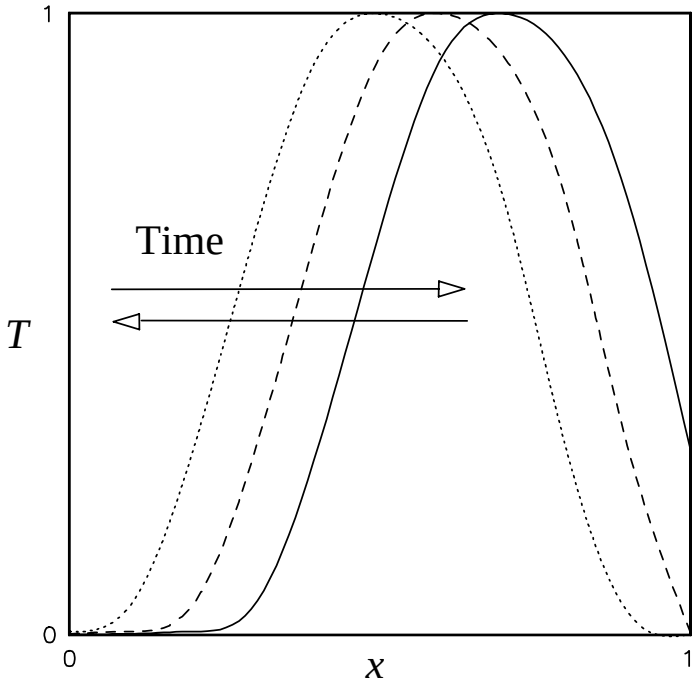

Figure 1.5 Typical temperature fronts in a fixed-bed catalytic reactor during the reverse flow.

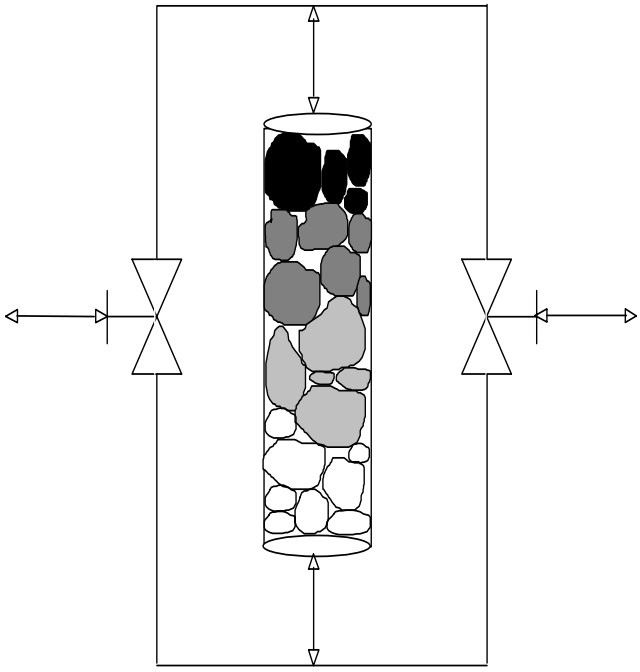

Figure 1.6 A switching arrangement for the flow reversal.

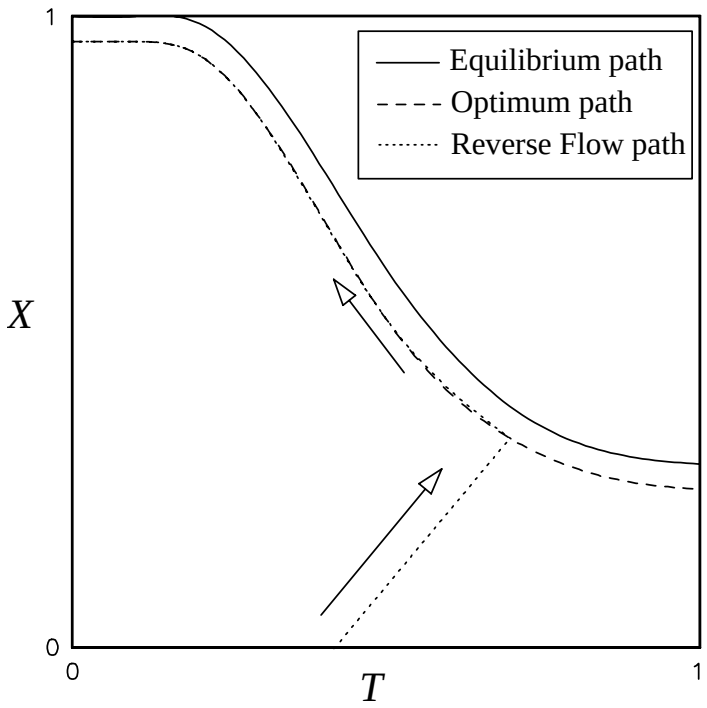

Figure 1.7 Temperature versus conversion diagram for a flow reversal process.

the reverse process (Matros, 1989). This not only increases the yield of the process, it also helps eliminate the need for intermittent cooling required in a process including staged adiabatic reactors which are conventionally used.

1.2.3 The *RE-GAS* Process

All of the above cited literature deals with the cyclic operation of fixed-bed regenerators and fixed-bed reactors. A typical cyclic operation of a fixed-bed reactor involves two semi-cycles. During a semi-cycle, the reactants are fed into the fixed-bed reactor from one end and during the next semi-cycle the reactants are fed into the bed from the other end. These repeated swings, or flow-reversals, of the feed result in an inverted U shaped temperature profile which travels in the bed from one position to other.

The references cited so far discussed only the bi-directional fixed-bed reactors subject to the same type of reaction throughout the cyclic operation i.e., the same feed

is introduced into the reactor during two successive semi-cycles. For example, in the catalytic oxidation of SO_2 the type of reaction that is occurring in the fixed-bed reactor is always catalytic oxidation of SO_2 during successive semi-cycles. The type of reaction does not change with the flow reversal of the feed (Matros, 1989, Eigenberger, 1988). Thus, the thermodynamic and dynamic nature of the system does not change with flow reversal.

Levenspiel (1988) proposed the *RE-GAS* process to produce synthesis gas. The process can involve gas phase or solid phase reactions. The fixed-bed reactor acts also like a heat regenerator. The *odd blow*, or the *odd semi-cycle*, involves feeding gaseous reactants which react exothermally in the fixed-bed reactor. During the *even blow*, or the *even semi-cycle*, another gaseous mixture, which contains reactants which undergo an endothermic reaction, is introduced from the opposite end of the fixed-bed. The product of interest is the product of the endothermic reaction which is carried out in the hot bed. The general idea is that the even blow is allowed to go on until the bed is sufficiently cooled down. These two semi-cycles constitute one complete cycle which is periodically repeated. In the production of synthesis gas by the RE-GAS process, even blows involve heating the bed by burning a hydrocarbon fuel, and odd blows involve the production of synthesis gas by endothermic reactions between steam and CO_2. The synthesis gas produced by this process, involving indirect coupling of exothermic and endothermic reactions, is not contaminated by N_2 unlike the bi-directional process proposed by Blanks et al. (1990) which uses direct coupling.

In the RE-GAS process, the type of reaction that takes place in the bed changes with each semi-cycle. Thus, two successive semi-cycles do not lead to mirror image solutions during the pseudo-steady state. The parameters like the maximum temperature, front velocity etc. are clearly different for even and odd semi-cycles especially since in one semi-cycle the reaction is exothermic (temperature rises) and in

the other it is endothermic (temperature falls). So far asymmetric bi-directional fixed-bed reactors subject to different reactions during even and odd semi-cycles have not been studied. Hence, there is a need to study RE-GAS type processes in order to develop an understanding of asymmetric fixed-bed operation under these new flow reversal conditions. This is the objective of the present study.

1.3 Objectives

The objectives of this research center around developing an understanding of how forced unsteady state can enhance the yield of an endothermic reaction in indirect presence of an exothermic reaction. The emphasis of the research is on development of a robust and accurate computational algorithm that would allow thorough investigation of the phenomena involved. Specifically, the objectives of this work are:

1. Develop a numerical algorithm which can simulate steep moving fronts.

2. Study the effect of forced flow reversal on a process involving homogeneous gas phase reactions where the yield of an endothermic reaction is enhanced by indirect coupling with an exothermic reaction. Investigate the parametric sensitivity and operability region.

3. Study the RE-GAS process through numerical simulation. Investigate the kinetics of reactions. Investigate parametric sensitivity and operability region.

The remainder of this thesis is divided into six Chapters. The developed numerical algorithm is discussed in the next (Chapter 2). Parametric sensitivity of fixed-bed reactors is presented in Chapter 3. A study of RE-GAS type processes is

discussed in Chapters 4 and 5. Chapter 6 deals directly with the RE-GAS process. The last Chapter 7 presents the conclusions of this work.

The FORTRAN codes developed for the simulation of different processes discussed in this thesis can be obtained from Dr. M. P. Dudukovic′, Chemical Reaction Engineering Laboratory, Campus Box 1198, Chemical Engineering Department, Washington University, One Brookings Drive, Saint Louis, MO 63130.

2. THE NUMERICAL ALGORITHM

A spatially and temporally adaptive completely implicit finite difference algorithm, which can accurately capture the moving temperature and reaction fronts in fixed-bed reactors with highly exothermic reactions, is developed and presented. For spatial adaptation linear interpolation proved to be more robust than higher order interpolations. Node placement based on the magnitude of the second spatial derivative was implemented and shown to lead to more accurate results and a more robust algorithm than the traditional node placement based on the magnitude of the first derivative. For improved accuracy, the interdependence of the spatial mesh size and the time step size is taken into account by coupling spatial and temporal adaptation. Choice of the time step is also related to the physics of the problem. Advantages of the developed algorithm over traditional finite difference and polynomial approximation methods are discussed.

The validity of the developed algorithm is proven by comparing the computed results with analytical solution of a linear heat regenerator model. A nonlinear model of a fixed-bed reactor with highly exothermic reaction occurring in the gas phase is also solved and the results are presented. The reasonableness of the solution for this nonlinear model is shown by comparison of model calculated and approximate analytical equation for the front velocity. The robustness of the developed algorithm in solving multiple coupled equations is demonstrated by solving a nonlinear model of a fixed-bed reactor in which both exothermic and endothermic reactions occur in the gas phase.

2.1 Introduction

As mentioned in the previous Chapter, in many chemical engineering applications solution of time dependent partial differential equations becomes a necessity. In particular, mathematical models for unsteady state processes occurring in fixed-bed reactors involving heat and mass transfer between solids and gases and reactions in solid phase and/or in gas phase involve such a set of partial differential equations. Fixed-beds with exothermic reactions in gas or solid phase can exhibit steep temperature and concentration profiles. The steepness of these profiles depends on the reactor rate sensitivity to temperature (activation energy), the exothermicity of the reaction (heat of reaction) and the phase in which reaction takes place. Since the solids have a much larger volumetric heat capacity than the gas phase, and a finite gas-solid heat transfer resistance is pronounced at high reaction rates, it is clear that a reaction occurring in the gas phase will lead to much steeper temperature and composition gradients than a reaction (of the same order, same activation energy and heat of reaction) occurring in the solid phase. This is not to say that fast reactions in the solid phase do not produce very steep gradients, but merely to indicate that the same gas phase reaction will result in even steeper ones. Under a certain set of conditions (flow reversal, composition cycling, start-up etc.) these steep fronts will move through the bed. Hence, a truly robust algorithm should be capable of providing accurate results for moving fronts caused by highly exothermic reactions in the gas phase as this is the most demanding situation.

Such moving fronts have been studied for both reactions in the solid phase and in the gas phase. For example, the production of SO_3 by exothermic catalytic reaction between SO_2 and O_2 by forced flow reversal, which involves periodic switching of the direction of the flow of the feed gases into the fixed-bed (Matros, 1989), catalytic combustion with periodic flow reversal (Eigenberger and Nieken, 1988), a study of

production of synthesis gas by forced flow reversal (Blanks et. al, 1990) are three of the many examples available in the literature which involve exothermic reactions in the solid phase and the resulting moving fronts.

There are a few processes in which highly exothermic gas phase combustion reactions take place in a fixed-bed. The attempted thermal production of NO by oxidation of atmospheric N_2 with atmospheric O_2 in a fixed-bed reactor filled with inert solids (Ermenc, 1956) is but one example. The gas phase combustion of hydrocarbons can be accomplished by forced flow reversal in a regenerative fixed-bed exploiting the high temperatures reached due to the forced flow reversal. The processes in which the yield of a gas phase endothermic reaction is increased in the presence of an exothermic reaction in the gas phase in a catalytic or inert fixed-bed are of interest. The idea is to provide the energy necessary to drive the endothermic reaction by the heat produced by an exothermic reaction which is stored in the packed bed of solids. This can be accomplished by repeated flow reversals. In such processes, due to lower thermal capacity of the gas, gradients of the temperature and concentration profiles are very high.

Although the phase in which exothermic reaction occurs influences the steepness of the fronts in a fixed-bed reactor, as mentioned earlier, highly exothermic reactions in either gas or solid phase can exhibit steep temperature and concentration fronts. The majority of traditional numerical techniques used in solving the partial differential equations that simulate these processes have been finite differences and polynomial approximations. To minimize computer time and increase the accuracy of predictions, temporal and spatial grid adaptation based on various criteria are applied in many algorithms (Eigenberger and Butt, 1976; Il'in and Luss, 1992). It is not our objective to illustrate in detail all the numerical studies of moving steep fronts in packed bed reactors. The state of the art is such that there is a clear need to develop a

robust numerical algorithm which can accurately track steep moving fronts in fixed-bed reactors involving highly exothermic reactions in both gas and/or solid phases. Our objective was to respond to this need by developing such a robust algorithm. In describing below as to how this was accomplished we review only those elements of previous studies which are pertinent to understanding the advantages of the proposed new algorithm.

2.2 Polynomial Approximation Methods

2.2.1 Global and Sectional Approximations

As mentioned earlier both global polynomial approximations, representing the dependent variable as a polynomial over the entire length of the reactor and polynomial

approximations on finite elements (Finlayson, 1980; Villadsen and Michelsen, 1978) have been used in solution of moving front problems. Polynomial approximation on finite elements naturally captures the steep fronts more accurately than the global approximation methods. Higher order polynomials produce 'numerical wiggles' in the region of high second derivatives, as illustrated in Figure 2.1b, in which a steep step-like function shown in Figure 2.1a is approximated by polynomials of different orders. In popular finite element methods second order polynomial approximations of the dependent variables are generally used (Eigenberger and Butt, 1976; Finlayson, 1980).

For moving fronts and cyclic operation several approaches have been used. Ramachandran and Dudukovic′ (1983) developed a moving finite element collocation method for a moving temperature front in a packed bed heat regenerator. The lengths

and the locations of the elements were determined by the magnitude of the heat flux.

Ramachandran and Dudukovic′ (1984) also solved the packed bed regenerator model

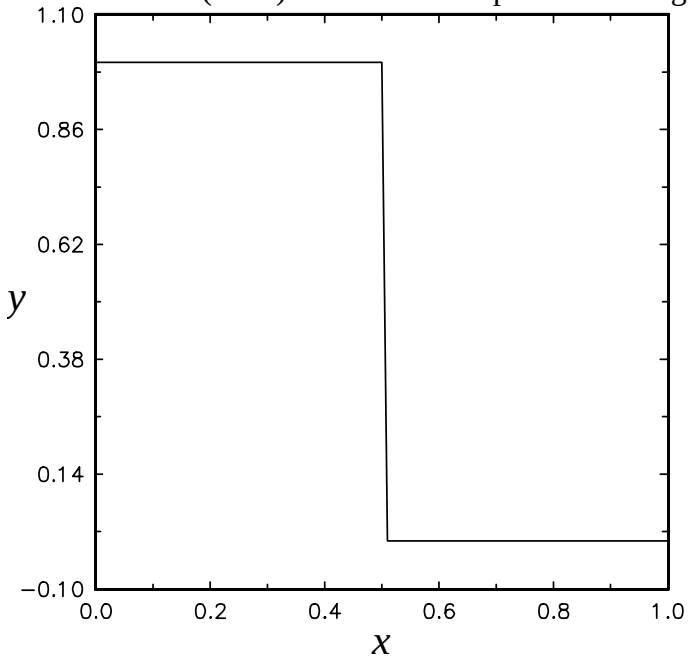

Figure 2.1a. A steep Function $y = f(x)$.

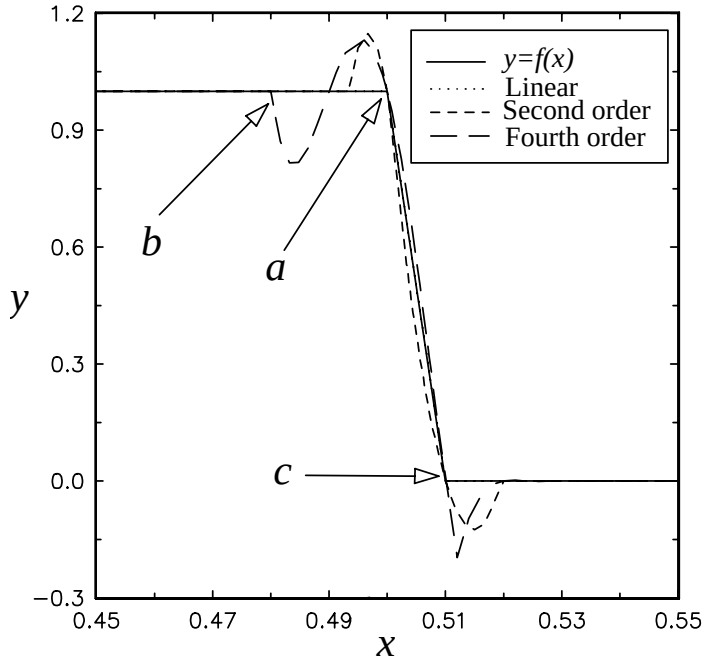

Figure 2.1b. Comparison between various orders of interpolation.

using dual collocation, i.e., collocation in space and time. Gawdzik and Rawkowski (1988, 89) studied the properties of an adiabatic tubular reactor forced through the reversal of flow of the reaction mixture using a combination of the method of characteristics and orthogonal collocation. Gupta and Bhatia (1991) simulated the cyclic operation (one cycle involves two half cycles—one half cycle is completed when the direction of the feed gases is switched) by using collocation on finite elements in space. They treated the differential equation system as a boundary value problem in time, with stationary catalyst temperature profiles at the beginning and the end of a half cycle being mirror images of each other. Eigenberger and Butt (1976) developed a modified Crank-Nicolson technique with non-equidistant space steps for moving fronts. The whole length of the bed is divided into finite elements and on each element the solution is approximated as a second order polynomial. However, in the regions of high second order derivatives the *Sag Effect*, which is basically caused by *numerical wiggles*, was observed. Eigenberger and Nieken (1988) studied catalytic combustion with periodic flow reversal using this algorithm. Carey (1979) developed an adaptive algorithm for stationary fronts in linear and nonlinear problems (e.g. diffusion-reaction in a porous catalyst, standard potential equation) which employs mesh refinement based on the equidistribution of the residual. Jiang and Carey (1988) employed the least squares method on a discrete level for weighted residual placement of nodes for moving fronts in flow problems (e.g. Burger's equation). They did encounter numerical instability for nonlinear problems and had to introduce numerical damping.

2.2.2 A Comparison between Polynomial Approximations of Different Orders

In fixed-bed reactors involving highly exothermic reactions, the reaction front is very steep and the concentration of the key reactant drops to zero over an extremely short distance at the reaction front. The concentration profile of the key reactant is continuous and the equations describing the front are nonlinear. However, the shape of the concentration front can often be closely approximated by a step-down function shown in Figure 2.1a. Such a step function looks like a piecewise linear function which can be clearly optimally represented by piecewise linear functions. This is illustrated by comparing the performance of different orders of interpolation. Lagrangian polynomials of various orders were employed. Since this kind of profile is subject to repeated polynomial approximations in the simulation of fixed-bed reactors with moving fronts, we approximated the step function twice using each polynomial. The first approximation was accomplished by using the data generated by the step function itself, and the second approximation was accomplished by using the data generated by the first approximation. A comparison between polynomial approximations of different orders is shown in Figure 2.1b. It is evident that the linear approximation proves to be the most accurate form of approximation. This is understandable since to calculate the dependent variable at node '*a*', higher order approximations use the points further from the point of interest, '*a*'. Values further away from the point of interest '*a*' , say at '*b*' and '*c*' (see Figure 2.1b) do not represent the values at the point of interest '*a*'. A large magnitude of the difference in values at 'b' and 'c' leads to incorrect approximation of the function even when many points are taken and a high order polynomial is used. A more accurate approximation of the dependent variable at point '*a*' is achieved by interpolation between a minimum number of grid points closest to '*a*'. Therefore the first order finite difference approximation, which is essentially a linear approximation, proves to be more accurate than higher order polynomial, or higher order finite difference approximations,

provided the grid points are placed very closely in the region where second derivatives are large in magnitude. A vast body of literature and experience shows that the concentration and reaction fronts in fixed-bed reactors, which are continuous and are described by nonlinear equations, bear close resemblance to piecewise linear functions, like the one in Figure 2.1a, in the region of the fronts. Hence, they are optimally represented by linear functions and this was done in the algorithm developed in this work.

2.3 Finite Differences

Based on the observations in the previous section, first order finite difference approximations are superior to higher order finite difference and polynomial approximations in representation of sharp fronts. Hence, an algorithm based on finite difference approximations for solution of moving front problems seems advisable. Finite differences, which can be derived from Taylor's series approximations (Finlayson, 1992), have been used quite extensively to solve partial differential equations which model fixed-bed reactors.

Explicit finite difference approximations use known dependent variable nodal values at time n to march on to time $n+1$ and are conditionally stable (Fletcher, 1991; Finlayson, 1992). When the fronts become very steep, stability and accuracy criteria for an explicit scheme require that both the spatial step and the temporal step be extremely small. This procedure is time consuming and impractical for very steep moving fronts with high second derivatives. It can be shown that if the difference approximations are made using mesh variables at time $n+1$ rather than at time n, the resulting finite difference implicit scheme is unconditionally stable (Fletcher, 1991). This scheme allows larger time steps and is robust.

Figure 2.2 shows a typical march in time for an implicit scheme. The sides of the mesh are defined by the boundary conditions and the base of the mesh is defined by the initial conditions. The rest of the mesh is defined by the implicit finite difference equations. However, in this case, unlike in the explicit scheme, the mesh variables are

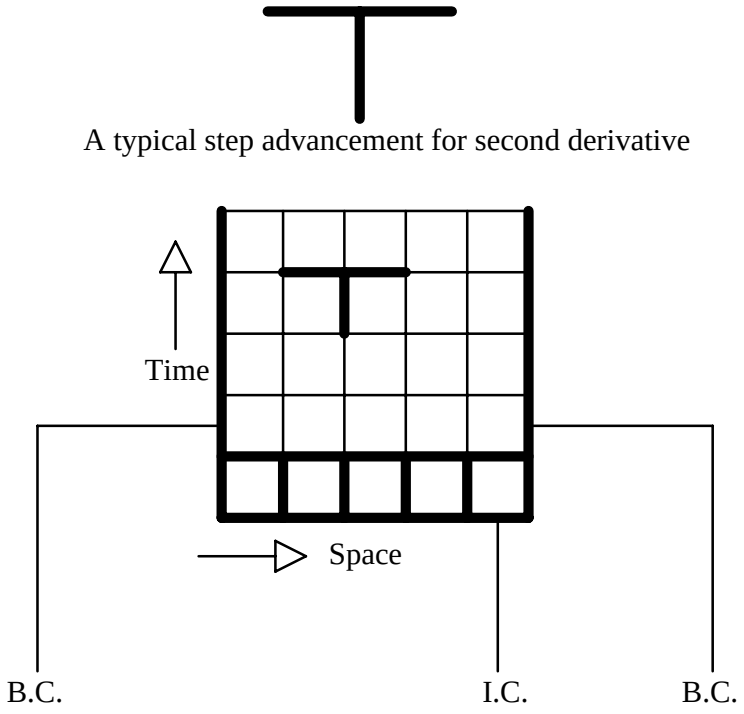

Figure 2.2. An implicit finite difference scheme

not known since difference equations are defined by mesh variables at time n+1. The system of nonlinear equations is implicit and tridiagonal. At every time step, the solution of this system of equations is required. However, if larger time steps are intelligently chosen, the implicit finite difference scheme is economical and robust compared to the explicit finite difference scheme.

Finite difference based algorithms have been used extensively to solve the models for moving fronts in fixed-bed reactors. Rhee et al (1973) used the cell model to simulate a fixed-bed reactor. Agar and Ruppel (1988) used implicit finite difference

approximations to study NOx removal in the presence of ammonia and air by forced flow reversal in a fixed-bed reactor. For accurate results the mesh is required to be very fine which increases the computation time dramatically and makes the use of finite differences impractical in prediction of very steep fronts. Il'in and Luss (1992) used an adaptive implicit finite difference scheme to simulate moving fronts. They used spline interpolation and the magnitude of the first derivative (first derivative control) as the criterion for mesh refinement. However, as shown in Figure 2.1, higher order interpolations are inaccurate in the region of high second order derivatives. Since the approximation of the front becomes more difficult in the region of high second order derivatives, a grid adaptation criterion based on the magnitude of second order derivatives, rather than the first order derivatives, is advisable as shown in this work.

Finlayson (1992) compared finite difference methods and finite elements methods on problems involving moving fronts. Basically his treatment involves non-reactive problems, explicit schemes are mainly treated, and highly nonlinear problems with many coupled variables are not discussed. Finlayson also suggests the mesh adaptation based on the second derivatives but advocates the application of higher order finite difference approximations over first order approximations for higher accuracy. However, as discussed earlier, first order approximations are more accurate in the regions where the magnitude of the second derivatives is high and hence should be used.

2.4 The Developed Adaptive Algorithm

Based on the above discussion we have concluded that a robust numerical algorithm should be based on the linear first order approximations. In the case of an explicit finite difference scheme, for very small spatial steps, time increments have to

be very small to satisfy stability criteria (Poulain and Finlayson, 1990; Fletcher, 1991) . However, completely implicit finite differences are unconditionally stable. If the time and spatial steps are intelligently chosen to satisfy accuracy, the computer time required to solve the problem is considerably reduced for an implicit scheme. Therefore, we have developed such a completely implicit, spatially and temporally adaptive, finite difference scheme, discussed below, for problems involving very steep moving fronts. Typical finite difference approximations for the first and second derivatives and for the source function are given below:

$$\left.\frac{\partial y}{\partial z}\right|_{z=z_i} = \frac{y_i^{n+1} - y_{i-1}^{n+1}}{z_i - z_{i-1}} \tag{2.1}$$

$$\left.\frac{\partial^2 y}{\partial z^2}\right|_{z=z_i} = \frac{\dfrac{y_{i+1}^{n+1} - y_i^{n+1}}{z_{i+1} - z_i} - \dfrac{y_i^{n+1} - y_{i-1}^{n+1}}{z_i - z_{i-1}}}{0.5\left(z_{i+1} - z_i\right) + 0.5\left(z_i - z_{i-1}\right)} \tag{2.2}$$

$$f(z,y)\big|_{z=z_i, y=y_i} = f(z_i^{n+1}, y_i^{n+1}) \tag{2.3}$$

The upwind approximations used above may introduce excessive numerical dispersion (Finlayson, 1992). However, the algorithm we have developed greatly minimizes such numerical dispersion as discussed below. Instead of the upwind approximations other first order approximations can also be used.

While an implicit finite difference scheme is unconditionally stable, the accuracy of the solution is limited by the employed accuracy criterion (Finlayson, 1992). For good accuracy, in the region where first and second derivatives are high, the time and spatial steps are required to be small. To simulate a steep moving front it is required that the magnitude of all spatial and time steps be determined by the smallest space and time step. Thus, the number of equations to be solved at each time

step increases along with the number of time steps, which renders the procedure very uneconomical.

Temporal and spatial adaptation of the mesh are then needed to reduce the number of equations to be solved at each time step along with the number of time steps. The accuracy criterion requires that spatial steps be small only where steep temperature and concentration fronts exist. Thus, by using an appropriate accuracy criterion, if the number of nodes at the temperature and concentration fronts is increased, while the rest of the grid maintains a sparse mesh, the system can meet the chosen accuracy criterion. The same procedure is applied for temporal grid adaptation. If a new node is placed at time n+1 between z_i and z_{i+1}, as defined at time n, it is necessary to interpolate n values onto n+1 values for a new mesh generation at time n+1. This procedure is explained in Figure 2.3.

Traditionally two methodologies are used for spatial adaptation. One of them employs the weighted distribution of the fixed number of nodes based on some equidistribution criterion. This methodology is elegant, since the total number of equations to be solved remains constant, and the nature of the system of equations does not change. The solution of this system of equations gives the final results. However, if the fronts become very steep, and the fixed number of nodes do not meet the accuracy criterion, the solution becomes far from accurate. The other method of adaptation is based on node addition-deletion based on the accuracy criterion. This method is not very elegant, since as the number and the position of nodes change, the system of equations changes. Therefore, to arrive at the final solution, it is necessary to iterate with intermediate solutions. However, this method is very robust because it can handle very steep moving fronts. Temporal adaptation is performed along with the spatial adaptation. The magnitude of the second derivative of the profile of the dependent variable at each node is maintained within a tolerance criterion by adjusting

the time and space steps at each time step. Figure 2.4 depicts a typical mesh refinement for a moving front.

2.4.1 The Accuracy Criterion and the Interpolation Scheme

The steepness of the profiles in space is defined by the magnitude of the first spatial derivative. Hence it appears that the accuracy criterion for mesh refinement should be based on the magnitude of the first derivative. However, in finite element methods it has been shown that for linear trial functions the error is proportional to the

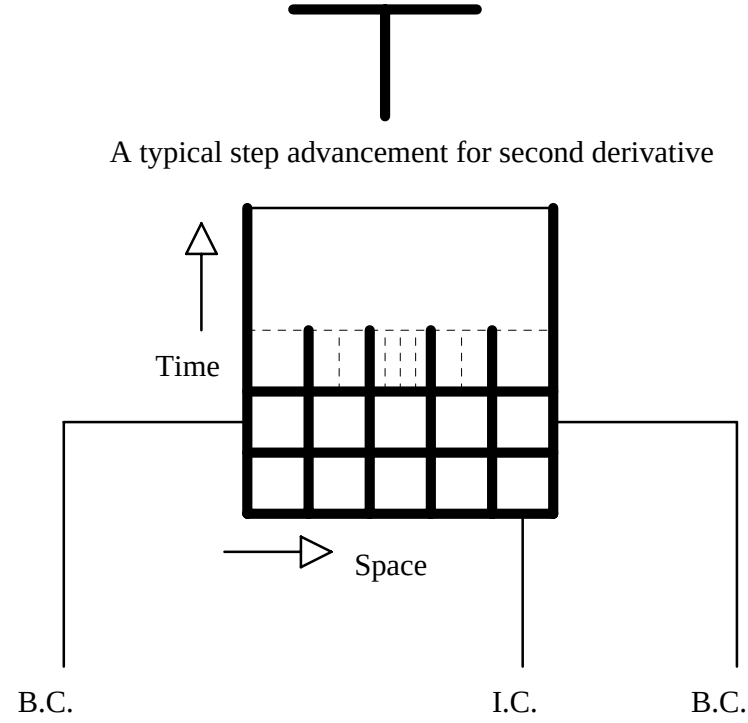

Figure 2.3. An interpolation scheme for spatial adaptation.

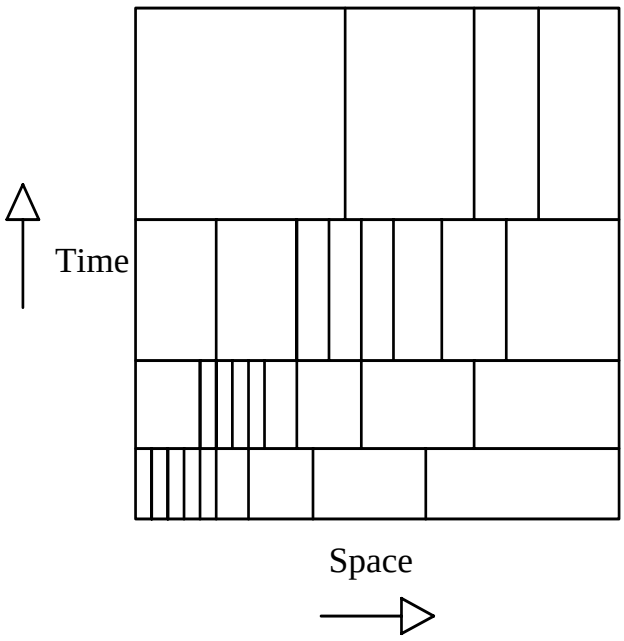

Figure 2.4. A complete picture of temporally and spatially adapted mesh.

second derivative of the solution (Finlayson, 1992). Also, in the region of the front, where the magnitude of the first derivative is very high, the front is almost a straight line which requires only a few nodes for accurate representation. Only in the region where the second derivative is very high the solution tends to get unstable and generates oscillations. The numerical dispersion introduced by the finite difference approximation itself, leads to the highest error in the regions of high second order derivatives. Therefore, we select an accuracy criterion based on the second derivative to refine the spatial mesh. The criterion used for second derivative control is

$$\left.\frac{\partial^2 y}{\partial z^2}\right|_i^{n+1} \times \frac{\left[\left(z_{i+1}^{n+1} - z_i^{n+1}\right) \times \left(z_i^{n+1} - z_{i-1}^{n+1}\right)\right]^2}{4} \leq \delta_2 \qquad (2.4)$$

where δ_2 is the tolerance set by the user. This allows us to always have a sufficient number of nodes at the 'edges' of the steep front where the second derivatives are very high, and, hence, this reduces numerical dispersion by positioning the nodes where they are most needed.

The conventionally used accuracy criterion is based on first derivative control and is given by

$$\frac{y_i^{n+1} - y_{i-1}^{n+1}}{y_i^{n+1}} \times 100 \le \delta_1 \qquad (2.5)$$

where δ_1 is a tolerance set by the user. We have compared numerous cases with first and second derivative control, and our method of using second derivative control was always superior without exception.

The time steps, in contrast, are always restricted by the first derivative control. Also, the maximum time step to be taken, t_{mx}, is set by the user based on the physics of the problem. In the case of fast reactions, t_{mx} should be of the order of the characteristic reaction time of the fastest reaction. If the rate of heat transfer is higher than the rate of reaction, t_{mx} should be of the order of the characteristic heat transfer time. Thus, the maximum allowable size of the time step is controlled by the physics of the problem. Hence, the size of the time steps taken is determined by the following accuracy criteria:

$$\frac{y_i^{n+1} - y_i^n}{y_i^n} \times 100 \le \delta_t \ldots \text{First Derivative Control} \qquad (2.6)$$

and

$$t^{n+1} - t^n \le t_{mx} \ldots . \text{Characteristic time control} \qquad (2.7)$$

where δ_t is the tolerance set by the user. The time step is increased by a factor of 1.25 after each iteration to allow for the maximum time step that can be taken within the bounds set by the accuracy criterion. The size of the time step is reduced by a factor of two if the accuracy is not satisfied.

Linear interpolation is used every time the mesh is refined. In the region where the second derivatives are high, higher order interpolations are inaccurate and give oscillatory results. The linear interpolation scheme used is

$$if \quad z_{i+1}^{n} > z_{i}^{n+1} > z_{i}^{n} \ then$$
$$y_{i,new}^{n} = y_{i}^{n} + \frac{y_{i+1}^{n} - y_{i}^{n}}{z_{i+1}^{n} - z_{i}^{n}} \times \left(z_{i,new}^{n} - z_{i}^{n} \right) \tag{2.8}$$

2.4.1.1 Multiple Point Interpolation and Multiple Point Elimination

To overcome numerical dispersion and improve the accuracy of results, multiple point interpolation and multiple point elimination are employed along with second derivative control. If the accuracy criterion is not satisfied at node *i*, nodes are added between nodes *i*-*ni* and *i*-(*ni*-1), *i*-(*ni*-1) and *i*-(*ni*-2)...*i* and *i*+1, *i*+1 and *i*+2,..*i*+*ni*-1 and *i*+*ni* where *ni* is the point interpolation index chosen by the user. If the elimination criterion (usually 0.01×accuracy criterion) is satisfied at *i*-*nt*, *i*-(*nt*-1), *i*-(*nt*-2)...*i*, *i*+1, *i*+2,..*i*+*nt*-1 and *i*+*nt*, where *nt* is the point node elimination index chosen by the user, a node at *i* is eliminated.

If computer time is a concern, a trade off between accuracy and time economy can be reached by various accuracy criterion relaxation techniques. We set the initial accuracy criterion in time by the tolerance δ_t and the spatial accuracy criterion by the tolerance δ_2. For accurate marching in time, the spatial accuracy is required to be very high and vice versa. The system of equations becomes very stiff if temporal tolerance and spatial tolerance are not in the comparable accuracy range. For example, if δ_2 is very low (high spatial accuracy) it requires that δ_t be low as well (high temporal accuracy). Therefore when time steps become smaller than the specified Δt_{min}, spatial and temporal accuracy criteria are relaxed by a small margin (usually $\delta_{2,new} = 1.1 \times \delta_{2,old}$ and $\delta_{t,new} = 1.1 \times \delta_{t,old}$) which allows bigger δ_t values and results in larger time steps. This results to a trade off between accuracy and computer time economy. Δt_{min} is chosen to be of one or two orders of magnitude smaller than the characteristic reaction time or characteristic heat transfer time. Since the size of the time step is

increased by a factor of 1.25 after each successfully converged calculation, time steps can become too large to satisfy the criterion $t^{n+1} - t^n \le t_{mx}$. Under these circumstances δ_t is decreased by a certain ratio to decrease the size of the time step needed to satisfy the specified t_{mx}. To maintain the comparable accuracy of the spatial step size, δ_2 is decreased by the same ratio as well. Thus, the size of a time step is bounded by t_{mx} and Δt_{min} to maintain accuracy and achieve computer time economy. The flow sheet of the algorithm is given in Figure 2.5.

The salient features of the developed algorithm can be summarized as follows.

1) Application of the spatial second derivative control

2) Use of the linear interpolation for spatial adaptation.

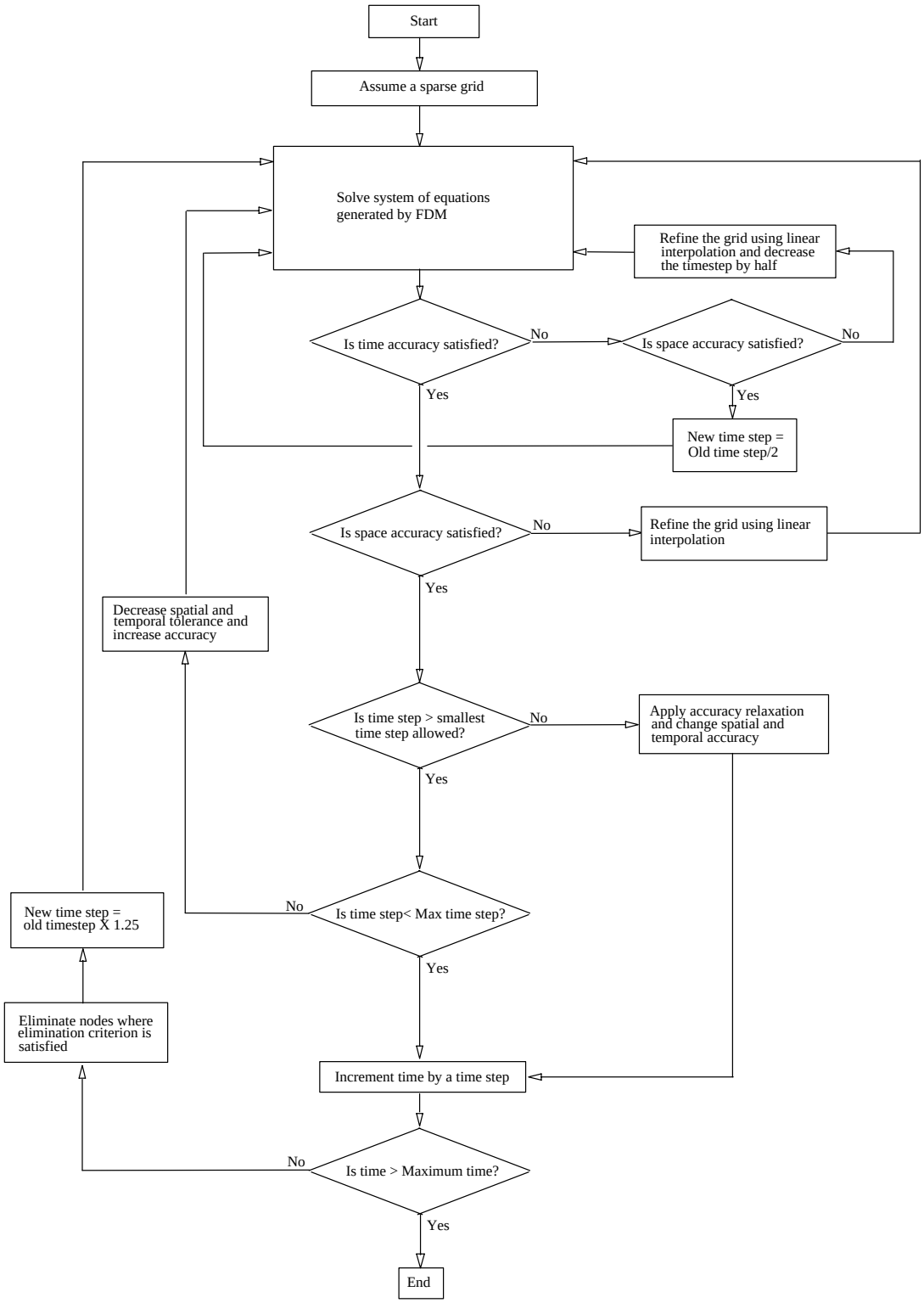

Figure 2.5. The flow sheet of the developed algorithm.

3) The incorporation of a chosen characteristic-time limited time step control along with the first derivative control for the time step management.

4) A variable space and time tolerance scheme which automatically varies the spatial and temporal tolerance if the finite difference system becomes too big for the computer to handle in a reasonable amount of time (trade off between accuracy and time).

2.5 Applications

2.5.1 The Heat Regenerator without Reaction

2.5.1.1 The Model

The first problem chosen for the verification of the performance of the developed algorithm is the classical heat regenerator problem. A packed bed filled with inert solids being heated by incoming hot gases is modeled by the following partial differential equations:

$$\frac{\partial \theta_g}{\partial z} = -St_g(\theta_g - \theta_s) \tag{2.9}$$

$$\frac{\partial \theta_s}{\partial \tau} = St_s(\theta_g - \theta_s) \tag{2.10}$$

Boundary conditions:

$@\, z = 0$

$\theta_g = 1;\ \theta_s = 1 - \exp(\tau St_s)$

and

Initial conditions:

$@\ \tau = 0$ and $0 \le z \le 1$

$\theta_s = 0$

where

$$\theta_g = \frac{T_g - T_{s,0}}{T_{g,in} - T_{s,0}}; \quad \theta_s = \frac{T_s - T_{s,0}}{T_{g,in} - T_{s,0}}; \quad z = \frac{x}{L}$$

$$\tau = \frac{t}{L/u_{in}}; \quad St_g = \frac{ha_p L}{\varepsilon \rho_{g,in} u_{in} C_{p,g}} \; ; \; St_s = \frac{ha_p L}{(1-\varepsilon)\rho_s u_{in} C_{p,s}}$$

Although in the process considered no reaction is occurring, the nature of the moving front is similar to that observed in fixed-bed reactors. In addition, the purely convective nature of the equations tests the robustness of the numerical algorithms. Since the analytical solution of this model is available, it is used for validation of our algorithm.

2.5.1.2 Analytical Solution

Analytical solution of this model is given by Nusselt, Anzelius and Schumann (Jakob, 1957). Here we use the analytical solution given by Schumann (Schmidt and Willmott, 1981) for (St_S τ)≥4.0 and (St_gz)≥4.0:

$$\theta_g(\tau, z) = 1 - \frac{1}{2}\left[1 + erf\left(\sqrt{zSt_g} - \sqrt{\tau St_s} - \frac{1}{8\sqrt{zSt_g}} - \frac{1}{8\sqrt{\tau St_s}}\right)\right] \qquad (2.11)$$

2.5.1.3 A Comparison between Analytical, Finite Difference and Polynomial Approximation on Finite Elements Solutions

The regenerator problem for the parameters given in Table 2.1 was solved first by the implicit finite difference method by using 101 equidistant node points. The problem was also solved by second order polynomial approximation on 50 equidistant finite elements. Thus, the total number of nodes used in the polynomial approximation method was also 101. In both methods a constant time step of 0.1 seconds was used.

The solutions obtained by both numerical methods are compared with the analytical solution given by Schumann in Figures 2.6a and 2.6b. It can be clearly seen that both methods give inaccurate results. In the case of the finite difference method (Figure 2.6a), the inaccuracy is caused by sparsely spaced nodes which is evident from the observed numerical dispersion. The finite difference method is stable and the magnitude of numerical dispersion can be reduced by using a fine mesh in the region of the high magnitude of second derivatives. The polynomial approximation on finite elements (Figure 2.6b), yields a highly unstable solution which is evident from numerical oscillations which are often referred to as 'wiggles'. This instability is caused by the inaccurate approximation of the dependent variable in the region of high magnitude of second order derivatives. Hence, it can be concluded that linear approximation used by finite differences is more robust and stable than the higher order approximations. However, to achieve accurate results using finite difference approximations a fine mesh is required. Computer time can be saved by using the adaptive algorithm that we have developed which places an increased number of nodes only in the region of high second order derivatives.

The finite element algorithm is very sensitive to the size of the mesh. An adaptive algorithm based on the finite element method failed to solve equations (2.9) and (2.10) with parameters given in Table 2.1. To capture the steepness of the front, additional elements are placed in the region of the high magnitude of second derivatives. However, as the number of elements in the region of high magnitude of second derivatives increases, the distance between two node points decreases considerably and the finite element method fails to converge. For example, for the problem under consideration, for a grid size of order 10^{-5}, the finite element method failed to converge. In a fixed-bed reactor involving highly exothermic reactions, the temperature and reaction fronts are steeper than the temperature front observed in the

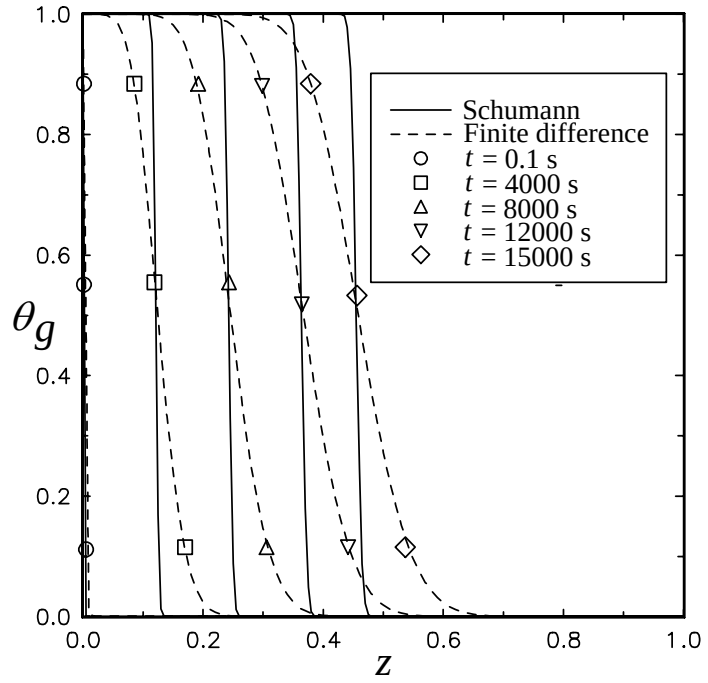

Figure 2.6a. A comparison of results obtained by using finite differences and Schumann

solution.

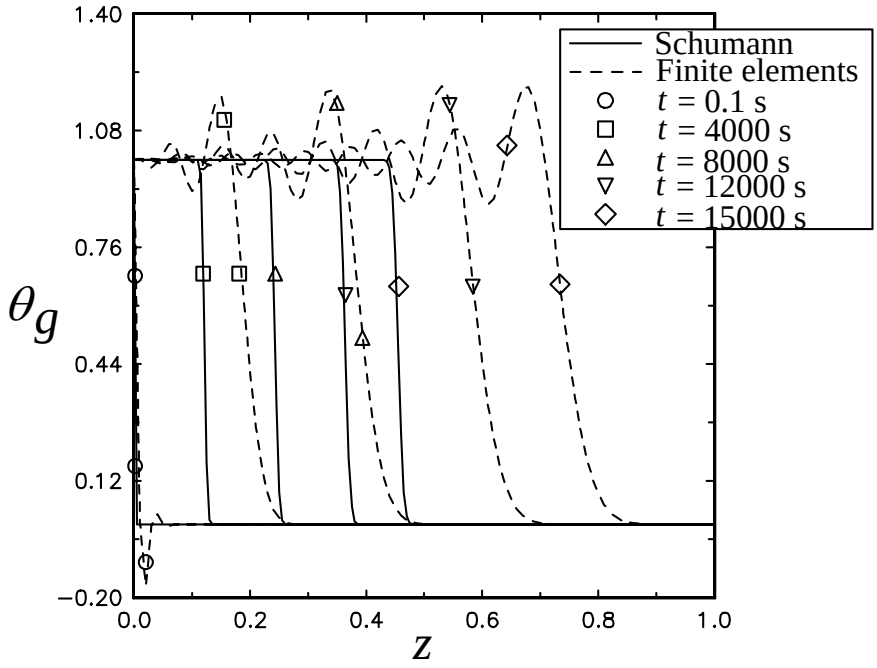

Figure 2.6b. A comparison of results obtained by using finite elements and Schumann

solution.

current problem. Therefore, polynomial approximation on finite element methods seem ill suited for simulation of steep fronts observed in a fixed-bed reactor.

2.5.1.4 A Comparison between Analytical Solution and the Developed Adaptive Algorithm

The classical regenerator model is solved using the developed adaptive algorithm and the results obtained are compared with the analytical solution. In this particular case a constant time step of 0.1 second (0.02 τ) was used, as it was not necessary to change the time steps because the front moves with a constant speed. As can be verified from Figure 2.7a, the adaptive algorithm accurately predicts the front movement. The node addition and deletion based on the accuracy criteria creates a cloud of nodes which moves with the front as shown in Figure 2.7b.

2.5.1.5 A Comparison between the First Derivative and Second Derivative Control

As already mentioned, the mesh adaptation based on the magnitude of the second derivative (second derivative control) is more accurate than that based on the magnitude of the first derivative (first derivative control). This can be verified by comparing the solutions of the heat regenerator problem obtained by using first and second derivative control. In the classical heat regenerator model, the heat capacity of the gas is neglected. Here, we incorporate the gas heat capacity in the model and we also include the axial dispersion term in the solid phase. The resulting model equations are given below.

$$\frac{\partial \theta_g}{\partial \tau} = -U \frac{\partial \theta_g}{\partial z} - St_g \frac{1}{\Omega_g}(\theta_g - \theta_s) \qquad (2.12)$$

$$\frac{\partial \theta_s}{\partial \tau} = \frac{1}{Pe_{h,s}} \frac{\partial^2 \theta_s}{\partial z^2} + St_s(\theta_g - \theta_s) \tag{2.13}$$

$$\Omega_g U = \text{constant} \tag{2.14}$$

Boundary conditions:

$@\, z = 0$

$$\theta_g = \theta_{g,in}; \quad \frac{\partial \theta_s}{\partial z} = 0$$

$$@\, z = 1; \quad \frac{\partial \theta_s}{\partial z} = 0$$

Initial conditions

$@\ \tau = 0$ and $0 \le z \le 1$

$$\theta_g = \theta_{g,0}; \quad \theta_s = \theta_{s,0}$$

where

$$\theta_g = \frac{T_g - T_{s,0}}{T_{g,in} - T_{s,0}}; \quad \theta_s = \frac{T_s - T_{s,0}}{T_{g,in} - T_{s,0}}; \quad z = \frac{x}{L}$$

$$\tau = \frac{t}{L / u_{in}}; \quad U = \frac{u}{\varepsilon u_{in}}; \quad St_g = \frac{h a_p L}{\varepsilon \rho_{g,in} u_{in} C_{p,g}}$$

$$St_s = \frac{h a_p L}{(1-\varepsilon)\rho_s u_{in} C_{p,s}}; \quad Pe_{h,s} = \frac{(1-\varepsilon)\rho_s u_{in} C_{p,s} L}{D_{e,s}}; \quad \Omega_g = \frac{\rho_g}{\rho_{g,in}}$$

The above model assumes plug flow of gas. The axial dispersion of heat in the solid phase was included in equation (2.13) and we have demonstrated that our algorithm can readily handle it. In the results presented here, however, this term is neglected since that leads to the steepest temperature profiles which present the most severe test to our algorithm. The Peclet number for heat transfer ($Pe_{h,s}$) as defined here is the ratio of the convective heat transfer by gas to the axial dispersion of heat in the solids

but multiplied with the ratio of the solid and gas heat capacity. Hence, $Pe_{h,s}$ is generally

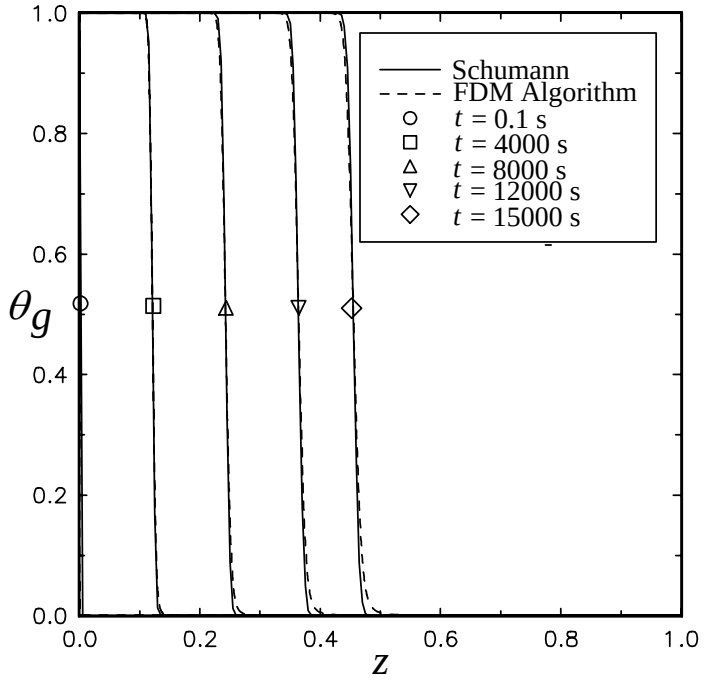

Figure 2.7a. A comparison of results obtained by using the adaptive algorithm and Schumann solution.

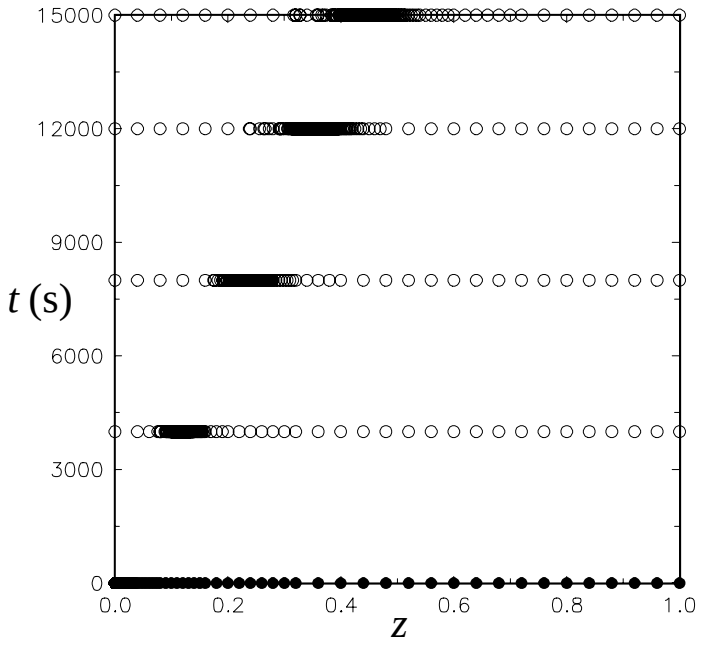

Figure 2.7b. The spatial position of grid points at different times.

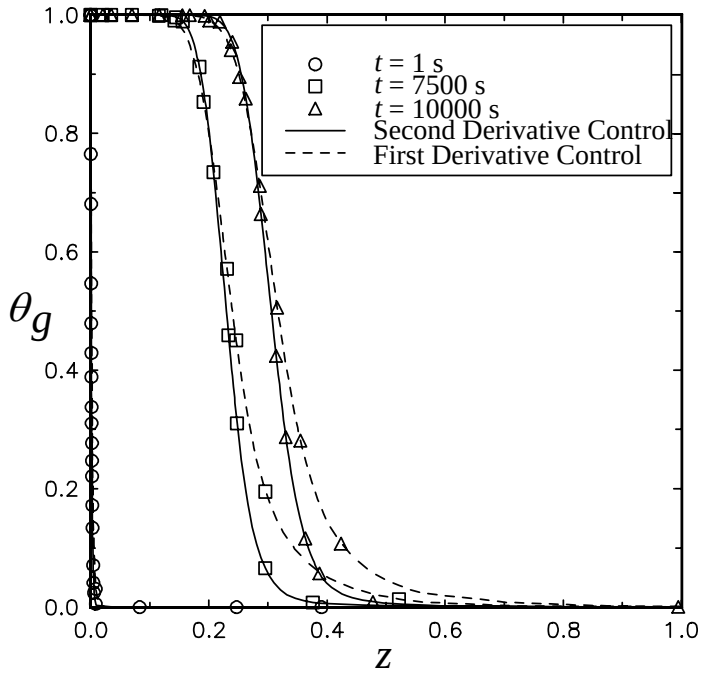

Figure 2.8. A comparison between first and second derivative control.

large and when it tends to infinity the term containing its reciprocal can be safely neglected. Plug flow models with no axial dispersion are known to be much more difficult to simulate numerically than dispersion models since dispersion of heat in the axial direction makes the temperature fronts smoother and broader. The gas Stanton number (St_g) is a measure of the relative magnitude of the rate of convective heat transfer between solids and the gas to the rate of convective heat transfer in the axial direction by the gas. Thus, a higher gas Stanton number indicates higher temperature change in the gas phase along the axial distance. The temperature fronts become steeper as the gas Stanton number increases. The solid Stanton number (St_s) is a measure of the relative magnitude of the rate of heat transfer between the gas and the solids compared to the product of volumetric heat capacity of the solids and the gas

velocity. Since the temperature drop in the solid phase is directly proportional to the rate of heat transfer between the gas and solids, and inversely proportional to the volumetric heat capacity of the solids, a higher solid Stanton number results in steeper temperature fronts in the bed. Since the gas and the solid temperature fronts follow each other closely, a system having higher gas and solid Stanton numbers involves steeper moving fronts. The parameters used in the simulation of the heat regenerator model are given in Table 2.1.

A comparison between the results obtained using the first and second derivative control is shown in Figure 2.8. As explained before, the temperature fronts predicted by using the accuracy criterion based on the magnitude of first derivative are less steep. If the tolerance is decreased in the case of first derivative control, the equations become very stiff and convergence becomes difficult to achieve. The size of a time step was bounded by t_{mx} = 1 s and Δt_{min} = 0.0001 s for both first and second derivative control. To save computer time, the accuracy relaxation criterion, $\delta_{new}=\delta_{old}\times 1.1$ is used every time the time step became smaller than 0.0001 s. It is clearly demonstrated here that the second derivative control works better than the first derivative control. Hence, only second derivative control is used for further applications.

2.5.2 Analysis of an Unsteady State Fixed-Bed Reactor

2.5.2.1 Model Equations

The accuracy and robustness of the developed numerical algorithm was established using the heat regenerator process. The prime objective of the algorithm is, however, to simulate the steep fronts in a fixed-bed reactor involving highly

exothermic reactions. Therefore, a simulation of a packed bed reactor subject to a highly exothermic reaction is undertaken. For the sake of generality the model incorporates two reactions—one exothermic and another endothermic, occurring in the gas phase in a fixed-bed reactor. The two reactions considered in this preliminary simulation are:

$$\begin{aligned} &A \rightarrow C && \Delta H_1 \langle 0 \\ &B \rightarrow D && \Delta H_2 \rangle 0 \end{aligned}$$

Plug flow of the gas and axial heat dispersion in the solid phase are assumed. As mentioned earlier the models based on the plug flow assumption alone predict steeper fronts than models that incorporate axial dispersion, because dispersion of heat and mass broadens the temperature and concentration fronts. Hence, a plug flow model is much more difficult to solve numerically than the dispersion model. The algorithm which can solve a plug flow model accurately can easily handle heat and mass dispersion in the gas phase. This was the reason for selecting the model equations below so as to expose our algorithm to the most demanding test. The gas is assumed to be compressible with the total mass flux of gas being constant (Kulkarni, 1992). The rate of conduction within solids is assumed to be very high compared to the convective heat transfer rate between the gas and the solids. The physical properties of the gases, including density, are assumed to be temperature dependent. Kinetics is assumed to have an Arrhenius type dependence on the temperature and to be first order. The model equations are

$$\frac{\partial \theta_g}{\partial \tau} = -U \frac{\partial \theta_g}{\partial z} + \tau_{s/r,g,A} TR_{g,A} \gamma_{g,A}^{\frac{1-\theta_g}{\theta_g+\theta_{g,d}}} y_A + \tau_{s/r,g,B} TR_{g,B} \gamma_{g,B}^{\frac{1-\theta_g}{\theta_g+\theta_{g,d}}} y_B - St_g \frac{1}{\Omega_g} (\theta_g - \theta_s) \quad (2.15)$$

$$\frac{\partial \theta_s}{\partial \tau} = \frac{1}{Pe_{h,s}} \frac{\partial^2 \theta_s}{\partial z^2} + St_s (\theta_g - \theta_s) \quad (2.16)$$

$$\frac{\partial y_A}{\partial \tau} = -U\frac{\partial y_A}{\partial z} - \tau_{s/r,g,A}\gamma_{g,A}^{\frac{1-\theta_g}{\theta_g+\theta_{g,d}}} y_A \tag{2.17}$$

$$\frac{\partial y_B}{\partial \tau} = -U\frac{\partial y_B}{\partial z} - \tau_{s/r,g,B}\gamma_{g,B}^{\frac{1-\theta_g}{\theta_g+\theta_{g,d}}} y_B \tag{2.18}$$

$$\frac{\partial \Omega_g}{\partial \tau} = -\frac{\partial\left(\Omega_g U\right)}{\partial z} = 0 \tag{2.19}$$

Boundary conditions:

$@\, z = 0$

$$\theta_g = \theta_{g,in};\quad \frac{\partial \theta_s}{\partial z} = 0;\quad y_A = y_{A,in};\quad y_B = y_{B,in}$$

$@\, z = 1$

$$\frac{\partial \theta_s}{\partial z} = 0$$

Initial Conditions:

$@\, t = 0$ and $0 \le z \le 1$

$$\theta_g = \theta_{g,0};\quad \theta_s = \theta_{s,0};\quad y_A = y_{A,0};\quad y_B = y_{B,0}$$

The dimensionless quantities used above are:

$$\tau = \frac{t}{L/u_{in}};\quad z = \frac{x}{L};\quad \theta_g = \frac{T_g - T_{g,in}}{\Delta T_{ad}};\quad \theta_s = \frac{T_s - T_{g,in}}{\Delta T_{ad}};\ \theta_{g,d} = \frac{2T_{g,in} - T_{g,in}}{\Delta T_{ad}}$$

$$\Omega_g = \frac{\rho_g}{\rho_{g,in}};\quad U = \frac{u}{\varepsilon u_{in}};\quad \gamma_{g,A} = e^{\frac{Ea_{g,A}}{RT_{g,ad}}};\quad \gamma_{g,B} = e^{\frac{Ea_{g,B}}{RT_{g,ad}}}$$

$$\tau_{s/r,g,A} = \frac{\tau_s}{\tau_{r,g,A}} = \frac{L/u_{in}}{\frac{1}{k_{0,g,A}/\varepsilon\, e^{-Ea_{g,A}/RT_{g,ad}}}};\quad \tau_{s/r,g,B} = \frac{\tau_s}{\tau_{r,g,B}} = \frac{L/u_{in}}{\frac{1}{k_{0,g,B}/\varepsilon\, e^{-Ea_{g,B}/RT_{g,ad}}}}$$

$$TR_{g,A} = \frac{1000(-\Delta H_{g,A})}{M_w C_{p,g}\Delta T_{ad}};\quad TR_{g,B} = \frac{1000(-\Delta H_{g,B})}{M_w C_{p,g}\Delta T_{ad}}$$

$$St_s = \frac{ha_p L}{(1-\varepsilon)\rho_s u_{in} C_{p,s}}; \quad St_g = \frac{ha_p L}{\varepsilon \rho_{g,in} u_{in} C_{p,g}}$$

; $$Pe_{h,s} = \frac{(1-\varepsilon)\rho_s u_{in} C_{p,s} L}{D_{e,s}}$$

Equation (2.19) is the mass balance for the gas phase i.e., the one dimensional equation of continuity. Essentially, equation (2.19) implies that the time derivative of density is negligible and hence the product of local density and local linear velocity (i.e., local mass flux) remains constant. This is a good approximation since the time scale of operation is very large, due to high $\frac{\rho_s c_{p,s}(1-\varepsilon)}{\rho_g c_{p,g}}$, compared to the time scale of change in density. For example, for a process which is carried on for 15,000 seconds and experiences a five fold density change (which is very high), the order of $\frac{\partial \Omega_g}{\partial \tau}$ is 10^{-5}. Since the inlet mass flux is known, and local density can be calculated by using ideal gas law (or an appropriate equation of state which is simultaneously solved with energy and species balances), local velocity is calculated as $U = \frac{\Omega_{g,in} U_{in}}{\Omega}$.

The gas and solid Stanton numbers and the heat transfer Peclet number $Pe_{h,s}$ are defined in the same manner as in the case of the heat regenerator without reaction. Thus, the higher the St_S, St_g, $Pe_{h,s}$ are, the steeper the temperature fronts in the system. The dimensionless quantity U is a constant equal to $1/\varepsilon$ for incompressible gases, and varies with the gas temperature for compressible gases. The deviation of U from $1/\varepsilon$ indicates the variation in the linear velocity of the gas due to its compressible nature. The dimensionless number $\tau_{S/r}$ is the ratio of the space time to the characteristic reaction time (subscripts 1 and 2 refer to the reaction number). Thus $\tau_{S/r}$ is a Damkohler number for first order reaction and indicates the extent of

conversion in the fixed-bed reactor. If $\tau_{s/r}$ <<1, the conversion in the reactor is negligible and the concentration fronts are flat. If $\tau_{s/r}$ >>1, nearly complete conversion (or thermodynamic equilibrium for reversible reactions) is achieved in the reactor and the concentration and reaction fronts are very steep. The dimensionless group TR_g (subscripts 1 and 2 refer to the reaction number) is a measure of the ratio of the enthalpy change caused by reaction to the gas heat capacity. Thus, it indicates the extent of the temperature change in the gas phase due to reaction. If the reaction involved has a very high heat of reaction and occurs in the gas phase which has a low heat capacity, the temperature change in the gas phase due to heat generated by the reaction is very high. Thus, a system having high Stanton numbers (St_g and St_s), and high TR_g and $Pe_{h,s}$ involves steep temperature fronts, and a system having high $\tau_{s/r}$ involves also steep concentration and reaction fronts.

Clearly, the above model is only an approximation of the physical reality. In the system discussed temperature variations of 1000s of degrees are expected. Over such a large temperature range it is unlikely that a reaction would obey the same order, or that other reactions will remain unimportant or that activation energies and heats of reactions as well as other parameters such as specific heats, heat transfer coefficients etc. can be assumed constants. While rigorous modeling of all of these quantities, including modeling of radiation heat transfer, would be needed for precise estimation of reactor performance, the model presented here is adequate for evaluation of the key features of the system. Since this type of system has not been examined before, the current model is adequate as a learning tool.

2.5.2.2 Semi-Analytical Tool for the Reaction Problem—Front velocity

The transient temperature and reaction fronts in a fixed-bed reactor spread while moving due to the finite heat transfer coefficient between the gas and solids and

due to mass and heat dispersion phenomena. Hence, the assumption of the existence of a constant front velocity is only an approximation. However, assuming such a constant front velocity and the gas to be incompressible, it is possible to analytically find an approximate expression for the approximate rate of the front movement in infinitely long catalytic packed beds (Rhee et al., 1973). We extend this treatment to homogeneous reactions occurring in a packed bed regenerator. A single homogeneous first order reaction is assumed to occur in the gas phase, but the treatment illustrated here remains the same for all types of kinetics. The axial heat dispersion and the radial temperature gradients in the solid phase are neglected. The following model is used for the analysis of the front velocity.

$$\frac{\partial \theta_g}{\partial \tau} = -\frac{1}{\varepsilon}\frac{\partial \theta_g}{\partial z} + \tau_{s/r,g} TR_{g,\gamma_g}\left(\frac{1-\theta_g}{\theta_g+\theta_{g,d}}\right) y_A - St_g(\theta_g - \theta_s) \tag{2.20}$$

$$\frac{\partial \theta_s}{\partial \tau} = St_s(\theta_g - \theta_s) \tag{2.21}$$

$$\frac{\partial y_A}{\partial \tau} = -\frac{1}{\varepsilon}\frac{\partial y_A}{\partial z} - \tau_{s/r,g}\gamma_g\left(\frac{1-\theta_g}{\theta_g+\theta_{g,d}}\right) y_A \tag{2.22}$$

Boundary conditions:

$@\, z = 0$

$\theta_g = \theta_{g,in};\ \ y_A = y_{A,in}$

Initial Conditions:

$@\, t = 0$ and $0 \le z \le 1$

$\theta_g = \theta_{g,0};\quad \theta_s = \theta_{s,0};\quad y_A = y_{A,0}$

The gas heat capacity and the heat transfer coefficient between the gas and the solids are assumed to be constant and the gas to be incompressible. If the dimensionless front

velocity is $V_r = \frac{\omega_r}{u}$ and the length of the fixed-bed reactor is infinite, by using $\xi = z - V_r \tau$, equations (2.20) to (2.22) can be written as follows

$$-V_r \frac{\partial \theta_g}{\partial \xi} = -\frac{1}{\varepsilon}\frac{\partial \theta_g}{\partial \xi} + \tau_{s/r,g} TR_g \gamma_g^{\left(\frac{1-\theta_g}{\theta_g+\theta_{g,d}}\right)} y_A - St_g(\theta_g - \theta_s) \tag{2.23}$$

$$-V_r \frac{\partial \theta_s}{\partial \xi} = St_s(\theta_g - \theta_s) \tag{2.24}$$

$$-V_r \frac{\partial y_A}{\partial \xi} = -\frac{1}{\varepsilon}\frac{\partial y_A}{\partial \xi} - \tau_{s/r,g} \gamma_g^{\left(\frac{1-\theta_g}{\theta_g+\theta_{g,d}}\right)} y_A \tag{2.25}$$

with

$@\, z = -\infty$

$\theta_g = \theta_{g,in}; \quad \theta_s = \theta_{g,in}; \quad y_A = y_{A,in}$

$@\, z = \infty$

$\theta_g = \theta_{g,mx}; \quad \theta_s = \theta_{g,mx}; \quad y_A = y_{A,eq}$

Eliminating source terms $\tau_{s/r,g} TR_g \gamma_g^{\left(\frac{1-\theta_g}{\theta_g+\theta_{g,d}}\right)} y_A$, $\tau_{s/r,g} \gamma_g^{\left(\frac{1-\theta_g}{\theta_g+\theta_{g,d}}\right)} y_A$, and $(\theta_g - \theta_s)$ from equations (2.23) to (2.25) we get

$$V_r\left(St_s \frac{d\theta_g}{d\xi} + St_g \frac{d\theta_s}{d\xi} + St_s TR_g \frac{dy_A}{d\xi}\right) = \frac{St_s}{\varepsilon}\frac{d\theta_g}{d\xi} + \frac{St_s TR_g}{\varepsilon}\frac{dy_A}{d\xi} \tag{2.26}$$

Integrating equation (2.26) from -∞ to ∞ and rearranging we get

$$V_r = \frac{1}{\varepsilon}\frac{1}{1 + \frac{St_g \Delta\theta_{mx}}{St_s \Delta\theta_{mx} + St_s TR_g \Delta y_{A,mx}}}$$

$$= \frac{1}{\varepsilon} \frac{1}{1 + \dfrac{\dfrac{\Delta T_{mx}}{\varepsilon \rho_g C_{p,g}}}{\dfrac{\Delta T_{mx}}{(1-\varepsilon)\rho_s C_{p,s}} + \dfrac{1000\left(-\Delta H_g\right)\Delta y_{A,mx}}{(1-\varepsilon) M_w \rho_s C_{p,s} C_{p,g}}}} \qquad (2.27)$$

In the above development the difference between the gas and bed temperatures is ignored. Thus θ and T refer to generic dimensionless and dimensional temperatures, respectively. Δ indicates the maximum change in the variable.

For a typical system under consideration, an order of magnitude estimate of the variables in equation (2.27) yields:

$\Delta T_{mx} \approx 10^2$ or 10^3 K; $M_w \approx 10^2$ g / mole; $\rho_g \approx 10^0$ kg / m^3; $\rho_s \approx 10^3$ kg / m^3,
$C_{p,g} \approx C_{p,s} \approx 10^3$ J / (kg.K); $\Delta H \approx 10^5$ or 10^6 J / mol

Thus, $\dfrac{\Delta T_{mx}}{(1-\varepsilon)\rho_s C_{p,s}} + \dfrac{1000\left(-\Delta H_g\right)\Delta y_{A,mx}}{(1-\varepsilon) M_w \rho_s C_{p,s} C_{p,g}}$ is of the order 10^{-3} to 10^{-2} and

$$\frac{\dfrac{\Delta T_{mx}}{\varepsilon \rho_g C_{p,g}}}{\dfrac{\Delta T_{mx}}{(1-\varepsilon)\rho_s C_{p,s}} + \dfrac{1000\left(-\Delta H_g\right)\Delta y_{A,mx}}{(1-\varepsilon) M_w \rho_s C_{p,s} C_{p,g}}} \approx 10^2 \text{ to } 10^3 >> 1$$

Therefore equation (2.27) can be rewritten as

$$V_r = \frac{\rho_g C_{p,g}}{(1-\varepsilon)\rho_s C_{p,s}} + \frac{1000\left(-\Delta H_g\right)\Delta y_{A,mx} \rho_g}{(1-\varepsilon)\Delta T_{mx} M_w \rho_s C_{p,s}} \qquad (2.28)$$

using the adiabatic energy balance to eliminate the heat of reaction $\left(-\Delta H_g\right) = \frac{C_{p,g} M_w \Delta T_{ad}}{1000\left(-\Delta y_{A,mx}\right)}$, equation (2.28) can be condensed to the following form:

$$V_r = \frac{\rho_g C_{p,g}}{(1-\varepsilon)\rho_s C_{p,s}}\left(1 - \frac{\Delta T_{ad}}{\Delta T_{mx}}\right) \tag{2.29}$$

In dimensional form the front velocity is:

$$\omega_r = \frac{u\rho_g C_{p,g}}{(1-\varepsilon)\rho_s C_{p,s}}\left(1 - \frac{\Delta T_{ad}}{\Delta T_{mx}}\right) = \omega\left(1 - \frac{\Delta T_{ad}}{\Delta T_{mx}}\right) \tag{2.30}$$

where ΔT_{mx} has to be numerically estimated using approximate equations (Nieken et al., 1995). The procedure is quite elaborate. Hence, in this thesis we use direct numerical simulation for accurate computation of ΔT_{mx}.

Thus, the temperature front velocity in a fixed-bed with reaction is always smaller than the front velocity in the same bed without reaction and is dependent on the ratio of the gas adiabatic temperature rise caused by reaction and the maximum change in the temperature in the bed. A similar expression for the front velocity was obtained by Rhee et al. (1973) for catalytic processes by using a cell model. Thus, the front velocity in a fixed-bed reactor does not change with reaction kinetics or phase in which reaction occurs. It is thermodynamically defined.

This expression for front velocity is compared to the actual front velocity for an exothermic reaction computed by the developed algorithm in this Chapter. Chapter 4 discusses the front velocity for both exothermic and endothermic reactions.

2.5.2.3 Simulation of a Fixed-bed Reactor—Single Pass

The developed temporally and spatially adaptive algorithm is used to solve Equations (2.15) to (2.19). Reactions with Arrhenius frequency factors of the order of 10^5 s^{-1}, activation energies and heats of reactions of the order of 10^5 J/mol were simulated on a DEC ALPHA 3000/600 desktop workstation. The parameters used for simulation are listed in Table 2.1. Although model equations are derived for the temperature dependent physical properties of the gas, gas heat capacity and heat transfer coefficient are assumed to be constant in this computation.

The simulation results for a fixed-bed reactor subject to a single exothermic reaction are shown in Figures 2.9 and 2.10. The adiabatic temperature rise for this system is 714.3 K and the observed maximum temperature is around 2400 K. The maximum temperature rise in the system (1700 K) is always higher than the adiabatic temperature rise due to the heat provided by the solids in the bed. The front velocity calculated using the model equations and the developed algorithm is 1.900×10^{-4} m/s while equation (2.30), based on inlet gas properties, predicts 1.884×10^{-4} m/s. This is a good agreement (relative percentage difference = 1.06) considering that there is a four fold temperature change in the system and that the approximate analytical expression for the front velocity was based on the assumption that the gas was incompressible.

Figures 2.11 and 2.12 depict the temperature and concentration fronts when only an endothermic reaction occurs in the initially hot packed bed. Initially the gas is heated to the temperature where the reaction rates are moderate. As the reaction occurs in the bed, the gases are cooled due to the endothermic reaction. As time passes by, the bed is further cooled and the conversion along the fixed-bed reactor decreases (concentration of the reactant along the bed increases). A comparison of the theoretically estimated front velocity with the numerically computed front velocity for an endothermic reaction is discussed in Chapter 4.

2.5.2.4 Simulation of Direct Coupling of an Exothermic and Endothermic Reaction—Periodic Operation

In complex kinetics involving several species both endothermic and exothermic reactions can occur simultaneously. A simple case of such a system would be two first order reactions—one endothermic and one exothermic, occurring simultaneously at a comparable rate. If the adiabatic temperature rise of the mixture is greater than zero, a temperature front with a hot spot higher than the initial bed temperature develops in the fixed-bed reactor as shown in Figures 2.13 and 2.14. Parameters used in the simulation are listed in Table 2.1. For the exothermic reaction $k_{0,1}$ was 1×10^{5} s^{-1} , *Ea* was 1×10^{5} J/mol and ΔH_1 was -2.0×10^{5} J/mol. Initially the temperature in the bed is low, hence the rates of both reactions are low and conversion is low. However, as time proceeds, the reaction mixture effectively generates heat in the bed and the gases get heated up which in turn increases the rate of reaction. Therefore, the temperature and concentration fronts similar to those exhibited by a single exothermic reaction are established, as illustrated by Figure 2.13 for the temperature and by Figure 2.14 for the concentration. A hot spot migrates down the bed (Figure 2.13) and steep concentration fronts (Figure 2.14) move down the bed. These two figures are quite similar to figures 2.9 and 2.10 for a single exothermic reaction.

A reverse process could be operated so that the source of heat is an exothermic reaction which occurs simultaneously with the desired endothermic reaction. When the two reactions occur with a comparable rate, and if the adiabatic temperature rise of the mixture is greater than zero, a temperature front with a hot spot higher than the initial bed temperature (Figures 2.13 and 2.14) develops in the fixed-bed reactor. The parameters used in the simulation are listed in Table 2.1. However, if such a single blow process is carried on for a long time, the temperature and concentration fronts

eventually exit the fixed-bed and the yield approaches zero. It is, therefore necessary to maintain the temperature and reaction fronts in the reactor. This can be accomplished by switching the direction of the flow of the feed gases before the hot spot moves out of the bed. Now the incoming cold reactive gases encounter the hotter part of the bed (Figure 2.15) where they react and move towards the exit which is at a lower temperature. Thus, an inverted U shaped temperature profile now traverses the whole bed as shown in Figure 2.15. Since the gases encounter a high temperature region in the reactor, the conversion in the reaction is always complete as shown in Figure 2.16. The next flow reversal is accomplished when the temperature front starts moving out of the bed. After the seventh semi-cycle, the temperature and concentration fronts in the

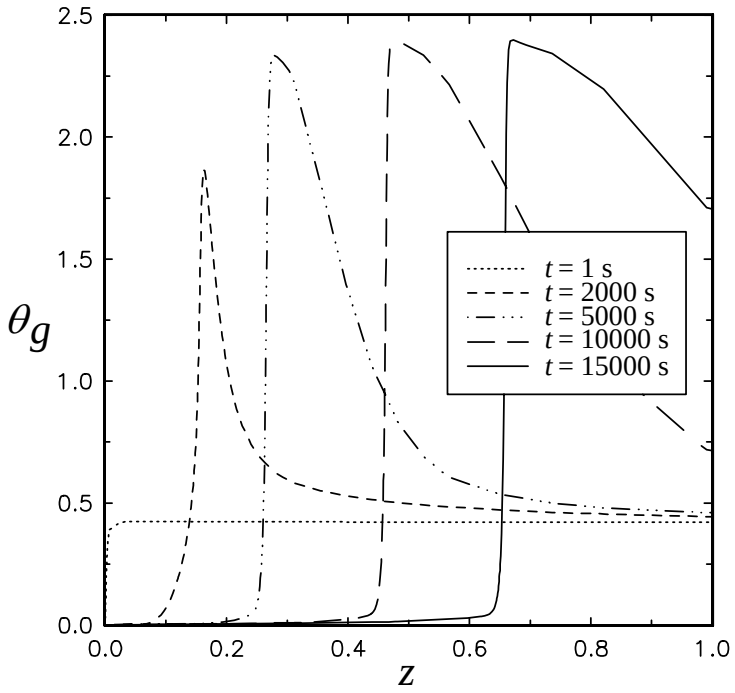

Figure 2.9. Axial gas temperature profiles in a fixed-bed reactor with an exothermic reaction (Temperature range 700-2400 K).

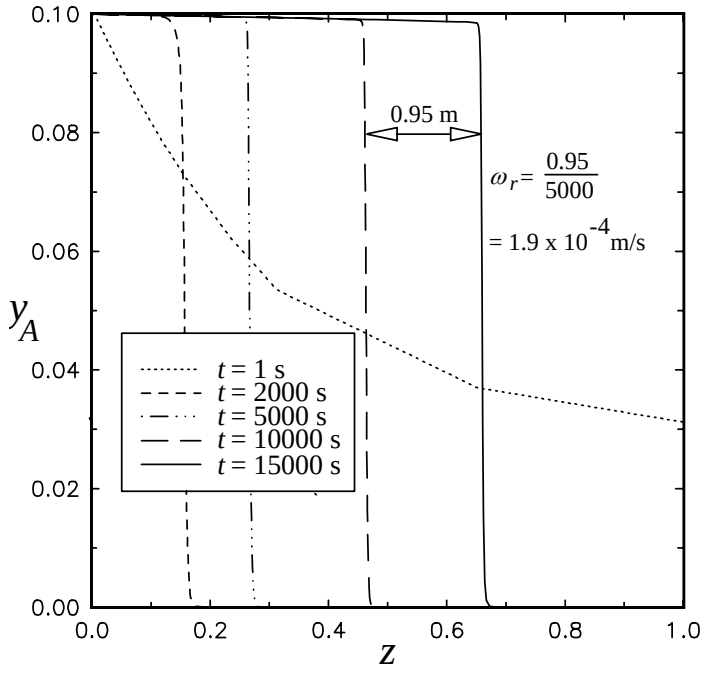

Figure 2.10. Axial concentration profiles in a fixed-bed reactor with an exothermic reaction.

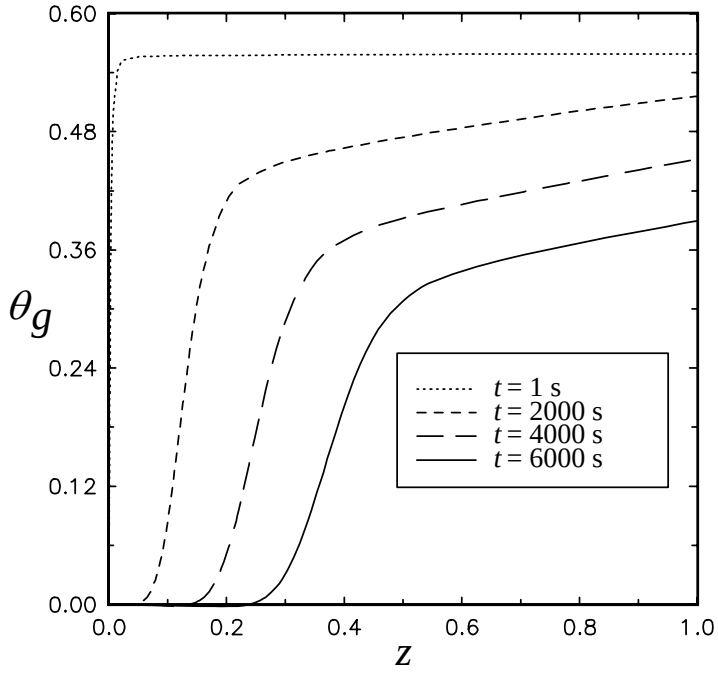

Figure 2.11. Axial temperature profiles in a fixed-bed reactor with an endothermic reaction.

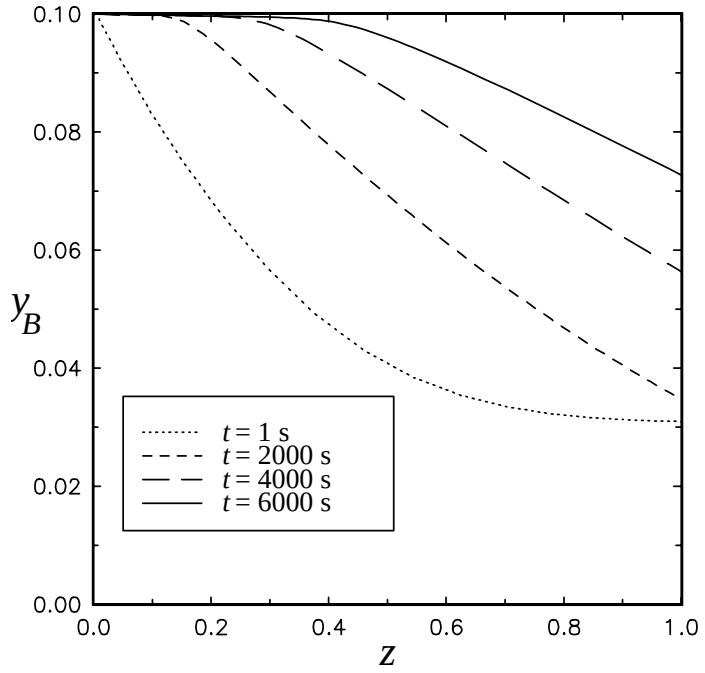

Figure 2.12. Axial concentration profiles in a fixed-bed reactor with an endothermic reaction.

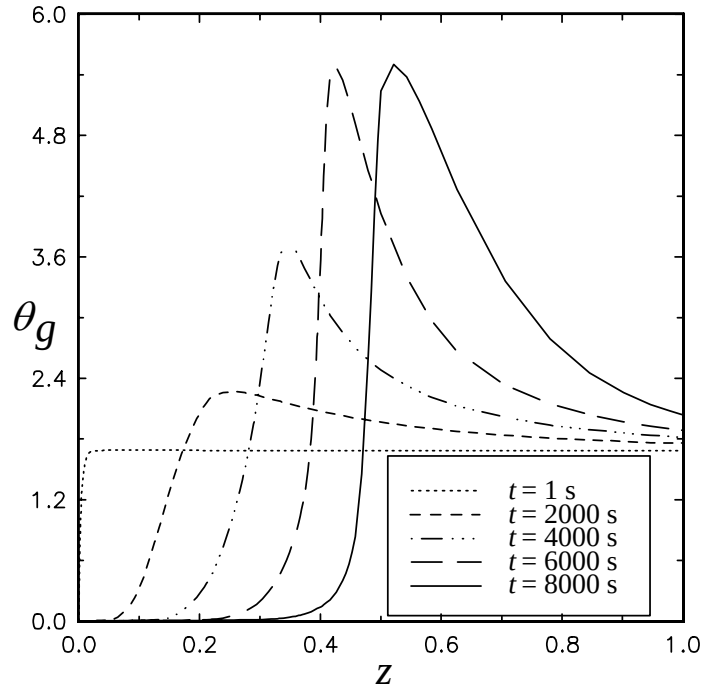

Figure 2.13. Axial temperature profiles in a fixed-bed reactor with both endothermic and exothermic reactions.

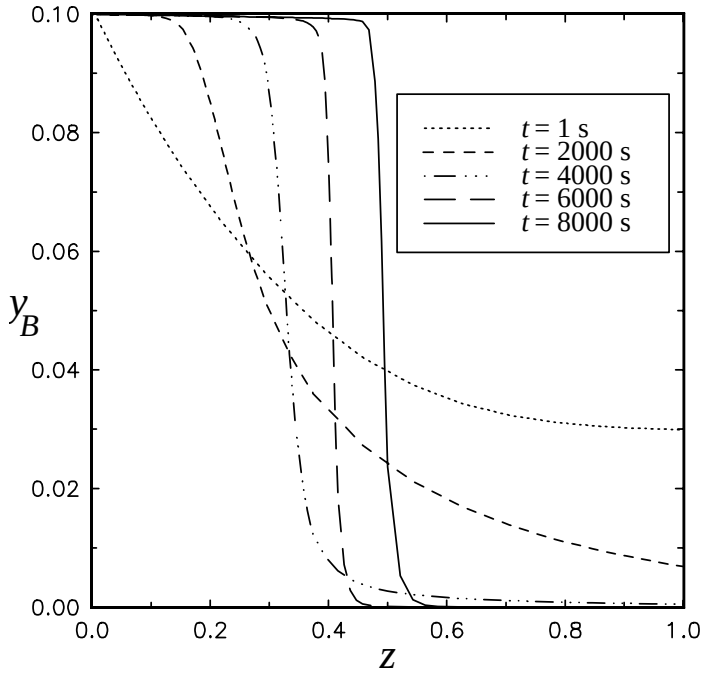

Figure 2.14. Axial concentration profiles in a fixed-bed reactor with both endothermic and exothermic reactions.

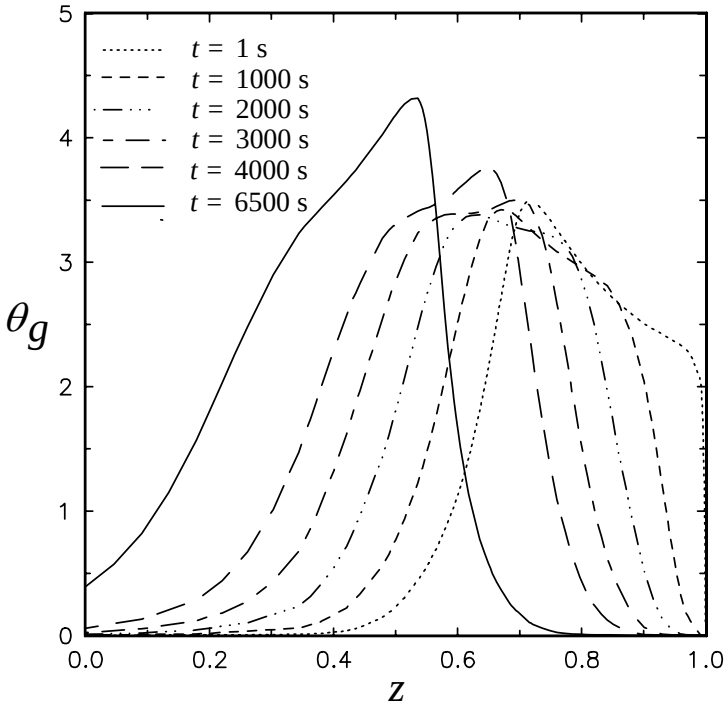

Figure 2.15. Axial temperature fronts in the fixed-bed during the second semi-cycle (endothermic + exothermic reactions).

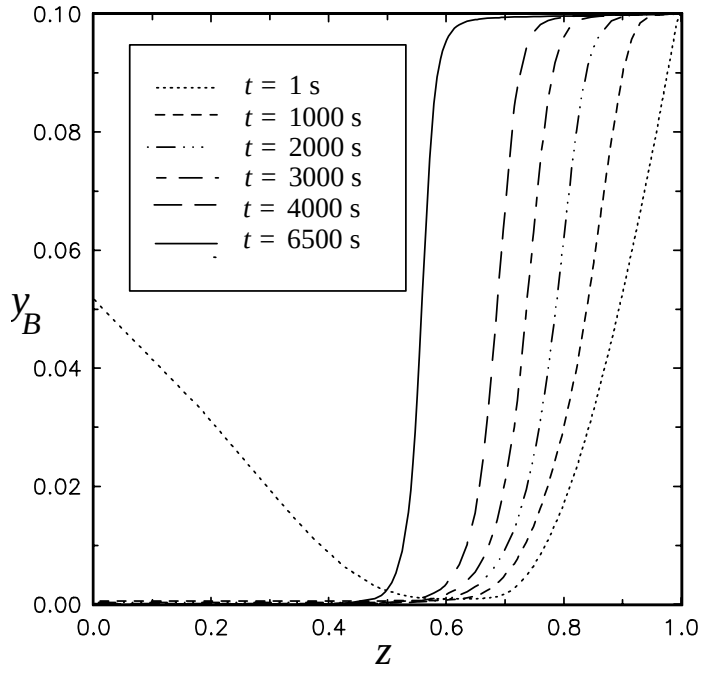

Figure 2.16. Axial concentration fronts of the key reactant in the fixed-bed during the second semi-cycle (endothermic+exothermic reactions).

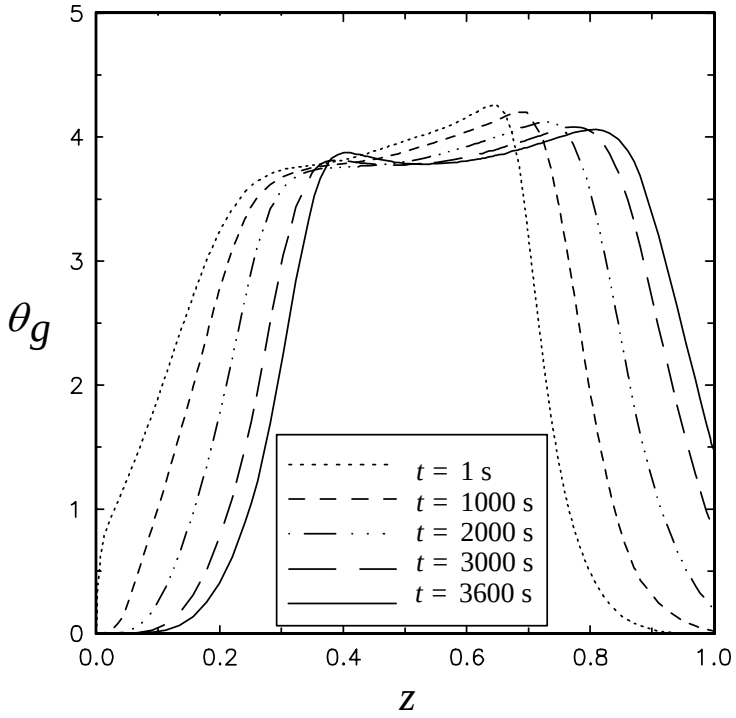

Figure 2.17. Axial temperature fronts in the fixed-bed during the seventh semi-cycle (endothermic + exothermic reactions).

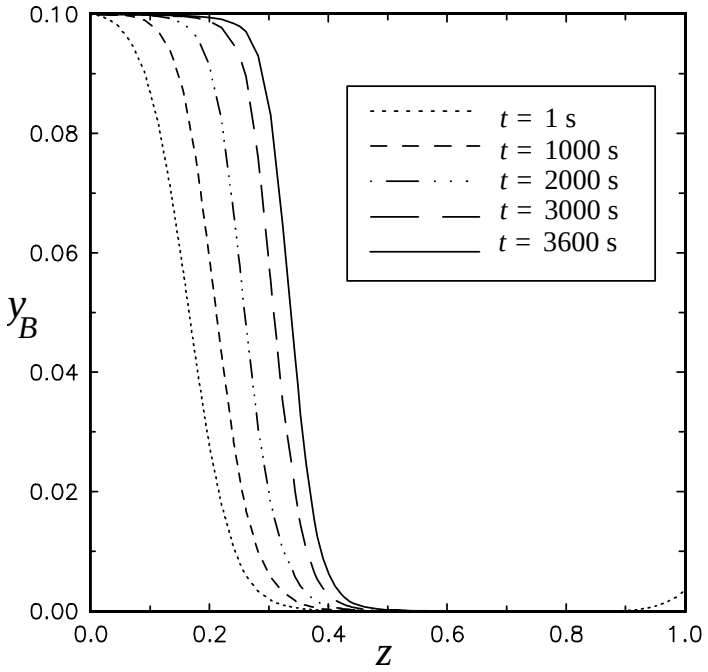

Figure 2.18. Axial concentration fronts of the key reactant in the fixed-bed during the seventh semi-cycle (endothermic+exothermic reactions).

fixed-bed are as shown in Figures 2.17 and 2.18. The conversion of the reactant undergoing the endothermic reaction is complete and the exit gases are cold.

The model used to simulate the above discussed bi-directional fixed-bed reactor is given by equations (2.15) to (2.19) which is also used in the simulation of the discussed single blow process. However, in the case of a bi-directional fixed-bed, for each switch in the semi-cycle, following modifications are required.

$$\begin{aligned} y_{N+1-i,even} &= y_{i,odd} \ldots\ldots i = 1,\ldots N \\ u_{N+1-i,even} &= u_{i,odd} \ldots\ldots i = 1,\ldots N \\ x_{N+1-i,even} &= L - x_{i,odd} \ldots\ldots i = 1,\ldots N \end{aligned} \tag{2.20}$$

where y is a scalar variable (temperature, concentration etc.) and u is the gas velocity.

The flow reversal process provides the necessary heat required to drive the endothermic reaction. In addition, the shape of the temperature profiles established in the fixed-bed reactor have distinct advantage for the processes where immediate

cooling of the product is required as in the case of thermal NO production. In thermal NO production, it is necessary to cool the product gases immediately after the reaction to freeze the yield of NO. In this case the reaction occurs in the high temperature region in the fixed-bed and the immediate cooling is accomplished in the part of the bed where temperatures are low. Thus, the product gases exit at low temperature.

2.6 A Note on Discretization

As discussed in this chapter implicit finite differences are unconditionally stable and allow larger step sizes without generating numerical wiggles. However, for large time-steps, the accuracy of the results decreases. Thus, the temporal accuracy criterion sets time-steps quite small to meet the accuracy criterion. Under such circumstances, for the dynamic fixed-bed reactor processes involving many cycles, a set of implicit equations, resulting from the implicit finite difference discretization, has to be repeatedly solved. Hence, the computational time can be very long even for the adaptive numerical algorithm developed in this chapter. In this section a few formulations that can be used to avoid solution of a large number of implicit equations are discussed.

2.6.1 Linear Convective Equations

Consider the following linear equation;

$$\frac{\partial y}{\partial t} = \kappa_1 \frac{\partial y}{\partial z} + \kappa_2 y \qquad (2.21)$$

$$@t = 0, \quad y = y_{in}; \; @z = 0, \quad y = y_0$$

Using implicit Euler's scheme and backward differences this equation can be discretized and the difference equation manipulated to yield an explicit equation as shown below.

$$\frac{y_i^{n+1}-y_i^n}{\Delta t}=\kappa_1\frac{y_{i-1}^{n+1}-y_i^{n+1}}{\Delta x}+\kappa_2 y_i^{n+1}$$

$$\Rightarrow y_i^{n+1}=\frac{y_i^n+\frac{\Delta t}{\Delta x}\left(\kappa_1 y_{i-1}^{n+1}\right)}{1+\kappa_1\frac{\Delta t}{\Delta x}+\kappa_2\Delta t} \tag{2.22}$$

$$\Rightarrow y_i^{n+1}=f(y_i^n,y_{i-1}^{n+1}) \tag{2.23}$$

Equation (2.23) is an explicit equation because at time t=0, y_i^n is given by the initial condition and y_{i-1}^{n+1} is given by the boundary condition (Figure 2.19). Thus, explicit marching in spatial as well as temporal direction is possible even for this completely implicit unconditionally stable formulation.

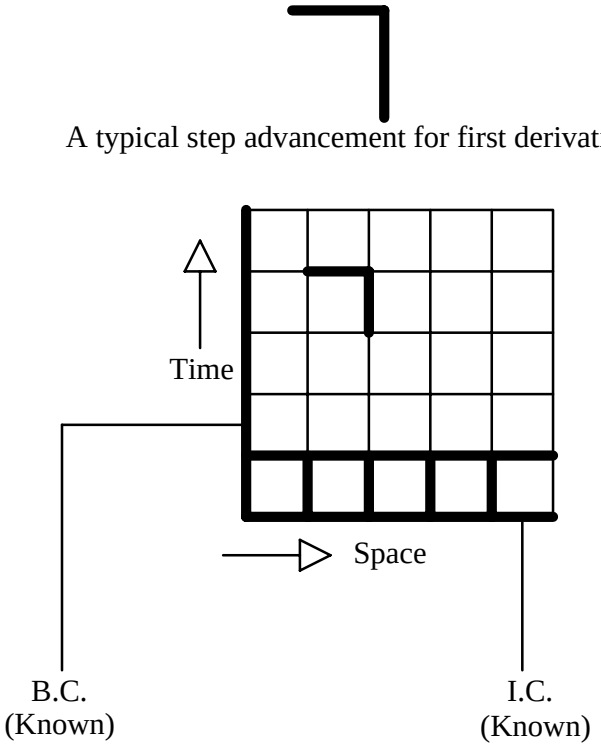

Figure 2.19. A graphical explanation for solution of equations (2.21) and (2.24).

2.6.2 Nonlinear Convective Equations

Consider the following nonlinear equation;

$$\frac{\partial y}{\partial t} = \kappa_1 \frac{\partial y}{\partial z} + F(y) \qquad (2.24)$$

$@t = 0, \quad y = y_{in}; \; @z = 0, \quad y = y_0$ where $F(y)$ is a nonlinear function.

Again using the implicit Euler's scheme and backward differences this equation can be discretized to result in explicit equations as shown below (Figure 2.19). The formulation is again unconditionally stable.

$$\frac{y_i^{n+1}-y_i^n}{\Delta t}=\kappa_1\frac{y_{i-1}^{n+1}-y_i^{n+1}}{\Delta x}+F\left(y_{i-1}^{n+1}\right)$$

$$\Rightarrow y_i^{n+1}=\frac{y_i^n+\frac{\Delta t}{\Delta x}\left(\kappa_1 y_{i-1}^{n+1}\right)+F\left(y_{i-1}^{n+1}\right)\Delta t}{1+\kappa_1\frac{\Delta t}{\Delta x}} \tag{2.25}$$

$$\Rightarrow y_i^{n+1}=f(y_i^n,y_{i-1}^{n+1}) \tag{2.26}$$

Equation (2.26) is an explicit equation. Thus, for this completely implicit formulation explicit temporal and spatial marching is possible (Figure 2.19).

2.6.3 Linear or Nonlinear Diffusion-Convection Equations

Consider the following nonlinear equation;

$$\frac{\partial y}{\partial t}=\kappa_2\frac{\partial^2 y}{\partial z^2}+\kappa_1\frac{\partial y}{\partial z}+F(y) \tag{2.27}$$

with given boundary and initial conditions where $F(y)$ is a nonlinear function.

With formulations discussed in sections 2.6.1 and 2.6.2 the nonlinear term $F(y)$ and the convective term can be discretized. However, the second order term of equation (2.27) has now to be formulated explicitly for explicit time and space step marching as illustrated below:

$$\frac{y_i^{n+1}-y_i^n}{\Delta t}=\kappa_2\frac{y_{i+1}^n-2y_i^n+y_{i-1}^n}{\Delta x^2}+\kappa_1\frac{y_{i-1}^{n+1}-y_i^{n+1}}{\Delta x}+F\left(y_{i-1}^{n+1}\right)$$

$$\Rightarrow y_i^{n+1}=\frac{y_i^n+\frac{\Delta t}{\Delta x}\left(\kappa_1 y_{i-1}^{n+1}\right)+F\left(y_{i-1}^{n+1}\right)\Delta t+\kappa_2\frac{\Delta t}{\Delta x^2}\left(y_{i+1}^n-2y_i^n+y_{i-1}^n\right)}{1+\kappa_1\frac{\Delta t}{\Delta x}} \tag{2.28}$$

$$\Rightarrow y_i^{n+1}=f(y_{i-1}^n,y_i^n,y_{i+1}^n,y_{i-1}^{n+1}) \tag{2.29}$$

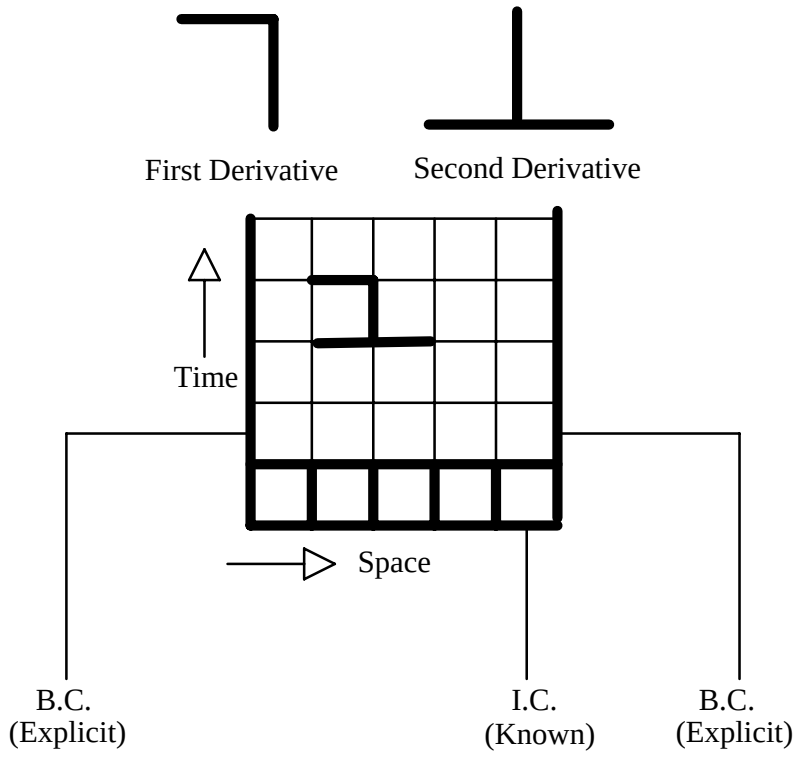

Figure 2.20 A graphical explanation for solution of equation (2.27).

Equation (2.29) is an explicit equation and thus using this formulation explicit marching in temporal and spatial direction is possible (Figure 2.20). However, the formulation is now not unconditionally stable because the second order terms are approximated using an explicit formulation. This imposes an additional stability criterion which needs to be satisfied along with the temporal and spatial adaptation criteria. Therefore caution must be exercised when using this formulation.

2.7 Conclusions

The developed completely implicit temporally and spatially adaptive algorithm works better than algorithms based on the polynomial approximation on finite elements for fixed-bed reactors involving reaction, heat transfer and steep moving

fronts. Linear approximation works better than higher order polynomial approximations for steep fronts having high second order derivatives. Finite difference approximations of the first order are more robust and accurate than higher order polynomial or higher order finite difference approximations especially in the region of high second derivatives where higher order differences are not very accurate. Although steepness of the front is measured by the magnitude of the first derivative, to capture the front accurately, a greater number of nodes must be placed in the region of the highest magnitude of second derivatives. By placing the greatest number of nodes in the region of high second derivatives, the second derivative control minimizes the numerical dispersion and, hence, captures the steepness of the front better than the first derivative control which places the nodes in the steeper regions of the front where the front can be readily approximated by linear functions. For grid adaptation linear interpolation is preferred over higher order interpolation. The physics of the problem is incorporated by employing the chosen characteristic-time limited time step control along with the first derivative control for the time step management. The temporal and spatial adaptation are coupled to give more accurate results. An optional intelligent trade off between accuracy and computer time is achieved by a variable space and time tolerance scheme which automatically varies the spatial and temporal tolerances if the finite difference system becomes too big for the computer to handle in a reasonable amount of time.

For a system of equations involving only convective terms, an implicit discretization using backward differences (section 2.6) can lead to a system of unconditionally stable explicit equations which allows explicit marching in spatial as well as temporal directions. A combination of explicit-implicit discretization for the diffusion-convection equations results in a conditionally stable system of explicit

equations which can allow larger time steps than only the explicit discretization can allow.

The developed adaptive algorithm is applicable to various types of linear and nonlinear problems for the fixed-bed reactor involving steep and steep moving fronts as illustrated by examples presented above.

Table 2.1: The Parameters Used in the Simulation of Various Processes.

Parameter	Equations (2.9) to (2.10)	Equations (2.12) to (2.14)	Equations (2.15) to (2.19) (only A→ C)	Equations (2.15) to (2.19) (only B→ D)	Equations (2.15) to (2.19) (A→C, B→ D)
$T_{g,in}$ (K)	1500	1500	700	700	700
$T_{g,0}$ (K)	300	300	1000	1000	1000
$T_{s,0}$ (K)	300	300	1000	1000	1000
$y_{A,in}$	-	-	0.1	-	0.1
$y_{A,0}$	-	-	variable	-	variable
$y_{B,in}$	-	-	-	0.1	0.1
$y_{B,0}$	-	-	-	variable	variable
$k_{0,A}$ (s^{-1})	-	-	1.0×10^{5}	-	1.0×10^{5}
$k_{0,B}$ (s^{-1})	-	-	-	1.0×10^{5}	1.0×10^{5}
$Ea_{g,A}$ (J/mol)	-	-	1.0×10^{5}	-	1.0×10^{5}
$Ea_{g,B}$ (J/mol)	-	-	-	1.0×10^{5}	1.0×10^{5}
$\Delta H_{g,A}$ (J/mol)	-	-	-2.0×10^{5}	-	-2.0×10^{5}
$\Delta H_{g,B}$ (J/mol)	-	-	-	1.5×10^{5}	1.5×10^{5}
h ($J/m^2.K.s$)	500	100	150	100	100
$C_{p,g}$ (J/kg.K)	1000	1000	1000	1000	1000
$C_{p,s}$ (J/kg.K)	1000	1000	1000	1000	1000
ρ_s (kg/m^3)	3000	3000	3000	3000	3000
a_p (m^2/m^3)	1500	300	300	300	300
u_{in} (m/s)	1	1	1	1	1
P (Pa)	1.013×10^{5}	1.013×10^{5}	1.013×10^{5}	1.013×10^{5}	1.013×10^{5}
L (m)	5	5	5	5	5
ε	0.5	0.5	0.5	0.5	0.5
M_w	28	28	28	28	28
$D_{e,s}$ (J/m.K.s)	-	0	0	0	0

3. THE WRONG-WAY BEHAVIOR OF FIXED-BED REACTORS

Volumetric thermal capacity of solids is higher than that of gases by three orders of magnitude. We show that this leads to a dynamic response of a fixed-bed reactor involving a solid phase reaction which is sluggish compared to that involving a gas phase reaction of the same kinetic and thermodynamic parameters. In the *dynamic regime*, where the inlet gas temperature is lower than the initial bed temperature, fixed-bed reactors exhibit the *wrong-way behavior*. We show that in this regime, the transient maximum temperature rise and the steepness of the temperature front are affected by the phase in which reaction occurs, by the inlet gas temperature and by the volumetric heat transfer coefficient. The maximum temperature rise in the bed is lower for the solid phase reaction and decreases with a decrease in the volumetric heat transfer coefficient. These and other new findings are obtained by our newly developed robust, completely implicit, spatially and temporally adaptive numerical algorithm which can capture steep moving fronts in fixed-bed reactors.

3.1 Introduction

In many chemical engineering applications study of moving fronts becomes a necessity. In particular, unsteady state processes occurring in fixed-bed reactors involving heat and mass transfer between solids and gases and reactions in the solid phase and/or in the gas phase involve such moving fronts. Fixed-beds with exothermic reactions in the gas or solid phase can also exhibit steep temperature and concentration profiles. The steepness of these profiles depends on the reaction rate sensitivity to temperature (activation energy), the exothermicity of the reaction (heat of reaction) and the phase in which the reaction takes place. Since the solids have a much larger volumetric heat capacity than the gas phase, and a finite gas-solid heat transfer

resistance is pronounced at high reaction rates, a reaction occurring in the gas phase will lead to much steeper temperature and composition gradients than a reaction (of the same order, same activation energy and heat of reaction) occurring in the solid phase. This is not to say that fast reactions in the solid phase do not produce very steep gradients, but merely to indicate that the same gas phase reaction will result in even steeper ones. Under a certain set of conditions (flow reversal, composition cycling, start-up etc.) these steep fronts will move through the bed (Rhee et al, 1973; Matros, 1989).

The maximum transient temperature rise and the front speed depend upon the phase in which the reaction occurs, on the inlet gas temperature (Il'in and Luss, 1992; Chen and Luss, 1989; Matros, 1989; Pinjala et al, 1988; Mehta et al, 1981; Sharma and Hughes, 1979; Van Doesburg and DeJong, 1976a; Van Doesburg and DeJong, 1976b; and Crider and Foss, 1966) and the rate of heat transfer. Since many chemical reactions take place in a fixed-bed either catalytically (i.e., in the solid phase) or homogeneously in the gas phase, the design of a fixed-bed reactor should also consider the phase in which most of the reaction occurs in addition to the inlet gas temperature. There is a need to understand the effect of the phase in which reaction occurs in a fixed-bed on reactor dynamics since this has not received adequate attention. Since the temperature and concentration fronts involved in highly exothermic reactions are very steep, the robust numerical algorithm which is developed by us (Chapter 2) to capture steep moving fronts encountered in such fixed-bed reactors is used in this study.

3.2 Model Equations: Gas Phase Reaction

First, we consider a packed bed reactor with a highly exothermic reaction occurring in the gas phase. The parametric values used in the computation (Table 3.1) correspond to a typical combustion system. The reaction is:

Exothermic: $A \rightarrow C \qquad \Delta H_{g,A} < 0$……(Gas Phase)

Axial dispersion of heat and mass in the gas as well as solid phase is assumed to be negligible. The assumption of plug flow of gas holds true for long reactors at high gas velocities. The assumption of negligible dispersion in the solid phase holds true for solid packings which allow minimal area of contact between two solid particles. The gas is assumed to be compressible with the total mass flux of gas being constant (Kulkarni, 1992). The rate of conduction within solids is assumed to be very high compared to the convective heat transfer rate between the gas and solids. The physical properties of the gas, including density, are assumed to be temperature dependent. Since the purpose of the study is to compare the thermal response of the bed for gas phase and solid phase reactions, pore diffusion in the solids and external mass transfer resistances between the gas and solids are incorporated into the overall kinetic expression for the reaction occurring in the solid phase. Kinetics is assumed to have an Arrhenius type dependence on the temperature and to be first order. This model should be adequate to establish the effect of the gas velocity, the phase of reaction and of volumetric heat transfer rate on the maximum transient temperature rise which is the focus of this study. The model equations consist of the energy balance for the gas and solid phase, equations (3.1) and (3.2), respectively, reactant *A* mass balance, equation (3.3), and the overall continuity, equation (3.4):

$$\frac{\partial \theta_g}{\partial \tau} = -U \frac{\partial \theta_g}{\partial z} + \tau_{s/r,g,A} TR_{g,A} \gamma_{g,A} e^{\frac{\theta_g}{\theta_g + \theta_{g,d}}} y_A - St_g \frac{1}{\Omega_g} (\theta_g - \theta_s) \qquad (3.1)$$

$$\frac{\partial \theta_s}{\partial \tau} = St_s \left(\frac{\Omega_g}{\theta_g} - \theta_s \right) \tag{3.2}$$

$$\frac{\partial y_A}{\partial \tau} = -U \frac{\partial y_A}{\partial z} - \tau_{s/r,g,A} \gamma_{g,A}^{\frac{1-\theta_g}{\theta_g + \theta_{g,d}}} y_A \tag{3.3}$$

$$\frac{\partial \Omega_g}{\partial \tau} = -\frac{\partial \left(\Omega_g U \right)}{\partial z} = 0 \tag{3.4}$$

The boundary conditions are:
$@ z = 0$

$\theta_g = \theta_{g,in}; \quad y_A = y_{A,in}$

The initial conditions are:
$@ t = 0$ and $0 \le z \le 1$

$\theta_g = \theta_{g,0}; \quad y_A = y_{A,0}$

The dimensionless quantities used above are:

$$\tau = \frac{t}{L / u_{in}}; \quad z = \frac{x}{L}; \quad \theta_g = \frac{T_g - T_{g,in}}{\Delta T_{ad}}; \quad \theta_s = \frac{T_s - T_{g,in}}{\Delta T_{ad}}; \; \theta_{g,d} = \frac{2T_{g,in} - T_{g,in}}{\Delta T_{ad}}$$

$$\Omega_g = \frac{\rho_g}{\rho_{g,in}}; \quad U = \frac{u}{\varepsilon u_{in}}; \quad \gamma_{g,A} = e^{\frac{Ea_{g,A}}{RT_{g,ad}}}; \quad \tau_{s/r,g,A} = \frac{\tau_s}{\tau_{r,g,A}} = \frac{L / u_{in}}{\frac{1}{k_{0,g,A} / \varepsilon \, e^{-Ea_{g,A}/RT_{g,ad}}}}$$

$$TR_{g,A} = \frac{1000 \left(-\Delta H_{g,A} \right)}{M_w C_{p,g} \Delta T_{ad}}; \quad St_s = \frac{ha_p L}{(1-\varepsilon) \rho_s u_{in} C_{p,s}}; \quad St_g = \frac{ha_p L}{\varepsilon \rho_{g,in} u_{in} C_{p,g}}$$

The dimensionless group TR_g is a measure of the ratio of the enthalpy change caused by reaction in the gas phase to the volumetric gas heat capacity. Thus, it indicates the extent of the temperature change in the gas phase due to reaction in the gas phase. If the reaction involved has a very high heat of reaction, the temperature change in the gas phase is very high. The physical significance of the rest of the dimensionless parameters is discussed in Chapter 2. A system having high Stanton

numbers (St_g and St_s), and high TR_g, involves steep temperature fronts, and a system having high $\tau_{s/r}$ involves also steep concentration and reaction fronts.

3.3 The Wrong-way Behavior: Gas Phase Reaction

Equations (3.1-3.4) were solved using the algorithm discussed in Chapter 2 and only the gas phase reaction ($A \rightarrow C$). The evolution of the axial temperature profiles in the fixed-bed reactor in time for inlet gas temperature of 700 K and initial bed temperature of 1000 K are shown in Figure 3.1. The maximum temperature rise is four folds higher than the adiabatic temperature rise. For the inlet gas temperature equal to the initial bed temperature of 1000 K, the axial temperature profiles in the bed are shown in Figure 3.2. In this case, the maximum temperature rise in the bed is equal to the adiabatic temperature rise. Hence, it can be concluded that for any intermediate inlet gas temperature between 700 K and 1000 K, the maximum temperature rise should lie between the maximum temperature rise observed for inlet gas temperature of 700 K and of 1000 K. Figure 3.3 illustrates the maximum temperature rise as a function of the inlet gas temperature and shows that the minimum value of the maximum temperature rise is equal to the adiabatic temperature rise. This phenomenon is known as the *wrong-way behavior* of fixed-bed reactors and has been reported and studied for catalytic fixed-bed reactors with solid phase reactions by Il'in and Luss, 1992; Chen and Luss, 1989: Matros, 1989; Pinjala et al, 1988; Mehta et al, 1981; Sharma and Hughes, 1979; Van Doesburg and DeJong, 1976a; Van Doesburg and DeJong, 1976b; and Crider and Foss, 1966. Here we show it for gas phase reactions.

As illustrated here the maximum temperature rise in the bed is a dynamic property only for the inlet gas temperatures below the initial bed temperature. Figure 3.3 indicates that the operating range for a fixed-bed reactor consists of two regimes: a

thermodynamic regime in which the maximum temperature rise is equal to the adiabatic temperature rise (occurs at gas inlet temperatures equal to or larger than the initial bed temperature) and a *dynamic regime* where the maximum temperature rise depends on the inlet gas temperature (for feed gas temperatures lower than the initial bed

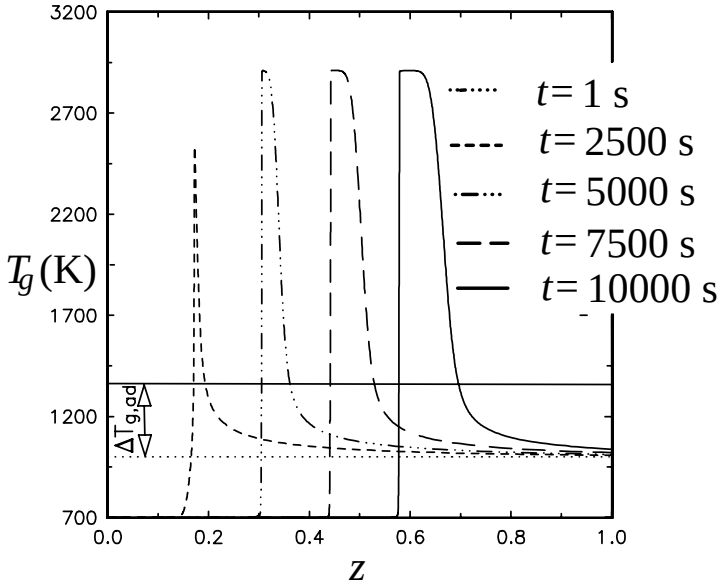

Figure 3.1. The evolution of axial gas temperature profiles for gas phase reaction ($T_{g,in}$=700 K < $T_{s,0}$=1000 K).

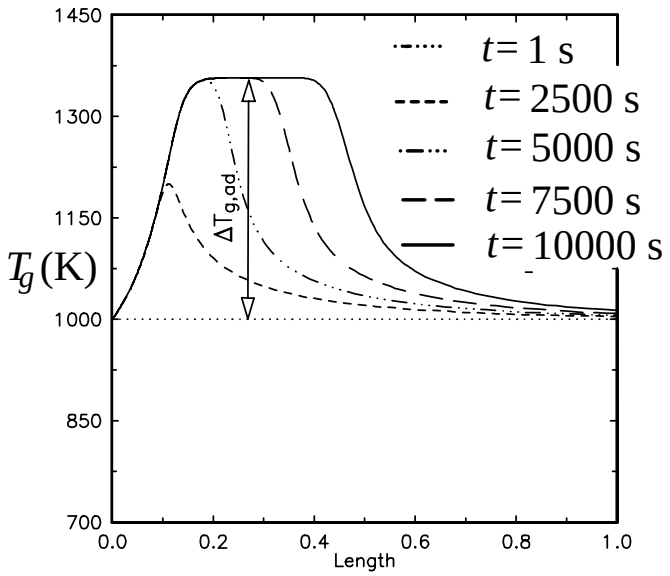

Figure 3.2. The evolution of axial gas phase temperature profiles for gas phase reaction

($T_{g,in}$=$T_{s,0}$=1000 K).

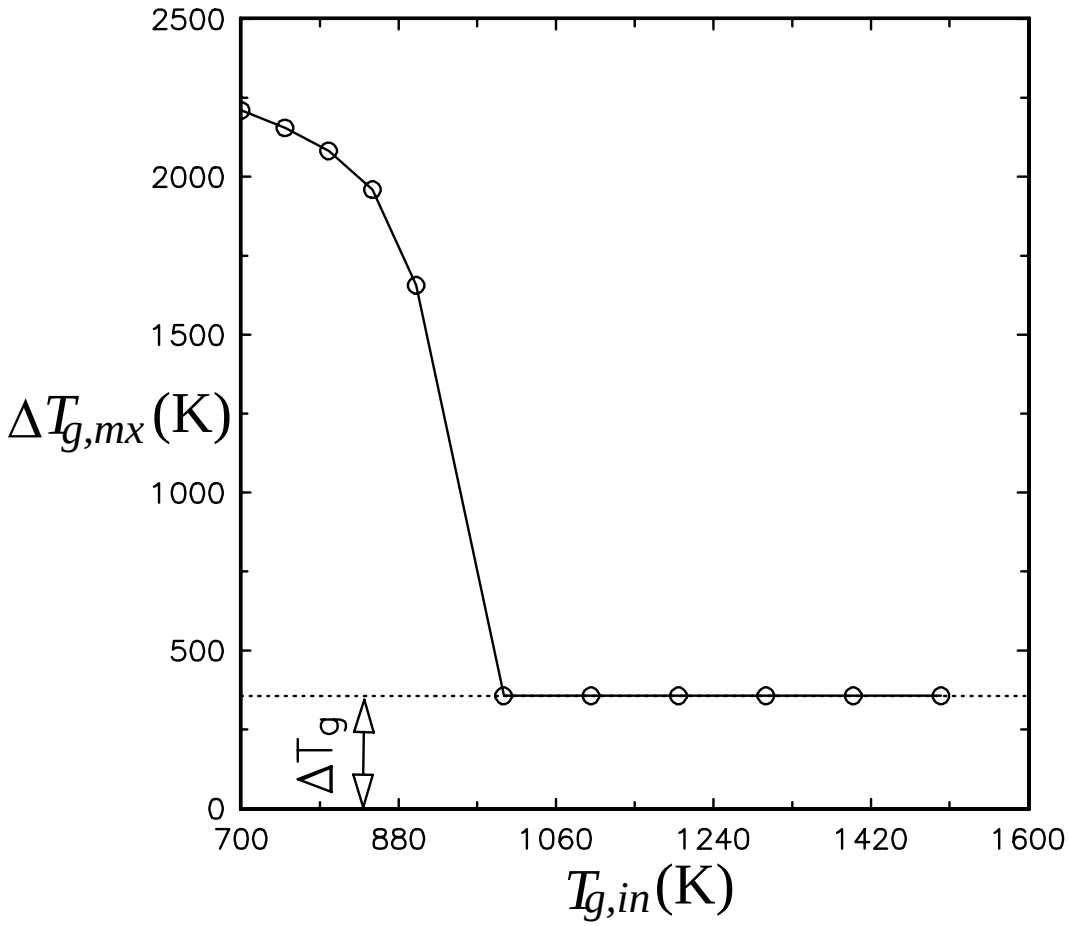

Figure 3.3. The effect of the inlet gas temperature, $T_{g,in}$ on the maximum temperature rise, $\Delta T_{g,mx}$ for the gas phase reaction.

temperature). In the *dynamic regime* a sudden decrease in the feed temperature decreases the conversion in the upstream section of the reactor; consequently, the still hot solids in the down stream section are exposed to higher reactant concentration leading to an increase in heat generation by reaction which increases the transient temperature rise in the bed (Il'in and Luss, 1992). This, of course, can happen only when there is interphase heat transfer—in this case, the gas coming in the bed encounters already hot solids. In the *thermodynamic regime* the incoming gas is already hotter than the inlet solid temperature and hence the maximum temperature rise can not exceed the adiabatic temperature rise.

3.4 The Wrong-way Behavior: The Effect of Heat Transfer Rate

Since the rate of change (steepness of the fronts) influences the maximum temperature rise in the *dynamic regime*, the rate of heat transfer along with the rate of reaction should also affect the maximum temperature rise. Lower heat transfer rates between the gas and the solids lead to a dispersed temperature front. In this case the temperature in the bed gradually increases along the length of the bed and the rates of reaction in the upstream section of the bed are finite. This results in the gradual and slower decrease in the reactant concentration along the length of the bed and, hence, the magnitude of the maximum temperature rise is moderate. However, for higher heat transfer rates the temperature fronts are steeper and sharper and the upstream section of the bed is too cold to support the exothermic reaction. Thus, the still hot solids in the down stream section are exposed to higher reactant concentration leading to an increase in heat generation by reaction which increases the transient temperature rise in the bed as illustrated in Figure 3.4.

3.5 The Model Equations: Solid Phase Reaction

Here, we consider a packed bed reactor with the same highly exothermic reaction discussed in Section 3.2, but occurring now in the solid phase. The parametric values used in the computation (Table 3.1) correspond to a typical combustion system. The reaction is:

$$\text{Exothermic:} \quad A \rightarrow C \qquad \Delta H_{s,A} < 0 \text{.....(Solid Phase)}$$

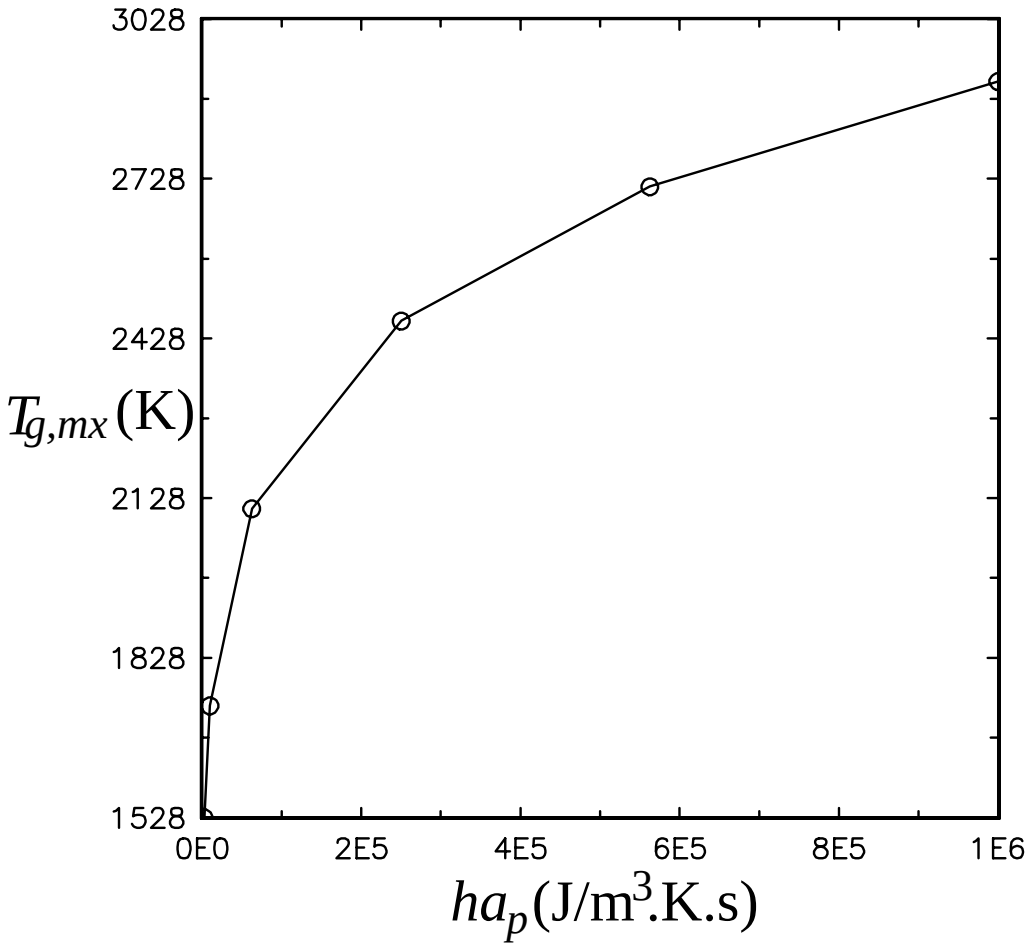

Figure 3.4. The effect of rate of heat transfer on the maximum temperature rise, $\Delta T_{g,mx}$.

The same assumptions made in the formulation of the model for the gas phase reaction are used in the formulation of the model for the solid phase process. The model equations consist of the energy balance for the gas and solid phase, equations (3.5) and (3.6), respectively, reactant *A* mass balance, equation (3.7), and the overall continuity, equation (3.8):

$$\frac{\partial \theta_g}{\partial \tau} = -U \frac{\partial \theta_g}{\partial z} - St_g \frac{1}{\Omega_g} \left(\theta_g - \theta_s \right) \tag{3.5}$$

$$\frac{\partial \theta_s}{\partial \tau} = \tau_{s/r,s,A} TR_{s,A} \gamma_{s,A}^{\frac{\theta_g - \theta_{g,d}}{\theta_g + \theta_{g,d}}} y_A + St_s \left(\theta_g - \theta_s \right) \tag{3.6}$$

$$\frac{\partial y_A}{\partial \tau} = -U\frac{\partial y_A}{\partial z} - \tau_{s/r,s,A}\gamma_{s,A}^{\frac{\theta_g}{\theta_g+\theta_{g,d}}} y_A \tag{3.7}$$

$$\frac{\partial \Omega_g}{\partial \tau} = -\frac{\partial\left(\Omega_g U\right)}{\partial z} = 0 \tag{3.8}$$

The boundary conditions are:
$@z = 0$

$\theta_g = \theta_{g,in}; \quad y_A = y_{A,in}$

The initial conditions are:
$@t = 0$ and $0 \le z \le 1$

$\theta_g = \theta_{g,0}; \quad y_A = y_{A,0}$

The dimensionless quantities used above are:

$$\tau = \frac{t}{L/u_{in}}; \quad z = \frac{x}{L}; \quad \theta_g = \frac{T_g - T_{g,in}}{\Delta T_{ad}}; \quad \theta_s = \frac{T_s - T_{g,in}}{\Delta T_{ad}}; \; \theta_{g,d} = \frac{2T_{g,in} - T_{g,in}}{\Delta T_{ad}}$$

$$\Omega_g = \frac{\rho_g}{\rho_{g,in}}; \quad U = \frac{u}{\varepsilon u_{in}}; \quad \gamma_{s,A} = e^{\left(\frac{Ea_{s,A}}{RT_{g,ad}}\right)}$$

$$\tau_{s/r,s,A} = \frac{\tau_s}{\tau_{r,s,A}} = \frac{L/u_{in}}{\frac{1}{k_{0,s,A}/(1-\varepsilon)\, e^{\left(\frac{Ea_{s,A}}{RT_{g,ad}}\right)}}}; \quad TR_{s,A} = \frac{P\,(-\Delta H_{s,A})}{RT_g \rho_s C_{p,s} \Delta T_{ad}}$$

$$St_s = \frac{ha_p L}{(1-\varepsilon)\rho_s u_{in} C_{p,s}}; \quad St_g = \frac{ha_p L}{\varepsilon \rho_{g,in} u_{in} C_{p,g}}$$

The dimensionless group TR_S is a measure of the ratio of the enthalpy change caused by reaction in the solid phase to the volumetric solid heat capacity. Thus, it indicates the extent of the temperature change in the solid phase due to reaction. TR_S is three orders of magnitude smaller than TR_g due to the high volumetric solid heat capacity compared to that of the gas phase. Hence, even if the reaction in the solid phase has a

very high heat of reaction, the rate of temperature change in the solid phase due to heat generated by the reaction is smaller than the rate of change in the temperature of the gas phase if the same reaction were to occur in the gas phase. Since the gas and solid temperatures follow each other quite closely, it is evident that the thermal response of the fixed-bed reactor involving only solid phase reaction is much slower than the thermal response of the bed if the same reaction were to occur in the gas phase. Physical significance of the rest of the dimensionless parameters is discussed in Chapter 2.

3.6 The Wrong-way Behavior: Solid Phase Reaction

The transient response of a bed with a solid phase reaction is similar to that in the case of a gas phase reaction (Figure 3.5). However, the phase in which combustion reaction occurs affects the maximum transient temperature rise. For the same kinetic parameters, the maximum transient temperature rise in the bed is lower for solid phase combustion compared to that for gas phase combustion. This difference is attributed to the slower dynamics of the solid phase caused by the higher thermal capacity of the solids compared to faster dynamics of the gas phase caused by the lower thermal capacity of the gas. The difference between the maximum transient temperature rise in the bed for the gas phase combustion and for the solid phase combustion can be very high. Since the rate of increase of the temperature in the bed is slower for a solid phase reaction, the rates of reaction in a fixed-bed reactor with a solid phase reaction increase slowly before the reactants are depleted. However, in the case of a gas phase reaction, the rate of change of reaction is sudden leading to faster production of the heat of reaction which increases the transient temperature rise. Since the rate of change in a solid phase is slower, in the *dynamic regime,* the maximum temperature rise for a solid

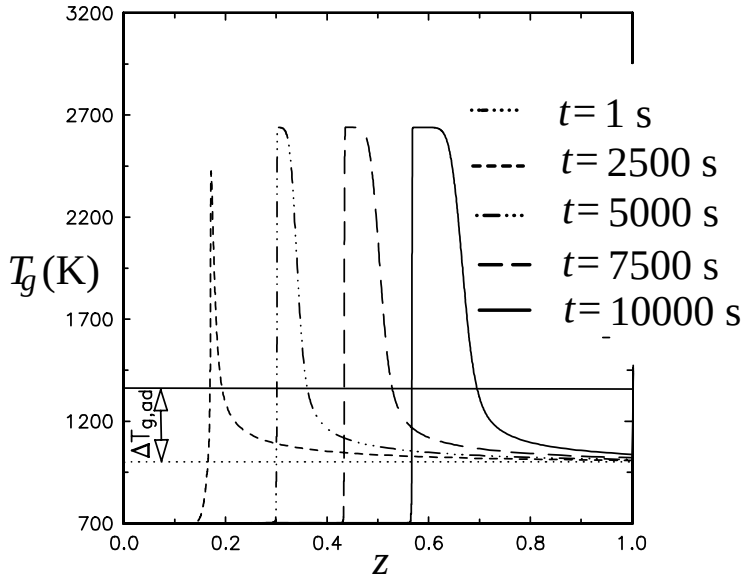

Figure 3.5. The evolution of axial gas temperature profiles for solid phase reaction ($T_{g,in}$=700 K < $T_{s,0}$=1000 K).

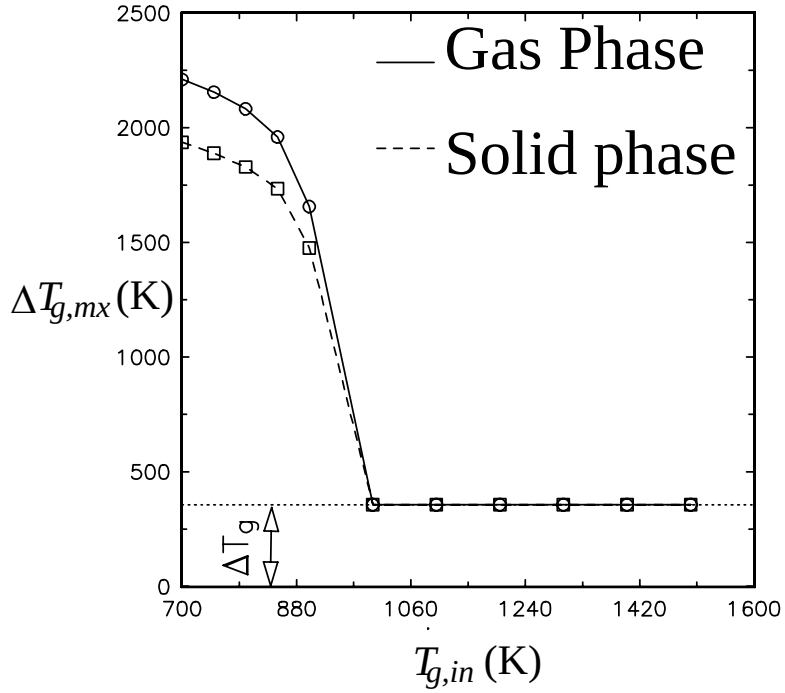

Figure 3.6. Comparison of the maximum temperature rise for gas and solid phase reactions.

phase reaction is much smaller than that for a gas phase reaction for the same kinetic parameters as shown in Figure 3.6.

3.7 A Note on the Solid Phase Temperature

The volumetric heat transfer coefficients and, hence, the volumetric heat transfer rates are very high in a fixed-bed reactor. Therefore, the solid temperature follows the gas temperature very closely and vice versa. The difference between the gas and solid temperatures cannot be appreciably shown in the figures presented in this Chapter. Hence, the arguments and figures presented for the gas phase temperatures also accurately represent the solid phase temperatures. For the parameters listed in Table 3.1, the fixed-bed reactor can be represented by a homogeneous model where the difference between the gas and the solid temperatures is zero.

3.8 Conclusions

The developed completely implicit, temporally and spatially adaptive numerical algorithm can accurately capture the steep moving temperature and reaction fronts in fixed-bed reactors. In the dynamic regime, where inlet gas temperature is lower than the initial bed temperature, the dynamic response of a fixed-bed reactor is sluggish for solid phase reactions. The maximum transient temperature reached in a fixed-bed reactor is higher for a gas phase reaction than that for a solid phase reaction due to higher thermal capacity of the solids which leads to sluggish response. Also, the maximum temperature rise in the bed increases with decreasing inlet temperature and increasing volumetric heat transfer coefficient. In the dynamic region, the rate of heat transfer, the rate of reaction and the phase in which reaction occurs all affect the maximum temperature rise in the bed.

Table 3.1: Parameters Used for Simulation.

Parameter	Value
$T_{g,in}$ (K)	700
$T_{g,0}$ (K)	1000
$T_{s,0}$ (K)	1000
y_{in}	0.1
y,	variable
k_0 (s^{-1})	1.0×10^5
Ea (J/mol)	1.0×10^5
ΔH_A(J/mol)	-2.0×10^5
ΔH_B (J/mol)	1.5×10^5
h ($J/m^2.K.s$)	1000
C_p (J/kg.K)	1000
ρ_s (kg/m^3)	3000
a_p (m^2/m^3)	1000
u_{in} (m/s)	1
P (Pa)	1.013×10^5
L (m)	5
ε	0.5
M_w	28

4. FUNDAMENTALS OF BI-DIRECTIONAL ASYMMETRIC FIXED-BED REACTOR OPERATION

The performance of a bi-directional fixed-bed reactor subject to both flow reversal and switching between exothermic and endothermic reactions is studied and simulated in this Chapter. During *odd semi-cycles (blows)* an exothermic reaction heats the bed, during *even semi-cycles* an endothermic reaction cools the bed and produces the desired product in the hot zone. It is shown that such operation is possible and efficient when the inlet gas temperature is lower than the initial bed temperature leading to the *wrong-way behavior* when the temperature front moves with a finite velocity (*creep velocity*) from the feed end to the exit during a semi-cycle. Since the dynamic nature of the fixed-bed reactor changes with each semi-cycle, the front velocity during an exothermic semi-cycle is different from the front velocity during an endothermic semi-cycle and an asymptotic expression is developed for the *differential creep (front) velocity* that quantifies this difference. Due to a non zero differential creep velocity the front exhibits an effective displacement after each cycle. This asymptotic expression for the creep velocity works very well except in the inlet and outlet region of the fixed-bed reactor. A developed expression for energy efficiency indicates that 100% efficiency can be reached only if the differential creep velocity is zero. A relation for the balanced operation of a reactor-regenerator is developed. Differences in reactor performance caused by reactions occurring in the gas or solid phase are also discussed.

4.1 Introduction

4.1.1 Modeling the Dynamic Operation of Fixed-beds

The processes dealing with heat storage in, and recovery from, packed beds received early attention. Among others Anzelius, Nusselt, Schumann, Hausen, Schmeidler and Ackermann (see Jakob, 1957), and Schmidt and Willmott (1981) studied the dynamic operation of packed bed heat regenerators without reactions. Ermenc (1956a and 1956b) added the possibility of running reactions in such systems and developed *The Wisconsin Process* for the thermal production of nitric oxide in which the cold reactants (nitrogen and oxygen in air) were heated and the products (NO + unreacted air) were cooled using heat regenerators. Levenspiel (1983) used the dispersion model to explain the spreading of the temperature front in a heat regenerator without reaction, while Ramachandran and Dudukovic′ (1984) developed a moving finite element collocation method for moving fronts in heat regenerators. Ramachandran and Dudukovic´ (1984) also solved the linear regenerator model using triple collocation, i.e. collocation in space and time, and developed the design criteria for periodic operation of heat regenerators (Dudukovic´ and Ramachandran; 1985).

Rhee et al. (1973), Matros (1989), Eigenberger and Butt (1988), Gupta and Bhatia (1991) are among many who studied the dynamic operation of fixed-bed reactors. Rhee et. al. (1973) developed an approximate expression for the speed of the temperature front. Matros (1989) showed that the yield of a thermodynamically reversible mildly exothermic catalytic reaction can be increased subject to forced flow reversal. Matros (1989), Snyder and Subramaniam (1993), Bunimovich et al. (1995) and others studied SO_2 oxidation in the solid phase in a reverse-flow reactor. Eigenberger and Nieken (1988) investigated the catalytic combustion of hydrocarbons

with periodic flow reversal using the Crank-Nicolson numerical algorithm developed by Eigenberger and Butt (1976). Agar and Ruppel (1988) used an implicit finite difference approximation to study NO_x removal in the presence of ammonia and air by forced flow reversal in a fixed-bed reactor. Gawdzik and Rakowski (1988, 89), using a combination of the method of characteristics and orthogonal collocation, investigated the operation of an adiabatic tubular reactor forced through the reversal of flow of the reaction mixture. Blanks et al. (1990) employed numerical simulation as well as a series of experiments in studying the production of synthesis gas by flow reversal. Gupta and Bhatia (1991) simulated the reactor cyclic operation by using collocation on finite elements in space and treated the differential equation system as a boundary value problem in time, with the stationary catalyst temperature profiles at the beginning and at the end of a half cycle being mirror images of each other. Wallace and Viljoen (1995) modeled the oxidation of CO in a monolithic catalytic bed with reciprocating flow.

All of the above cited literature deals with the cyclic operation of fixed-bed regenerators and fixed-bed reactors. A typical cyclic operation of a fixed-bed reactor involves two semi-cycles. During a semi-cycle, the reactants are fed into the fixed-bed reactor from one end and during the next semi-cycle the reactants are fed into the bed from the other end. These repeated swings, or flow-reversals, of the feed result in an inverted U shaped temperature profile which travels in the bed from one position to other. The references cited so far discussed only the bi-directional fixed-bed reactors subject to the same type of reaction throughout the cyclic operation, i.e., the same feed is introduced into the reactor during two successive semi-cycles. For example, in the catalytic oxidation of SO_2 the type of reaction that occurs in the fixed-bed reactor is always catalytic oxidation of SO_2 during every and each semi-cycle. The type of reaction does not change with the flow reversal of the feed (Matros, 1989,

Eigenberger, 1988). Thus, the thermodynamic and dynamic nature of the system does not change with flow reversal.

4.1.2 The *RE-GAS* Process

Levenspiel (1988) proposed the *RE-GAS* process to produce synthesis gas. The process can involve gas phase or solid phase reactions. The fixed-bed reactor now acts also like a heat regenerator. The *odd blow*, or the *odd semi-cycle*, involves feeding gaseous reactants which react exothermally in the fixed-bed reactor. During the *even blow*, or the *even semi-cycle*, another gaseous mixture, which contains reactants which undergo an endothermic reaction, is introduced from the opposite end of the bed. The product of interest is the product of the endothermic reaction which is carried out in the hot bed. The general idea is that the even blow is allowed to go on until the bed is sufficiently cooled down. These two semi-cycles constitute one complete cycle which is periodically repeated. For example, in the production of synthesis gas by the RE-GAS process, even blows involve heating the bed by burning a hydrocarbon fuel, and odd blows involve the production of synthesis gas by endothermic reactions between steam and CO_2. The synthesis gas produced by this process is not diluted with N_2 unlike in the bi-directional process proposed by Blanks et al. (1990).

In the RE-GAS process, the type of reaction that takes place in the bed changes with each semi-cycle. Thus, two successive semi-cycles do not lead to mirror image solutions during the pseudo-steady state. The parameters like the maximum temperature, front velocity etc. are different for even and odd semi-cycles. So far asymmetric bi-directional fixed-bed reactors subject to different reactions during even and odd semi-cycles have not been studied. Hence, there is a need to study RE-GAS type of processes in order to develop an understanding of asymmetric fixed-bed operation under these new flow reversal conditions. This is the objective of the present study.

4.1.3 Quantities of Interest

There are a few fundamental questions which need to be addressed for the proper understanding of the above discussed new reverse flow fixed-bed process. It is expected that the inlet gas temperatures for the exothermic and endothermic reactions in relation to the initial bed temperature affect the performance of the process. Also, periods of even and odd semi-cycles, t^*_{even} and t^*_{odd} respectively, should affect the yield of the process. In the traditional bi-directional processes t^*_{even} is equal to t^*_{odd} because the front speeds of odd and even semi-cycles are equal to each other. However, in the RE-GAS type process, due to different reactions occurring during odd and even semi-cycles, the velocity of the temperature front is different for the odd and even semi-cycles. Hence, the ratio t^*_{odd} / t^*_{even} can have a significant effect on the performance of the process. The possibility of achieving 100% energy efficiency by coupling endothermic and exothermic reactions arises and needs to be addressed. It is also necessary to investigate the effect of the phase in which reaction occurs, i.e., the process can occur mainly catalytically in the solid phase or homogeneously in the gas phase.

In this work we address the above questions by performing simulation studies to examine the effect of the inlet temperature ($T_{g,in}$), the phase in which the reaction occurs and the duration of the switching time t^* on a RE-GAS type of process. The purpose of this numerical simulation is not to optimize the process but to gain physical insight into the parametric sensitivity of the RE-GAS type of process.

4.2 Gas Phase RE-GAS Type Process

4.2.1 The Model

We consider a packed bed reactor with highly exothermic and endothermic reactions occurring in the gas phase. The parametric values used in the computation (Table 4.1) correspond to a typical combustion and endothermic gasification system. The two reactions are:

$$\text{Exothermic:} \quad A \rightarrow C \qquad \Delta H_{g,A} < 0 \text{.....(Gas Phase)}$$
$$\text{Endothermic:} \quad B \rightarrow D \qquad \Delta H_{g,B} > 0 \text{.....(Gas Phase)}$$

It is assumed that only the reaction $A \rightarrow C$ occurs in the bed during an odd semi-cycle when reactant A is fed to the system, and only the reaction $B \rightarrow D$ takes place during an even semi-cycle when reactant B is fed from the opposite end of the reactor. The heats of exothermic and endothermic reactions are set to be different (Table 4.1) to allow for different front speeds during odd and even semi-cycles but are assumed constant.

A model is now developed subject to the following additional assumptions.

1) Axial dispersion of heat and mass in the gas as well as in the solid phase is assumed to be negligible. The assumption of plug flow of gas holds true for long reactors at high gas velocities. The assumption of negligible dispersion in the solid phase holds true for solid packings which allow minimal area of contact between two solid particles. Clearly there will be some dispersion of heat in high temperature beds by various means, including radiation, but this is neglected at present as the zero dispersion model represents a useful limiting case to study in illustrating the features of the process.

2) The rate of conduction within the solids is assumed to be very high compared to the convective heat transfer rate between the gas and solids which is a fair assumption if particles are not too large.

3) The gas is assumed to be compressible with the total mass flux of gas being constant ($\rho_g u = \rho_{g,in} u_{in}$) (Kulkarni, 1992).

4) Pore diffusion in the solids, and external mass transfer resistances between the gas and the solids, are incorporated into the overall kinetic expression for the reaction occurring in the solid phase. Kinetics is assumed to have an Arrhenius type dependence on the temperature and to be first order.

Admittedly the above model that uses first order Arrhenius type kinetics which does not change over a wide range of temperature is a great simplification of reality. Over the extended temperature range the real gas phase reaction mechanism can change several times. Pore diffusion changes within 50 K and radiation heat transfer effects can be very important. However, this work concerns itself with a preliminary and fundamental study of an asymmetric operation of a fixed-bed reactor. The purpose of this work is to gain a physical insight into a RE-GAS type asymmetric process. Once the global features of the asymmetric fixed-bed reactor are well understood, the real RE-GAS process with real kinetics can be studied. The above numerical model is sufficient for our current purpose of understanding whether a periodic operation of asymmetric fixed-bed reactors is possible and how it is affected by initial gas temperature and characteristic reaction parameters.

The model based on all above assumptions should be adequate to establish the effect of the inlet temperature, $T_{g,in}$, the phase in which reaction occurs, the volumetric heat transfer rate and the front velocity on the RE-GAS process, all of which represent the focus of this study.

The model equations consist of the energy balance for the gas and solid phase, equations (4.1) and (4.2), respectively, reactant A and B mass balances, equations (4.3) to (4.4), respectively, and the overall continuity, equation (4.5):

$$\frac{\partial \theta_g}{\partial \tau} = -U\frac{\partial \theta_g}{\partial z} + \tau_{s/r,g,A} TR_{g,A} \gamma_{g,A}^{\frac{1-\theta_g}{\theta_g+\theta_{g,d}}} y_A + \tau_{s/r,g,B} TR_{g,B} \gamma_{g,B}^{\frac{1-\theta_g}{\theta_g+\theta_{g,d}}} y_B - St_g \frac{1}{\Omega_g}\left(\theta_g - \theta_s\right) \quad (4.1)$$

$$\frac{\partial \theta_s}{\partial \tau} = St_s \left(\frac{\Omega_g}{\theta_g} - \theta_s\right) \quad (4.2)$$

$$\frac{\partial y_A}{\partial \tau} = -U\frac{\partial y_A}{\partial z} - \tau_{s/r,g,A} \gamma_{g,A}^{\frac{1-\theta_g}{\theta_g+\theta_{g,d}}} y_A \quad (4.3)$$

$$\frac{\partial y_B}{\partial \tau} = -U\frac{\partial y_B}{\partial z} - \tau_{s/r,g,B} \gamma_{g,B}^{\frac{1-\theta_g}{\theta_g+\theta_{g,d}}} y_B \quad (4.4)$$

$$\frac{\partial \Omega_g}{\partial \tau} = -\frac{\partial\left(\Omega_g U\right)}{\partial z} = 0 \quad (4.5)$$

The boundary conditions are:

$@\, z = 0$

$\theta_g = \theta_{g,in}; \quad y_A = y_{A,in}; \quad y_B = y_{B,in}$

The initial conditions are:

$@\, t = 0$ and $0 \le z \le 1$

$\theta_g = \theta_{g,0}; \quad y_A = y_{A,0}; \quad y_B = y_{B,0}$

The dimensionless quantities used above are:

$$\tau = \frac{t}{L/u_{in}}; \quad z = \frac{x}{L}; \quad \theta_g = \frac{T_g - T_{g,in}}{\Delta T_{ad}}; \quad \theta_s = \frac{T_s - T_{g,in}}{\Delta T_{ad}}; \; \theta_{g,d} = \frac{2T_{g,in} - T_{g,in}}{\Delta T_{ad}}$$

$$\Omega_g = \frac{\rho_g}{\rho_{g,in}}; \quad U = \frac{u}{\varepsilon u_{in}}; \quad \gamma_{g,A} = e^{\frac{Ea_{g,A}}{RT_{g,ad}}}; \quad \gamma_{g,B} = e^{\frac{Ea_{g,B}}{RT_{g,ad}}}$$

$$\tau_{s/r,g,A} = \frac{\tau_s}{\tau_{r,g,A}} = \frac{L/u_{in}}{\frac{1}{k_{0,g,A}/\varepsilon\, e^{-Ea_{g,A}/RT_{g,ad}}}}; \quad \tau_{s/r,g,B} = \frac{\tau_s}{\tau_{r,g,B}} = \frac{L/u_{in}}{\frac{1}{k_{0,g,B}/\varepsilon\, e^{-Ea_{g,B}/RT_{g,ad}}}}$$

$$TR_{g,A} = \frac{1000(-\Delta H_{g,A})}{M_w C_{p,g} \Delta T_{ad}}; \quad TR_{g,B} = \frac{1000(-\Delta H_{g,B})}{M_w C_{p,g} \Delta T_{ad}}$$

$$St_s = \frac{ha_p L}{(1-\varepsilon)\rho_s u_{in} C_{p,s}}; \quad St_g = \frac{ha_p L}{\varepsilon \rho_{g,in} u_{in} C_{p,g}}$$

The variables that affect the operation of an asymmetric fixed-bed reactor are summarized in the form of appropriate dimensionless groups. The gas Stanton number (St_g) is a measure of the relative magnitude of the rate of convective heat transfer between solids and the gas to the rate of convective heat transfer in the axial direction by the gas. Thus, a higher gas Stanton number indicates a higher axial temperature gradient in the gas phase. The temperature fronts become steeper as the gas Stanton number increases. The solid Stanton number (St_s) is a measure of the relative magnitude of the rate of heat transfer between the gas and the solids compared to the product of the volumetric heat capacity of the solids and the gas velocity. Since the temperature gradient in the solid phase is directly proportional to the rate of heat transfer between the gas and solids, and inversely proportional to the volumetric heat capacity of the solids, a higher solid Stanton number results in steeper temperature fronts in the bed. As the gas and the solid temperature fronts are known to follow each other closely, a system having higher gas and solid Stanton numbers must involve steeper moving fronts. Thus, the higher the St_s, St_g are, the steeper the temperature fronts in the system.

The dimensionless quantity U is a constant equal to $1/\varepsilon$ for incompressible gases, and varies with the gas temperature for compressible gases. The deviation of U from $1/\varepsilon$ indicates the variation in the linear velocity of the gas due to its compressible nature. The dimensionless number $\tau_{s/r}$ is the ratio of the space time to the characteristic reaction time. Thus $\tau_{s/r}$ is a Damkohler number for first order reaction and indicates the extent of conversion in the fixed-bed reactor. If $\tau_{s/r} << 1$, the conversion in the reactor is negligible and the axial concentration profiles are flat. If $\tau_{s/r} >> 1$, nearly complete conversion (or thermodynamic equilibrium for reversible

reactions) is achieved in the reactor and the concentration and reaction fronts are very steep.

The dimensionless group TR_g is a measure of the ratio of the enthalpy change caused by reaction in the gas phase to the volumetric gas heat capacity. It indicates the extent of the temperature change in the gas phase due to reaction in the gas phase. If the reaction involved has a very high heat of reaction, the temperature change in the gas phase is very high. A system having high Stanton numbers (St_g and St_s), and high TR_g involves steep temperature fronts, and a system having high $\tau_{s/r}$ involves also steep concentration and reaction fronts.

4.2.2 The Wrong-way Behavior Revisited

Equations (4.1-4.5) were solved first using the algorithm developed in Chapter 2, considering only the exothermic gas phase reaction ($A \rightarrow C$). Figure 4.1 (Figure 3.3) illustrates the maximum temperature rise as a function of the inlet gas temperature, and shows that the minimum value of the maximum temperature rise is equal to the adiabatic temperature rise based on the inlet gas temperature and the exit gas conversion. When the initial bed temperature is below or equal to the inlet gas temperature, which is the case if a hot combustible mixture is passed through an initially cold bed, the maximum transient temperature rise ($\Delta T_{g,mx}$) in the bed is equal to the adiabatic temperature rise. However, when the initial bed temperature is moderately higher than the inlet gas temperature, and is sufficiently high to ignite the combustion mixture, the maximum transient temperature rise in the bed is much higher than the adiabatic temperature rise. This *wrong-way behavior* was discussed in Chapter 3.

As illustrated in Figure 4.1 (Figure 3.3), the maximum temperature rise in a packed bed reactor is a dynamic property only for the inlet gas temperatures below the

initial bed temperature. Figure 4.1 indicates that the operating range for a fixed-bed reactor consists of two regimes: a *thermodynamic regime* in which the maximum temperature rise is equal to the adiabatic temperature rise (occurs at gas inlet temperatures equal to or larger than the initial bed temperature) and a *dynamic regime* where the maximum temperature rise depends on the inlet gas temperature (for feed gas temperatures lower than the initial bed temperature). In the *dynamic regime* a low

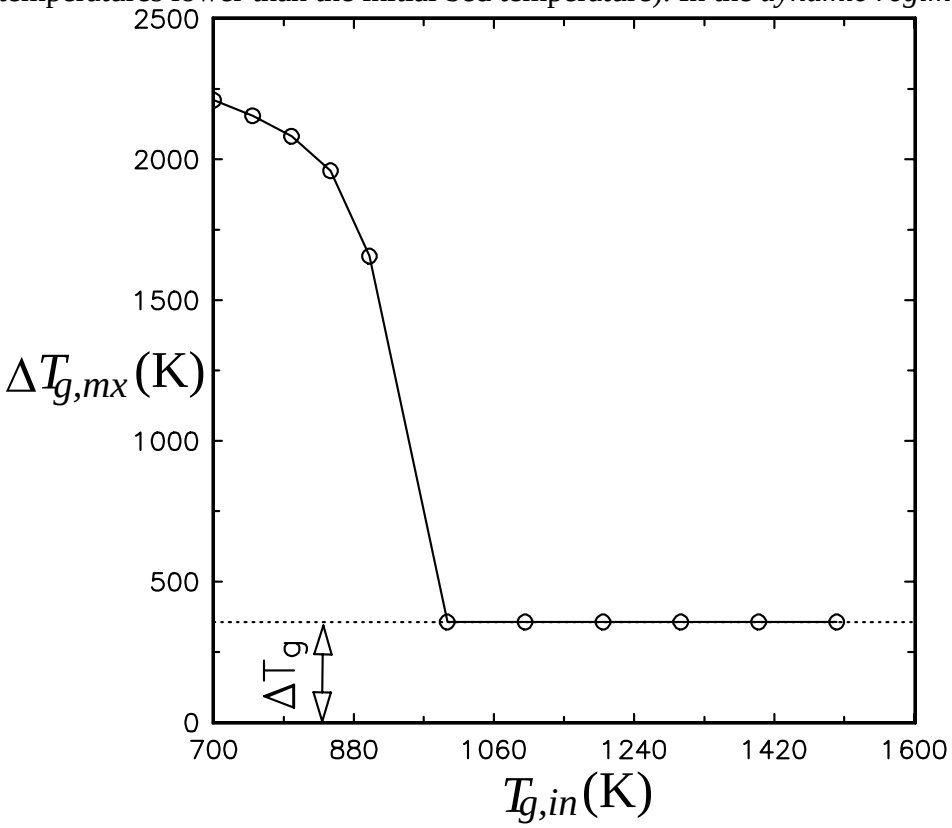

Figure 4.1. The effect of $T_{g,in}$ on $\Delta T_{g,mx}$ for the gas phase reaction.

feed temperature decreases the conversion reachable in the upstream section of the reactor where the reactants are getting heated; consequently, the still hot solids in the down stream section are exposed to higher reactant concentration leading to an increase in heat generation by reaction which increases the transient temperature rise in the bed (Il'in and Luss, 1992). This, of course, can happen only when there is interphase heat transfer—in this case, the gas coming in the bed encounters already

hot solids. In the *thermodynamic regime* the incoming gas is already hotter than the inlet solid temperature and, hence, the maximum temperature rise can not exceed the adiabatic temperature rise. Clearly the adiabatic temperature rise is always based on the inlet gas temperature.

The rates of endothermic reactions are dramatically enhanced by higher temperatures. Therefore, it seems plausible that the wrong-way behavior of the bed can be utilized to establish high temperature zones in the bed during a cyclic process so that the endothermic reaction can undergo completion in a short period of time in such a hot zone. Since a hot zone can be very short, the length of the bed can also be reduced without sacrificing the performance. The goal is to create zones in the bed with temperatures far in excess of the adiabatic temperature of the fuel-air mixture used in the exothermic part of the operating cycle. We now explore conditions under which this can be accomplished.

4.2.3 Sensitivity to the Inlet Temperature

Based on the results of numerical simulation it was observed that the wrong-way behavior of a fixed-bed reactor is indeed a property which can be exploited in a RE-GAS type process. Equations (4.1) to (4.5) were solved using implicit finite differences as suggested in Chapter 2, first for a RE-GAS type process with only gas phase reactions when solids serve to accumulate and release heat. The exothermic reaction $A \rightarrow C$ takes place during an odd semi-cycle, and the endothermic reaction $B \rightarrow D$ (with heat of reaction different from that of the exothermic reaction) takes place during an even semi-cycle. The direction of the feed gases is reversed for each semi-cycle.

Two different cases of a bi-directional process were studied—one with inlet gas temperature of 700 K and the other with inlet gas temperature of 1000 K. For both

cases the initial bed temperature was 1000 K. The first period in which only exothermic reaction takes place lasted for 15,000 s and each subsequent semi-cycle lasted for 1000 s. Figure 4.2 shows the temperature profiles at the end of the first semi-cycle for both cases. The situation in which the feed temperature is lower than the initial bed

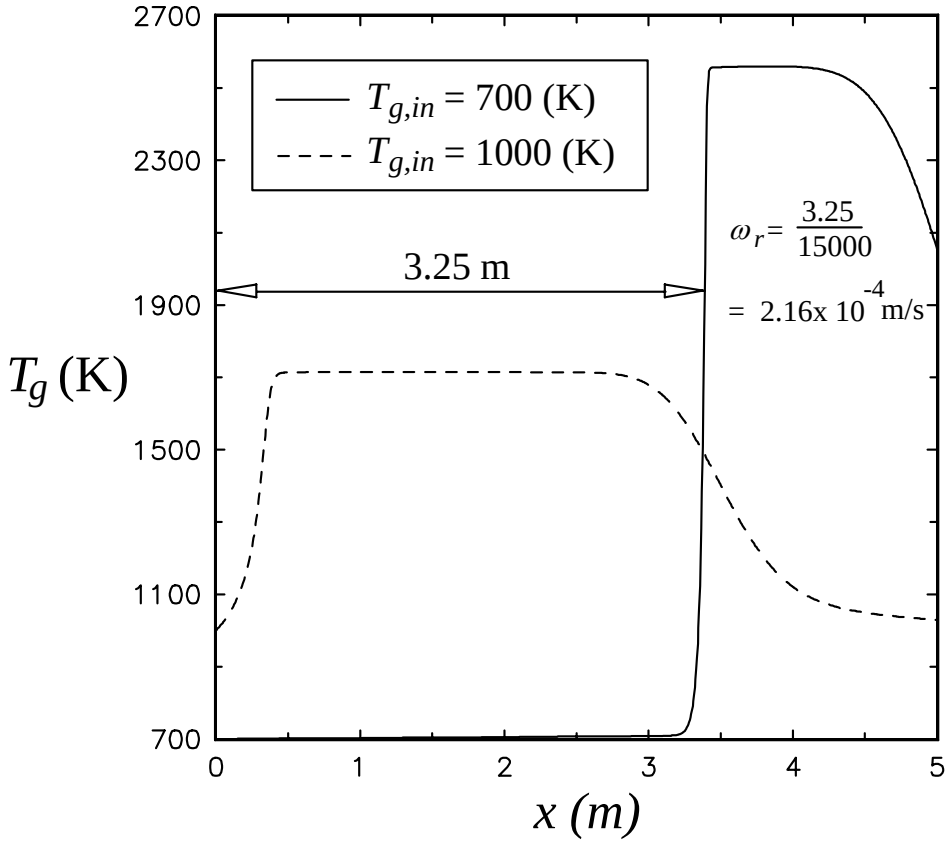

Figure 4.2. The axial temperature profile at the end of the first semi-cycle for the wrong-way and the normal process.

temperature is referred to in this paper as the *wrong-way process*. The case in which the feed temperature is equal (or higher) to the initial bed temperature is referred to in the paper as the *normal process*. As can be observed from Figure 4.2, the maximum transient temperature rise for the wrong-way process is more than three times greater than the maximum temperature rise for the normal process, therefore, more than three

times greater than the adiabatic temperature rise. Figure 4.3a shows the temperature profiles in the fixed-bed reactor at the end of the first and of the second semi-cycle for the wrong-way process. For clearer demonstration of the front movement for the endothermic semi-cycle, the endothermic semi-cycle period used for this particular figure was 5000 s. However, as mentioned before, subsequent semi-cycles lasted for 1000 s. Figure 4.3b displays the temperature profiles in the fixed-bed reactor at the end of the first and second semi-cycle for the normal process. As can be observed from Figures 4.3a and 4.3b, the maximum temperature rise is higher and the temperature fronts are sharper for the wrong-way process. Observe the difference in temperature scale of the ordinate of the two figures. More importantly, during the first semi-cycle of the wrong-way process, the temperature front moves along the length of the bed with a finite front velocity, and by the end of the first semi-cycle, which lasted for a period of 15000 s, the front is well inside the bed (Figure 4.3a). This gives room for the movement of the front in the opposite direction during the second semi-cycle. However, in the case of the normal process, the bed gets heated while the temperature front stays stagnant at the entrance (Figure 4.3b). Since the temperature front stays at the feed end for the first semi-cycle, right from the beginning of the second semi-cycle, when the flow is reversed, the temperature front starts moving out of the bed at the feed end of the first semi-cycle. This implies that even for short even semi-cycle periods the hot spot can quickly move out of the bed.

Figures 4.4a and 4.4b exhibit the pseudo-steady state temperature profiles at the end of the odd and even semi-cycle periods for the wrong-way process and for the normal process, respectively. From these figures it is evident that the pseudo-steady state temperature profiles for both the wrong-way process and the normal process are somewhat similar. It can also be observed that even the normal process now produced the maximum temperature rise in excess of the adiabatic temperature rise (Figure

4.4b). This occurs because in multiple cycling, while advancing towards pseudo-steady state, during endothermic (even) semi-cycles the high temperature region gets pushed towards the entrance of the bed for the odd (exothermic) semi-cycles. Hence, at the start of the subsequent odd (exothermic) semi-cycles the bed temperature in the vicinity of the entrance is higher than the feed temperature which now allows the wrong-way

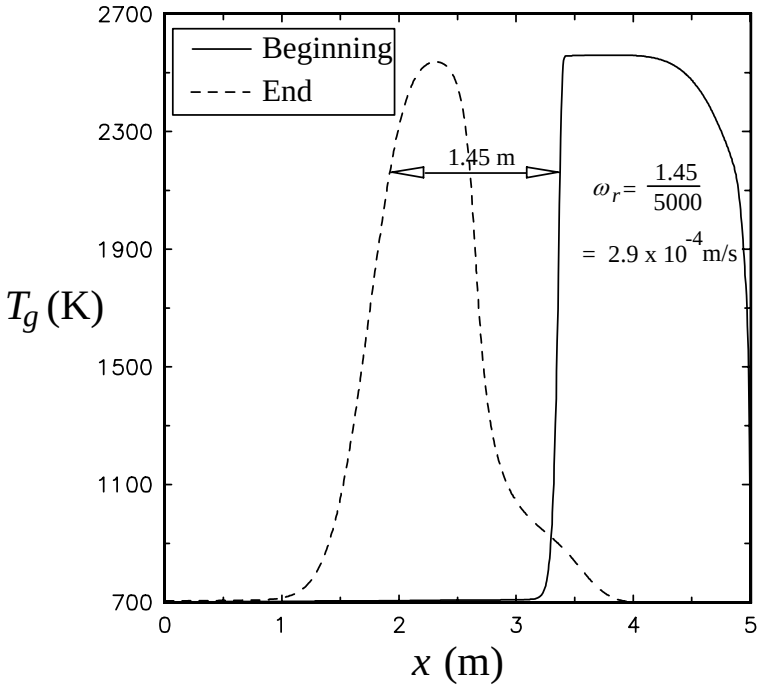

Figure 4.3a. The gas phase wrong-way process: the temperature profiles at the beginning and end of the second semi-cycle.

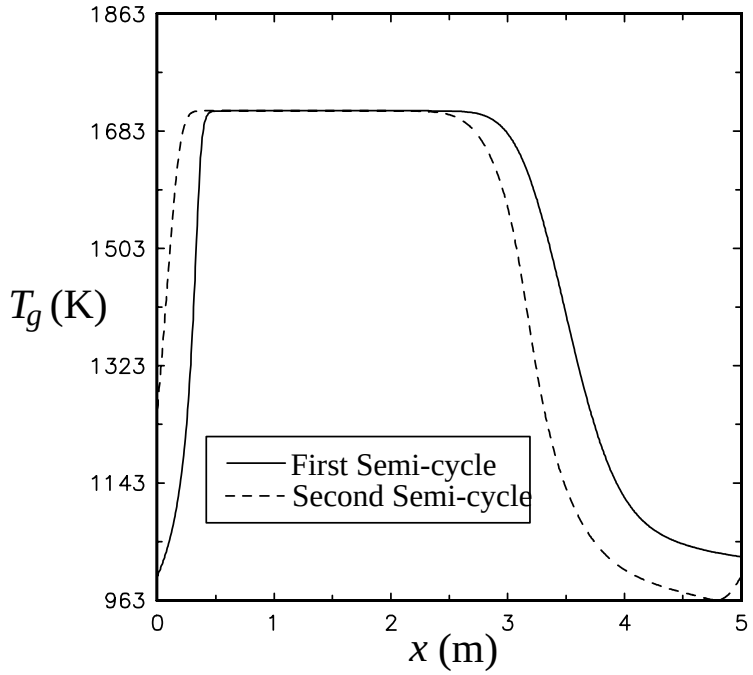

Figure 4.3b. The gas phase normal process: the temperature profiles at the end of the first and second semi-cycle.

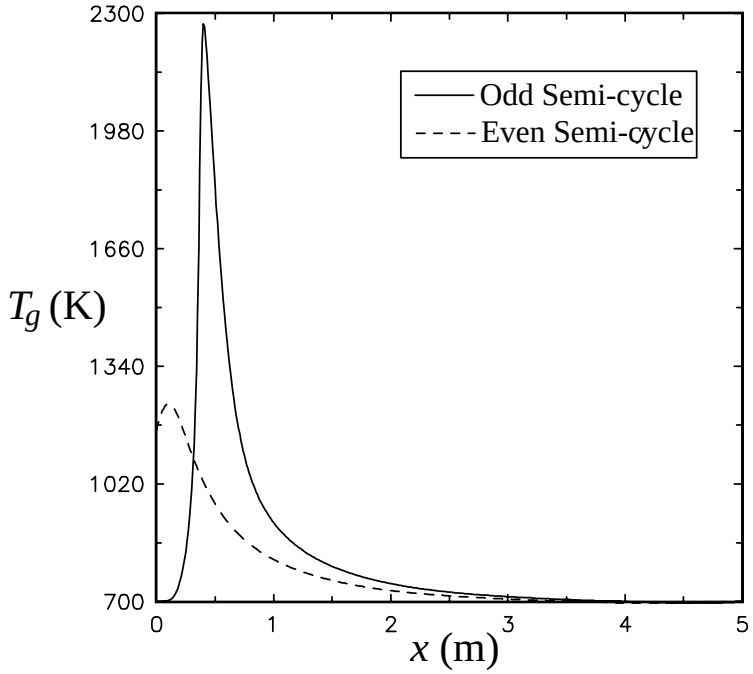

Figure 4.4a. The gas phase wrong-way process: the temperature profiles at pseudo steady state at the end of odd and even semi-cycle periods.

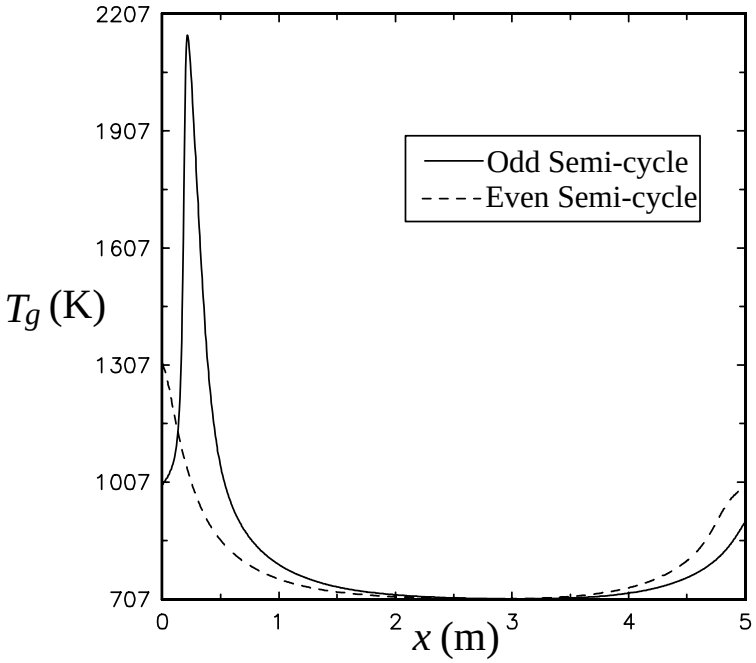

Figure 4.4b. The gas phase normal process: the temperature profiles at pseudo steady state at the end of odd and even semi-cycle periods.

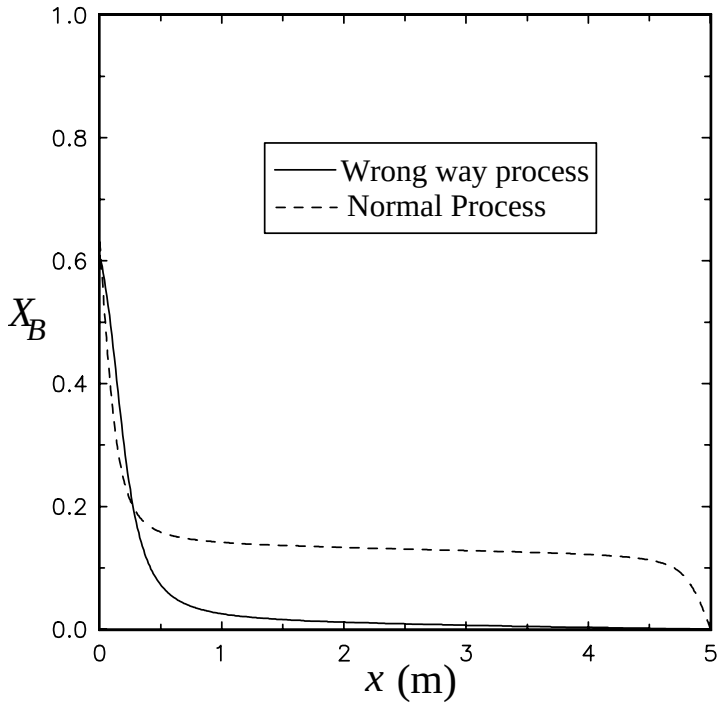

Figure 4.5. The pseudo steady state conversion profiles at the end of even semi-cycles for the gas phase wrong-way and normal process.

behavior to occur for the normal process. As can be observed from Figure 4.4a, the pseudo steady state temperature front moved towards the feed end of the odd semi-cycle (x=0) even for the wrong-way process. Due to the temperature hot spot in the proximity of the feed end for the odd semi-cycle, during the even semi-cycles, the hot spot quickly moves out of the bed. This degrades the performance of the wrong-way process and makes it similar to that of the normal process in as much that the exit conversion for the endothermic reaction (even semi-cycles) is now well below unity, as illustrated in Figure 4.5. Thus, the apparent advantage of the wrong-way process over the normal process during the initial transient operation was lost at the pseudo steady state. This finite creep of the temperature front from the first semi-cycle to the pseudo-steady state should be avoided in order to achieve higher conversion of the key reactant during the endothermic reaction conducted during the even semi-cycles. We will now consider as to how this could be done.

4.2.4 The Effect of Semi-Cycle Periods on the Steady State

4.2.4.1 Differential Creep Velocity

At pseudo steady state, the temperature and the concentration profiles at the beginning or the end of two successive even or odd semi-cycles should be identical. However, as can be observed in Figure 4.6, the temperature profiles in repeated cycles prior to establishment of periodic stationary operation, seem to be moving towards the feed end for odd semi-cycles (x=0) with a certain finite *differential creep velocity*. For the inverted U shaped temperature profile to exist in the bed at pseudo-steady state, the differential creep velocity should be equal to zero. The existence of the finite differential creep velocity indicates that the inverted U shaped temperature profile will eventually depart the fixed-bed reactor. In the above simulation (Figures 4.6 and 4.9)

the duration of the first semi-cycle was 15000 seconds and time periods of subsequent semi-cycles were 5000 seconds. The reason for the existence of the differential creep velocity is the difference in the velocities of the fronts during even and odd semi-cycles. The approximate expression for the front velocity for a single reaction was derived, using the coordinate transformation used by Rhee et al (1973), and is given by

$$\omega_r = \frac{u\rho_g C_{p,g}}{(1-\varepsilon)\rho_s C_{p,s}}\left(1-\frac{\Delta T_{ad}}{\Delta T_{mx}}\right) = \omega\left(1-\frac{\Delta T_{ad}}{\Delta T_{mx}}\right) \tag{4.6}$$

During an odd semi-cycle the exothermic reaction takes place with the adiabatic temperature rise equal to 714 K. During an even semi-cycle the endothermic reaction

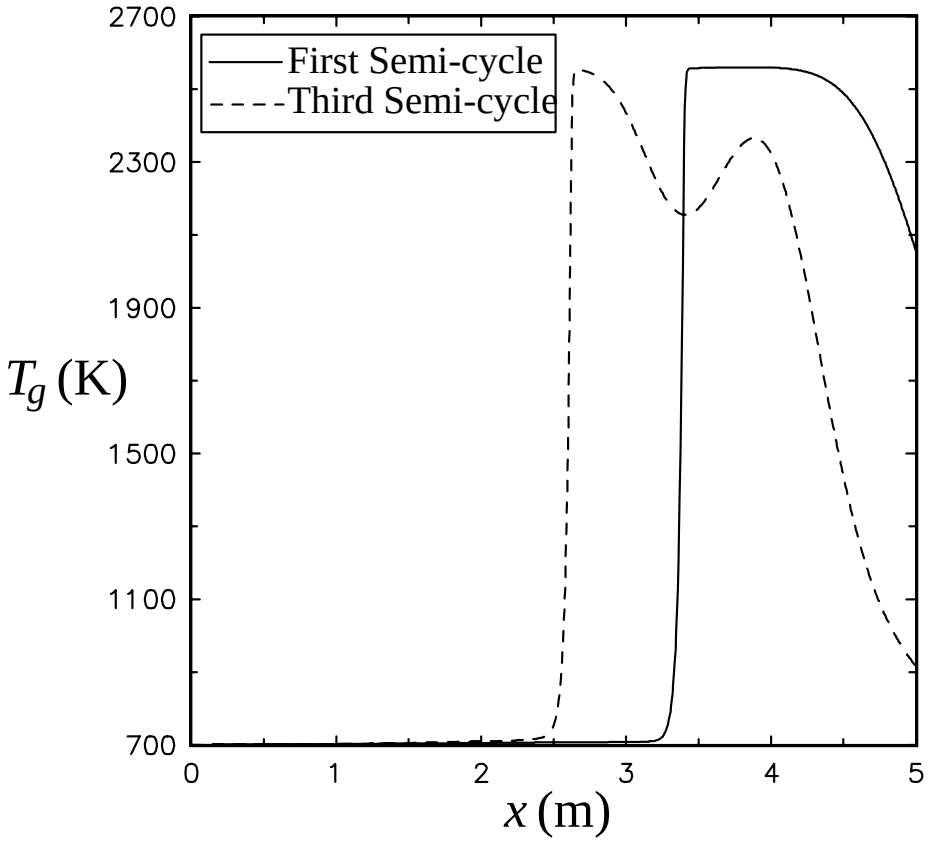

Figure 4.6. The temperature profiles at the end of two early successive odd semi-cycles
for the wrong-way process.

takes place with the adiabatic temperature drop of approximately 515 K. This results in the difference in the front velocities for odd and even semi-cycles with the front velocity for the exothermic reaction (odd semi-cycle) being lower than that for the endothermic reaction (even semi-cycle). The theoretical front velocity computed using equation (4.6) is 1.923×10^{-4} m/s for the exothermic semi-cycle and is 2.3×10^{-4} m/s for the endothermic semi-cycle. The front velocity estimated using the simulation results (Figures 4.2 and 4.3a) is approximately equal to 2.16×10^{-4} m/s for the exothermic semi-cycle and is around 2.9×10^{-4} m/s for the endothermic semi-cycle. Although the front velocity is an asymptotic approximation derived assuming a constant gas density, the theoretical (equation (4.6)) and simulated results agree quite well for the exothermic semi-cycle and are of the same order or magnitude for the endothermic semi-cycle.

Since the semi-cycle period used to generate Figures 4.2a to 4.4a (except for Figure 4.3a) was constant and set at 1000 s, and the semi-cycle period used to generate Figure 4.6 was also a constant set at 5000 s for both even and odd semi-cycles, due to faster moving fronts during the even semi-cycles (i.e. endothermic reaction), the temperature front creeps towards the original feed end of the reactor as the number of cycles increases.

Thus, this difference in the front velocities for the even and odd semi-cycles is due to the difference in the thermodynamic parameters, namely, the heats of reaction of two different reactions taking place. A bi-directional process can now exhibit a differential front velocity if the inlet velocity, feed composition and thermodynamic parameters are different for the odd and even semi-cycles. If in a reverse process, the

reactions change with each semi-cycle, the difference in the front velocity could be appropriately compensated by the difference in the semi-cycle periods. The simplest criterion for such balanced operation is

$$\frac{\omega_{r,odd}}{\omega_{r,even}} = \frac{t^*_{even}}{t^*_{odd}} \tag{4.7}$$

The above criterion can readily be arrived at from the approximate expression for the differential creep velocity given by equation (4.8) by requiring zero differential creep velocity.

$$\omega_{r,diff} = \frac{\omega_{r,odd} \times t^*_{odd} - \omega_{r,even} \times t^*_{even}}{t^*_{odd} + t^*_{even}} \tag{4.8}$$

There is another important conclusion that can be drawn from equation (4.6). If the maximum temperature rise in the bed is equal to the adiabatic temperature rise, the front velocity becomes zero i.e., the cold bed gets heated up while the front stays stagnant. It also means that the temperature profile monotonically increases from the feed end during an odd semi-cycle. If the front velocity is zero for the exothermic reaction, and finite for the endothermic reaction, the front quickly creeps out of the feed end for the odd semi-cycles.

4.2.4.2 Discussion of Simulations

Equations (4.7) and (4.8) indicate that if the front velocities for even and odd semi-cycles are not equal to each other, the temperature front can depart the bed. However, as can be observed from Figure 4.4a, for $t^*_{odd} = t^*_{even}$ = 1000s and $\omega_{r,even} > \omega_{r,odd}$, this does not happen for the wrong-way process as the temperature

front moves towards the feed end of the odd semi-cycle during the even semi-cycle but partially remains in the bed without completely departing at pseudo steady state. The same bi-directional process was simulated for different bed lengths and the results are presented in Figures 4.7 and 4.8. It is observed, in each case, that during the even semi-cycle the temperature front moves towards the feed end of the odd semi-cycle and partially stays in the bed at pseudo-steady state. This phenomenon is similar to that of the normal process where the hot spot of the temperature profile stays near the feed end for the odd semi-cycles from the beginning to end of an odd semi-cycle and, hence, the temperature front partially departs from the bed during even semi-cycles, as shown in Figure 4.4b. This causes the exit conversion of the endothermic reaction at pseudo steady state, illustrated in Figure 4.5 for both processes, to be significantly lower than the conversion obtained for the wrong-way process during the initial few cycles. Obviously, at the entrance region of the bed (i.e. x=0), equation (4.6), which is an asymptotic approximation for an infinitely long fixed-bed reactor where no end effects are incorporated (Chapter 2), does not hold. Hence, equation (4.6) is approximate and applicable only to the interior region of the fixed-bed reactor where the temperature profile behaves as in an infinitely long bed. Therefore, it is important to have a negligible differential creep velocity in a bi-directional operation. Equation (4.7) provides an estimate of semi-cycle periods needed to achieve such negligible differential creep velocity. Since the maximum temperature of the bed also changes between two successive semi-cycles, the semi-cycle periods for even and odd semi-cycles should be determined by trial and error around the values calculated by equation (4.7).

Based on the kinetic parameters listed in Table 4.1 the front velocity for the exothermic reaction is calculated. Based on the assumption that an exothermic reaction and an endothermic reaction with the same kinetic and thermodynamic

parameters lead to the same front velocity, the front velocity for the endothermic reaction used in the RE-GAS type process is also calculated. Using these calculations, and some trial and error, the period for odd semi-cycles and for even semi-cycles were selected to be 1000 s and 550 s, respectively. The results of the simulation are shown in Figures 4.9 to 4.11. As can be seen from these figures, the temperature front now does not display a differential creep velocity, (Figure 4.9) and at pseudo-steady state hot spot stays in the bed (Figure 4.10). Hence, at dynamic steady state the front traverses from one position in the reactor to the other in a periodic fashion. Also, it can be observed that only the wrong-way process with zero creep velocity results in complete conversion for the endothermic reaction (Figure 4.11) because the high temperature zone stays well within the bed. As opposed to this, in the processes which display a finite differential creep velocity (both normal process and the wrong-way process without adjusted semi-cycle periods), the temperature front moves toward the entrance for the exothermic semi-cycle. During an endothermic semi-cycle, the hot spot moves out from the entrance for the exothermic semi-cycle and the temperature in the bed decreases. Hence, the average conversion for endothermic reaction decreases (Figure 4.11).

4.2.4.3 Energy Efficiency

In the processes simulated so far, there is always a finite amount of energy carried out of the bed by the departing gases. This situation always exists if the total heat produced by the exothermic reaction is greater than the total heat absorbed by the endothermic reaction. The energy efficiency of a cycle at pseudo steady state is given by

$$\eta_{cycle} = \frac{Q_{endo}}{Q_{exo}} = \frac{\rho_{gm,in,endo} u_{in,endo} X_B \Delta H_{g,B} \times t^*_{even}}{\rho_{gm,in,exo} u_{in,exo} X_A \Delta H_{g,A} \times t^*_{odd}} \qquad (4.9)$$

For 100% energy efficiency, the total heat absorbed by the endothermic reaction should be equal to the total heat produced by the exothermic reaction. i.e.,

$$Q_{exo} = Q_{endo}$$
$$\Rightarrow \rho_{gm,in,exo} u_{in,exo} X_A \Delta H_{g,A} \times t^*_{odd} = \rho_{gm,in,endo} u_{in,endo} X_B \Delta H_{g,B} \times t^*_{even} \quad (4.10)$$

and

$$\frac{\rho_{gm,in,endo} u_{in,endo} X_B \Delta H_{g,B}}{\rho_{gm,in,exo} u_{in,exo} X_A \Delta H_{g,A}} = \frac{t^*_{odd}}{t^*_{even}} \quad (4.11)$$

Thus, for equal inlet concentrations and temperatures for both exothermic and endothermic reactions, the semi-cycle periods should be determined by the ratio of the heats of reactions if we strive for high energy efficiency.

For the parameters used to simulate the RE-GAS type process, using equation (4.11), the even and odd semi-cycle periods were determined to be 1250 s and 1000 s, respectively. At pseudo-steady state, the temperature profile departed the fixed-bed

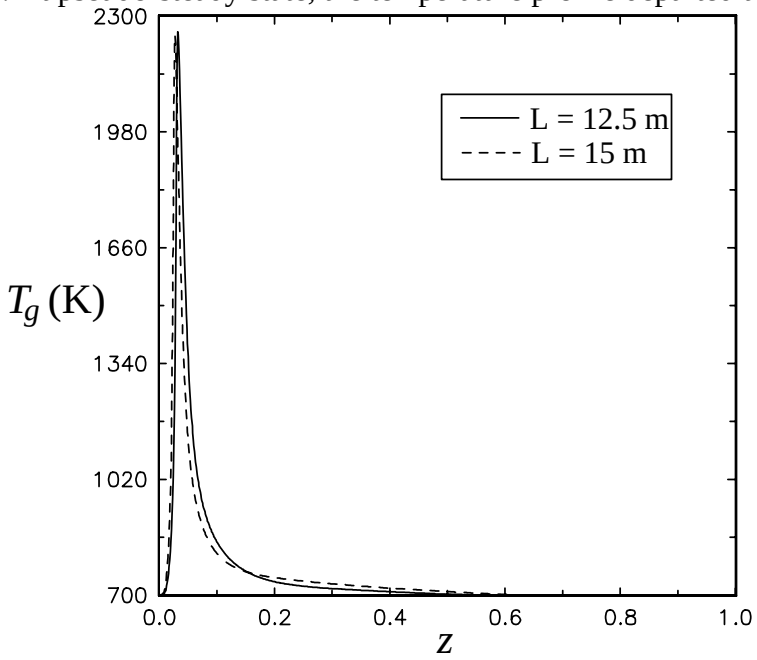

Figure 4.7. The gas phase wrong-way process: the pseudo steady state temperature profiles at the end of odd semi-cycles for different reactor lengths.

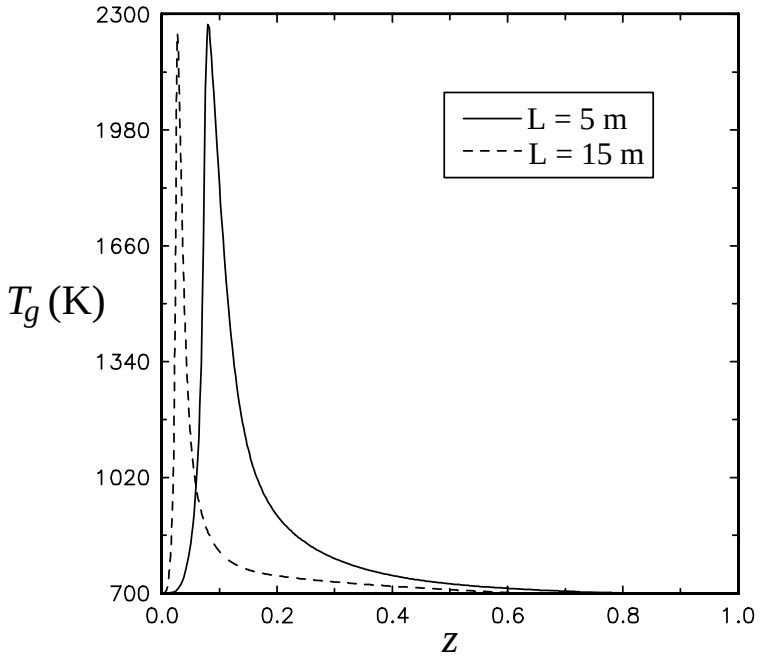

Figure 4.8. The gas phase wrong-way process: the pseudo steady state temperature profiles at the end of odd semi-cycles for different reactor lengths.

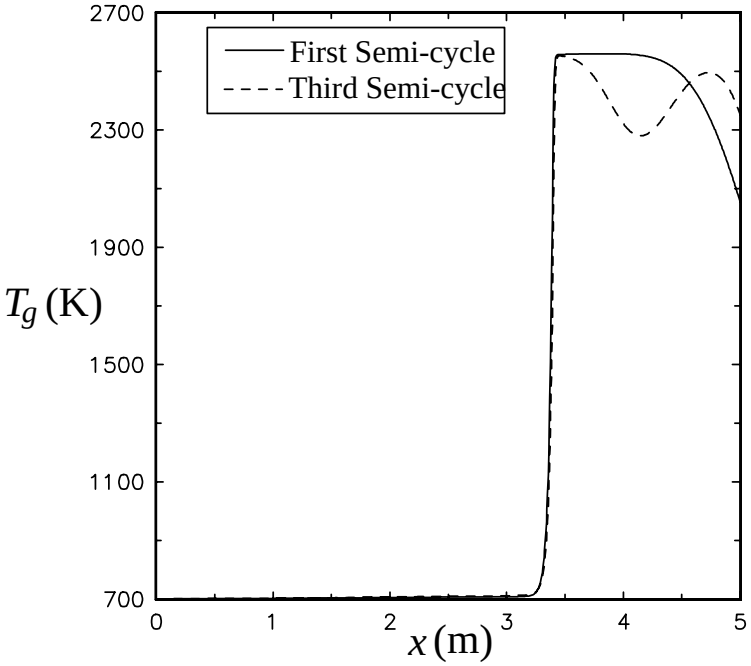

Figure 4.9. The wrong-way process with adjusted switching periods: the temperature profiles at the end of the first and third semi-cycles.

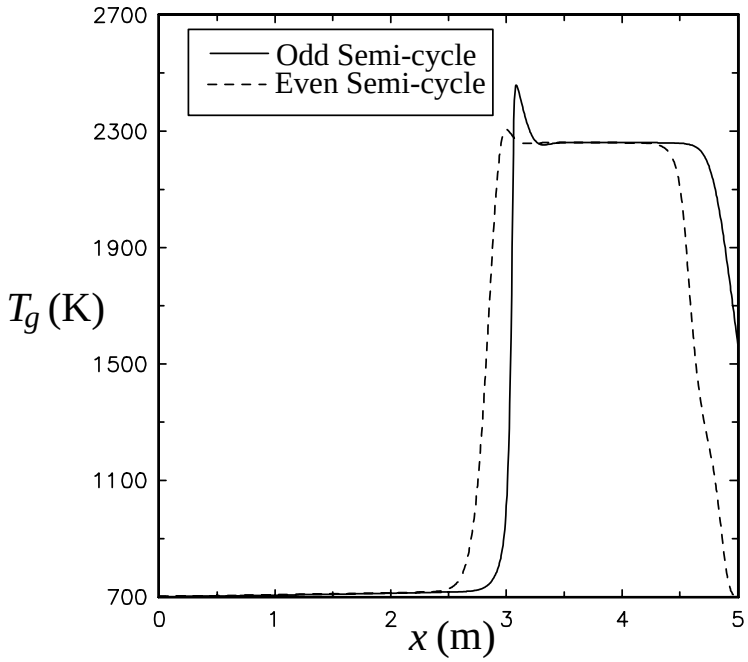

Figure 4.10. The wrong-way process with adjusted switching periods: the temperature profiles at pseudo steady state.

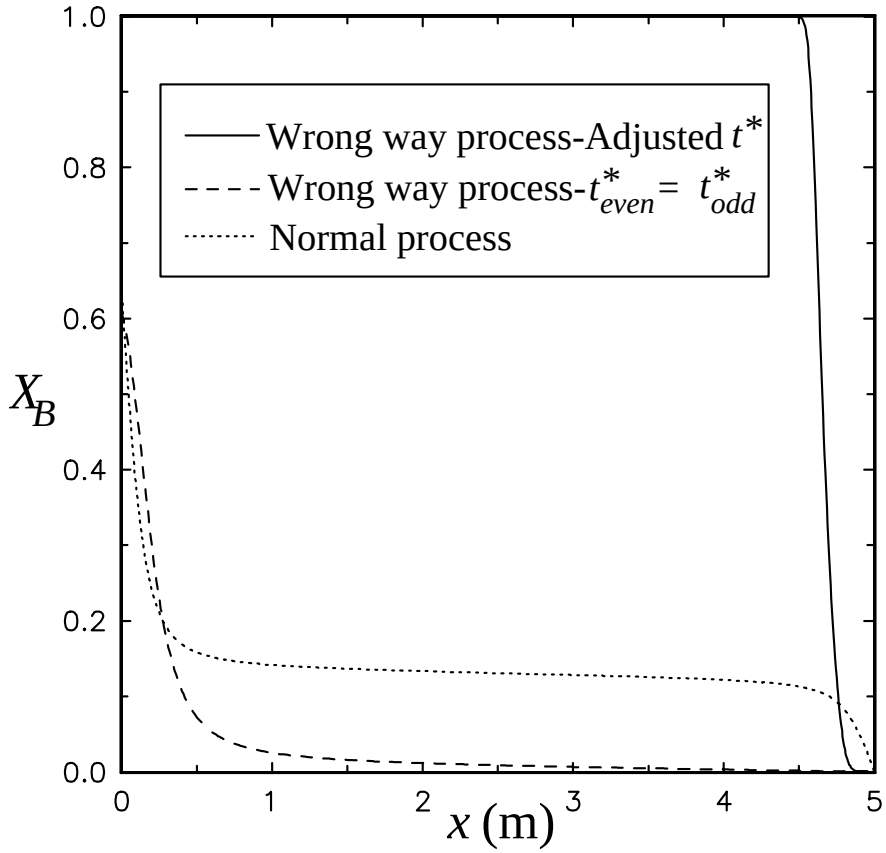

Figure 4.11. Comparison of the pseudo steady state conversion profiles at the end of even semi-cycles for the wrong-way process with adjusted semi-cycle periods, wrong-way process and the normal process.

reactor and no reaction occurred in the bed. This is because the criterion given by equation (4.7) for zero creep velocity is not satisfied by equation (4.11). Obviously, it follows from equations (4.7) and (4.11) that 100% energy efficiency can be achieved only when the following relation is satisfied;

$$\frac{\rho_{gm,in,endo} u_{in,endo} X_B \Delta H_{g,B}}{\rho_{gm,in,exo} u_{in,exo} X_A \Delta H_{g,A}} = \frac{\omega_{r,even}}{\omega_{r,odd}} = \frac{t^*_{odd}}{t^*_{even}} \qquad (4.12)$$

Although equation (4.12) is exact, the expression to estimate front velocity (equation (4.6)) is approximate. Hence, front velocities should be determined by trial and error to satisfy equation (4.12). The analysis of the achievable energy efficiency will be

discussed in the next chapter. The energy efficiency is further discussed in Chapters 5 and 6 in detail.

4.3 Solid Phase RE-GAS Type Process

4.3.1 The Model

Here we consider a packed bed reactor in a RE-GAS type process with both the exothermic and endothermic reaction occurring in the solid phase. The parametric values used in the computation (Table 4.1) correspond to a typical combustion-gasification system. The reactions are:

$$\text{Exothermic:} \quad A \rightarrow C \qquad \Delta H_{s,A} < 0 \text{.....(Solid Phase)}$$
$$\text{Endothermic:} \quad B \rightarrow D \qquad \Delta H_{s,B} > 0 \text{.....(Solid Phase)}$$

Analogously to the gas phase RE-GAS process, it is assumed that only reaction $A \rightarrow C$ occurs in the bed during an odd semi-cycle when reactant A is fed to the reactor, and only reaction $B \rightarrow D$ takes place during an even semi-cycle when B enters from the opposite side of the reactor. The heats of exothermic and endothermic reactions are set to be different (Table 4.1) to allow for different front speeds during odd and even semi-cycles.

The same assumptions made in formulation of the model for the gas phase RE-GAS type process are used in formulation of the model for the solid phase RE-GAS type process. The model equations consist of the energy balance for the gas and solid phase, equations (4.13) and (4.14), respectively, reactant A and B mass balances, equations (4.15) to (4.16), respectively, and the overall continuity, equation (4.17):

$$\frac{\partial \theta_g}{\partial \tau} = -U\frac{\partial \theta_g}{\partial z} - St_g\frac{1}{\Omega_g}\left(\theta_g - \theta_s\right) \tag{4.13}$$

$$\frac{\partial \theta_s}{\partial \tau} = \tau_{s/r,s,A}TR_{s,A}\gamma_{s,A}^{\frac{1-\theta_g}{\theta_g+\theta_{g,d}}}y_A + \tau_{s/r,s,B}TR_{s,B}\gamma_{s,B}^{\frac{1-\theta_g}{\theta_g+\theta_{g,d}}}y_B + St_s\frac{\Omega_g}{\theta_g}\left(\theta_g - \theta_s\right) \tag{4.14}$$

$$\frac{\partial y_A}{\partial \tau} = -U\frac{\partial y_A}{\partial z} - \tau_{s/r,s,A}\gamma_{s,A}^{\frac{1-\theta_g}{\theta_g+\theta_{g,d}}}y_A \tag{4.15}$$

$$\frac{\partial y_B}{\partial \tau} = -U\frac{\partial y_B}{\partial z} - \tau_{s/r,s,B}\gamma_{s,B}^{\frac{1-\theta_g}{\theta_g+\theta_{g,d}}}y_B \tag{4.16}$$

$$\frac{\partial \Omega_g}{\partial \tau} = -\frac{\partial\left(\Omega_g U\right)}{\partial z} = 0 \tag{4.17}$$

The boundary conditions are:
$@\, z = 0$

$\theta_g = \theta_{g,in};\quad y_A = y_{A,in};\quad y_B = y_{B,in}$

The initial conditions are:
$@\, t = 0$ and $0 \le z \le 1$

$\theta_g = \theta_{g,0};\quad y_A = y_{A,0};\quad y_B = y_{B,0}$

The dimensionless quantities used above are:

$$\tau = \frac{t}{L/u_{in}};\quad z = \frac{x}{L};\quad \theta_g = \frac{T_g - T_{g,in}}{\Delta T_{ad}};\quad \theta_s = \frac{T_s - T_{g,in}}{\Delta T_{ad}};\ \theta_{g,d} = \frac{2T_{g,in} - T_{g,in}}{\Delta T_{ad}}$$

$$\Omega_g = \frac{\rho_g}{\rho_{g,in}};\quad U = \frac{u}{\varepsilon u_{in}};\quad \gamma_{s,A} = e^{\frac{Ea_{s,A}}{RT_{g,ad}}};\quad \gamma_{s,B} = e^{\frac{Ea_{s,B}}{RT_{g,ad}}}$$

$$\tau_{s/r,s,A} = \frac{\tau_s}{\tau_{r,s,A}} = \frac{L/u_{in}}{\frac{1}{k_{0,s,A}/(1-\varepsilon)\, e^{-Ea_{s,A}/RT_{g,ad}}}};\quad \tau_{s/r,s,B} = \frac{\tau_s}{\tau_{r,s,B}} = \frac{L/u_{in}}{\frac{1}{k_{0,s,B}/(1-\varepsilon)\, e^{-Ea_{s,B}/RT_{g,ad}}}}$$

$$TR_{s,A} = \frac{P\,|\Delta H_{s,A}|}{RT_g\rho_s C_{p,s}\Delta T_{ad}};\quad TR_{s,B} = \frac{P\,|\Delta H_{g,B}|}{RT_g\rho_s C_{p,s}\Delta T_{ad}}$$

$$St_s = \frac{ha_p L}{(1-\varepsilon)\rho_s u_{in} C_{p,s}};\quad St_g = \frac{ha_p L}{\varepsilon\rho_{g,in} u_{in} C_{p,g}}$$

The dimensionless group TR_S is a measure of the ratio of the enthalpy change caused by reaction in the solid phase to the volumetric solid heat capacity. It indicates the extent of the temperature change in the solid phase due to reaction. TR_S is three orders of magnitude smaller than TR_g due to the high volumetric solids heat capacity compared to that of the gas phase. Hence, even if the reaction in the solid phase has a very high heat of reaction, the rate of temperature change in the solid phase due to heat generated by the reaction is smaller than the rate of change in the temperature of the gas phase if the same reaction were to occur in the gas phase. As the gas and solid temperatures follow each other quite closely, it is evident that the thermal response of a fixed-bed reactor involving only solid phase reaction is much slower than the thermal response of the bed if the same reaction were to occur in the gas phase. The significance of other dimensionless parameters is explained in the section dedicated to *The gas phase RE-GAS type process*.

4.3.2 The Process

The transient response of the bed in which reactions occur in the solids (catalytically) is similar to the case discussed above for gas phase reaction. The phase in which combustion reaction occurs affects the maximum temperature rise. For the same kinetic parameters, the maximum temperature rise in the bed is lower for the solid phase combustion compared to that for gas phase combustion. This difference is attributed to the slower dynamics of the solid phase caused by the higher thermal capacity of the solids compared to faster dynamics of the gas phase caused by the lower thermal capacity of the gas. The difference between the maximum temperature rise in

the bed for gas phase combustion and for solid phase combustion can be very high. Since the rate of increase of the temperature in the bed is slower for a solid phase

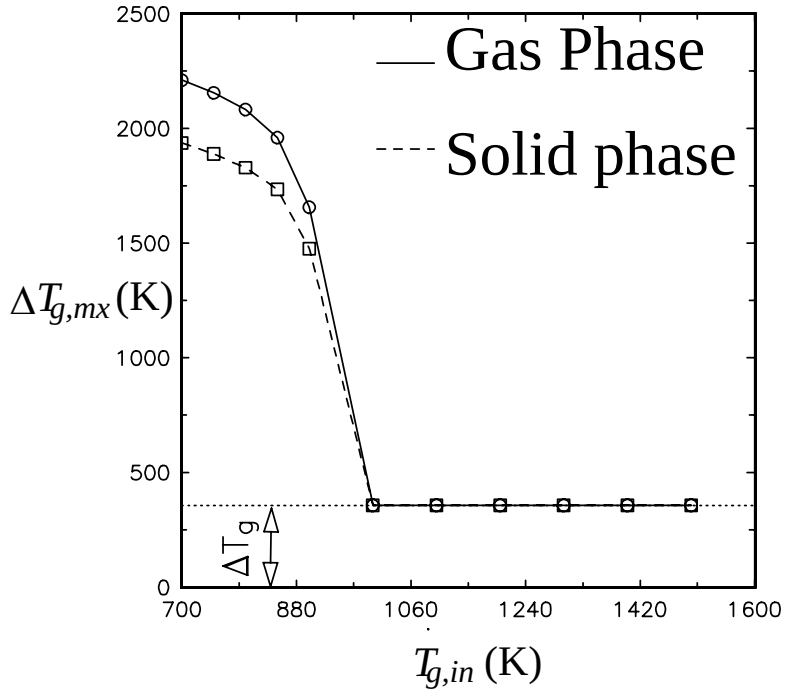

Figure 4.12. A comparison between wrong-way behavior of fixed-bed reactors with gas phase and solid phase reactions.

reaction, the rate of reaction in the fixed-bed reactor with solid phase reaction increases slowly before the reactants are depleted. However, in the case of a gas phase reaction, the rate of change of reaction is sudden leading to faster production of heat of the reaction which increases the transient temperature rise. Due to the fact that the rate of change in the solid phase is slower, in the *dynamic regime*, the maximum temperature rise for the solid phase reaction is much smaller than that for the gas phase reaction for the same kinetic parameters. This is shown in Figure 4.12.

4.3.4 Discussion of Simulations

A RE-GAS type process is simulated here considering only solid phase reactions. The parameters used are the same as those used in the simulation of the gas phase wrong-way process. The temperature profiles for the solid phase wrong-way

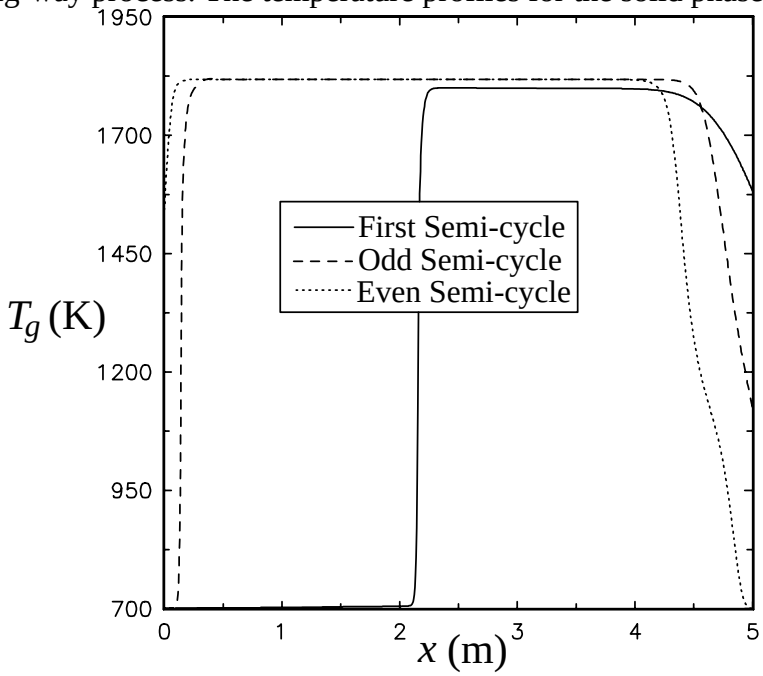

Figure 4.13. The solid phase wrong-way process: the temperature profiles at the end of first semi-cycle and at the end of an odd and even semi-cycle at the pseudo-steady state.

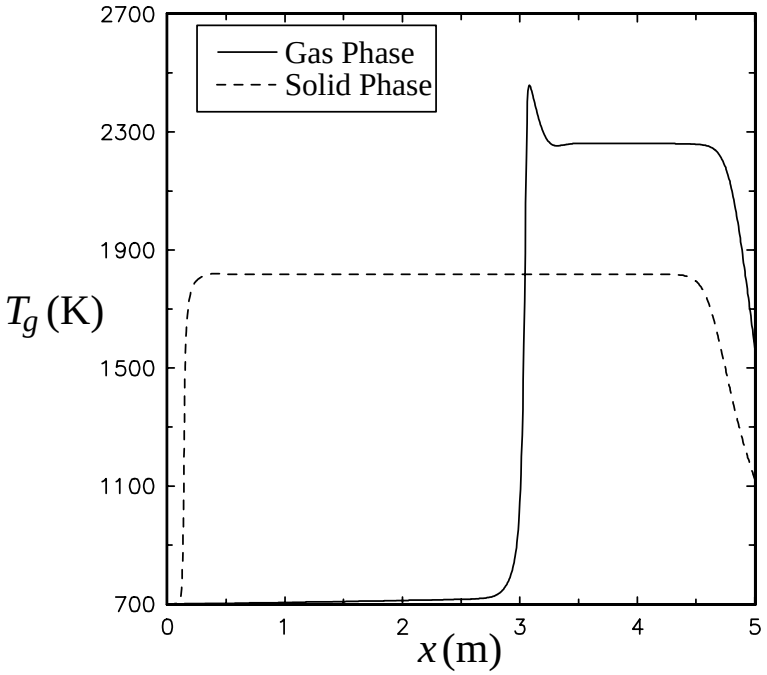

Figure 4.14. The wrong-way process: the temperature profiles for the gas and the solid phase reactions at the end of an odd semi-cycle at pseudo-steady state.

process are qualitatively similar to those in the case of the gas phase wrong-way process. Hence, the details of this process are not discussed here. Figure 4.13 illustrates the temperature profile at the end of the first semi-cycle and at pseudo steady state. The dfference in the thermal response of the bed for the gas phase and solid phase reactions is shown in Figure 4.14. In this figure it is clearly established that the temperature fronts for the gas phase reaction are much steeper, and that the maximum temperature reached in the fixed-bed for gas phase reactions is much higher.

4.4 Comparison of Discussed Processes

The average conversions and energy efficiencies during even and odd semi-cycles in various processes discussed in this paper are listed in Table 4.2. It is obvious that the wrong-way process with adjusted semi-cycle periods to meet the requirement of equation (4.7) for zero creep velocity leads to the highest conversion. The semi-

cycle periods of this process were determined by equations (4.6) and (4.7) which require greater t^*_{odd} than t^*_{even} to achieve zero differential creep velocity. This results from equations (4.6) and (4.7) which require $t^*_{odd} > t^*_{even}$ when $-\Delta H_{g,A} > \Delta H_{g,B}$ which esults in $Q_{exo} > Q_{endo}$. In contrast the requirement for 100% energy efficiency (equation 4.9) demands t^*_{even} greater than t^*_{odd}. Hence, the thermal energy efficiency of the wrong-way process with adjusted semi-cycle periods is the lowest of all processes discussed in this paper. In this situation, the temperature profile with well established hot spot stays well inside the bed which results in 100% conversion. The wrong-way process with equal odd and even semi-cycle periods and the normal process yield lower conversion because the hot spot departs quickly from the bed during even semi-cycles. When it is important to reach high conversions the wrong-way process with adjusted semi-cycle periods is highly desirable.

4.5 Conclusions

The maximum temperature rise and conversion are higher for the wrong-way process (where the inlet gas temperature for the exothermic reaction is below the initial bed temperature), than that for the normal process (where the inlet gas temperature is equal to or greater than the initial bed temperature). The temperature fronts during the odd and even semi-cycles exhibit different front velocities due to different reactions taking place during the two semi-cycles. This leads to a net displacement of the inverted U shaped temperature front after two successive even or odd semi-cycles. The rate of displacement is given by the differential creep velocity (Equation (4.8)). To establish a periodically moving temperature front at the pseudo-steady state, unequal switching periods given by equation (4.7) should be used. The normal process does not exhibit a finite front velocity during the heating period whereas during the cooling period a finite front velocity is displayed. Also, the

temperature in the bed monotonically increases during the odd semi-cycles. During the even semi-cycles this leads to the quick departure of the high temperature region from the original feed end of the reactor (i.e., feed end for odd semi-cycles) which leads to lower conversions during even semi-cycles.

The maximum energy efficiency is achieved only when total heat generated by the exothermic reaction is equal to the total heat absorbed by the endothermic reaction. The RE-GAS type process can also operate at 100% efficiency when equation (4.12) is satisfied.

The gas phase reactions result in steeper profiles compared to the solid phase reactions. Also, the maximum temperature rise for the gas phase reactions is higher than that for the solid phase reactions. The difference is observed in the dynamic regime and is explained by the higher thermal inertia of the solids compared to that of the gases.

Table 4.1: The Parameters Used in the Simulation of Various Processes.

Parameter	Value
$T_{g,in}$ (K)	700
$T_{g,0}$ (K)	1000
$T_{s,0}$ (K)	1000
y_{in}	0.1
y,	variable
k_0 (s^{-1})	1.0×10^5
Ea (J/mol)	1.0×10^5
ΔH_A(J/mol)	-2.0×10^5
ΔH_B (J/mol)	1.5×10^5
h ($J/m^2.K.s$)	100
C_p (J/kg.K)	1000
ρ_s (kg/m^3)	3000
a_p (m^2/m^3)	300
u_{in} (m/s)	1

P (Pa)	1.013×10^5
L (m)	5
ε	0.5
M_w	28

Table 4.2. Conversion and Thermal Efficiency of Various Processes.

Type of Process	X_{endo}	X_{exo}	η_{cycle}
Normal Process	0.691	0.882	58%
Wrong-way process	0.807	0.887	68%
Wrong-way process—Zero $\omega_{r,diff}$	1.0	1.0	41.3%
Wrong-way process—Solid phase (Zero $\omega_{r,diff}$)	1.0	1.0	41.3%

5. PERIODIC OPERATION OF ASYMMETRIC BI-DIRECTIONAL FIXED-BED REACTORS: ENERGY EFFICIENCY

Evaluation of the energy efficiency of a fixed-bed reactor in cyclic operation, subject to alternate swings of an exothermic and an endothermic reaction, is the focus of this chapter. During an *exothermic* semi-cycle an exothermic reaction takes place to heat the bed while during an *endothermic* semi-cycle that follows an endothermic reaction takes place in the bed, with reactants fed into the bed from the opposite direction. A fixed-bed operated periodically in the above described mode is *asymmetric* as the dynamic nature of the bed changes during each cycle. It is shown that to operate such an asymmetric fixed-bed reactor in a periodic steady state, two conditions need to be satisfied—the energy liberated during the exothermic semi-cycle should be equal to or greater than the energy consumed during the endothermic semi-cycle, and the product of the front velocity and semi-cycle period for the endothermic semi-cycle must be equal to or greater than that for the exothermic semi-cycle. The energy efficiency and conversions for both reactions increase with increasing bed length and decreasing semi-cycle periods for a fixed ratio of the exothermic and endothermic semi-cycle periods. The effect on operability and energy efficiency of the heats of reactions, inlet mass fluxes and front velocities during both semi-cycles, and of the ratio as well as the magnitude of individual semi-cycle periods is discussed.

5.1 Introduction

5.1.1 Symmetric and Asymmetric Fixed-Bed Reactors

Only a brief description of symmetric and asymmetric fixed-bed reactors is given in this section. A detailed discussion of similar reactors was presented in Chapter 4. Fixed-bed reactors can be operated under forced unsteady state conditions

to increase the yield of many nonlinear chemical processes (Matros, 1989). In a bi-directional fixed-bed reactor the yield and energy efficiency for irreversible exothermic reactions (Eigenberger and Nieken, 1988) and thermodynamically limited exothermic reactions (Matros, 1989) can be increased by repeated flow reversals. We call such a bi-directional fixed-bed reactor *symmetric* if its dynamic nature does not change with each flow reversal, as is the case for most bi-directional fixed-beds studied in the literature where the type of the reaction occurring in the bed does not change with flow reversal. Among many, Matros (1989), Sharma and Hughes (1976), Van Doesburg and DeJong (1976a, 1976b), Eigenberger and Nieken (1988), Gawdzik, and Rakowski (1988, 1989), Blanks et al (1990), Gupta and Bhatia (1991), Snyder and Subramaniam (1993), Bunimovich et al. (1995), have studied the operation of symmetric fixed-bed reactors.

In an *asymmetric fixed-bed reactor*, presented schematically in Figure 5.1, the dynamic nature of the bed changes with each flow reversal (Levenspiel, 1988) due to the change in the type of reaction that occurs in the bed with each flow reversal. The key dynamic parameters, such as the front speed and the maximum transient temperature rise, now also change with each flow reversal as shown in Chapters 3 and 4. These chapters also examined the effect of differential creep velocity, inlet temperatures, and the phase in which reaction occurs on the operation of an asymmetric fixed-bed reactor. However, the effect of kinetics and of other controllable parameters, such as the ratio of switching periods on the energy efficiency of the asymmetric fixed-bed reactors was not investigated, and this is the main objective of the present study. Our goal is to examine the effect of operating parameters on the energy efficiency of asymmetric fixed-bed reactors and to provide a rational explanation for all observed trends.

5.1.2 The *RE-GAS* Process

In this work the parametric sensitivity of the energy efficiency of a RE-GAS (Levenspiel, 1988) type process is studied. The fixed-bed reactor is operated cyclically in a bi-directional mode (Figure 5.1). Each cycle involves two semi-cycles consisting of an *odd semi-cycle*, or *exothermic semi-cycle*, and an *even semi-cycle*, or *endothermic* semi-cycle. During an odd (exothermic) semi-cycle an exothermic reaction takes place in the reactor which heats up the bed; during an even (endothermic) semi-cycle an endothermic reaction takes place in the reactor with reactants fed from the opposite end of the bed. The reaction front speed during an exothermic semi-cycle is different from the front speed during an endothermic semi-cycle, and this results in a finite displacement of the reaction front after two consecutive exothermic or endothermic semi-cycles. The rate of this displacement is given by the finite differential creep velocity (Chapter 4). It was shown, however, that the reaction front can be maintained in the bed under certain conditions; and a criterion, based on the differential creep velocity, needed for keeping the reaction front well inside the bed, was developed and presented. For further details the reader is referred to Chapter 4.

5.2 The Model: Gas Phase Reactions

Here we consider a packed bed reactor with highly exothermic and endothermic reactions occurring in the gas phase. The parameters used for the exothermic reaction are those typically encountered in hydrocarbon combustion and the parameters used for the endothermic reaction are those typically found in the steam reforming reaction. The parametric values used in the computation are listed in Table 5.1. The reactions are:

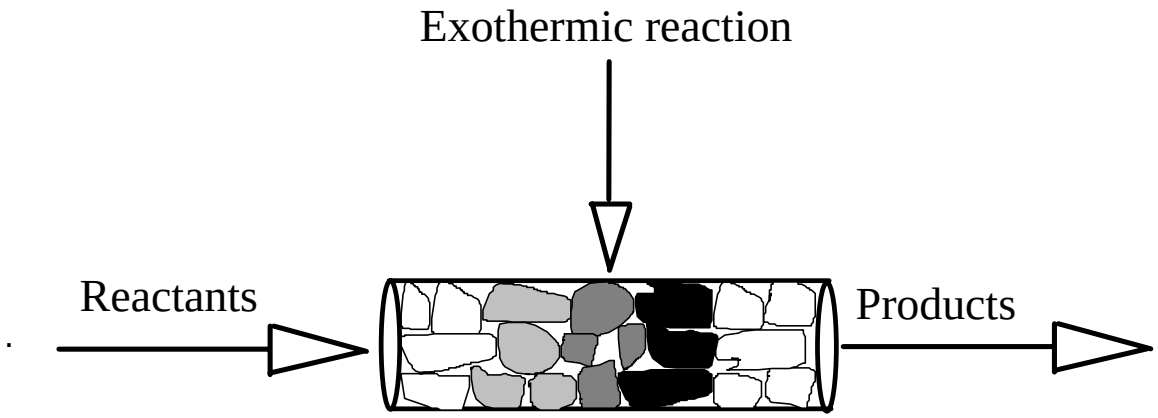

An exothermic reaction occurs in an *asymmetric* fixed-bed reactor during an exothermic semi-cycle

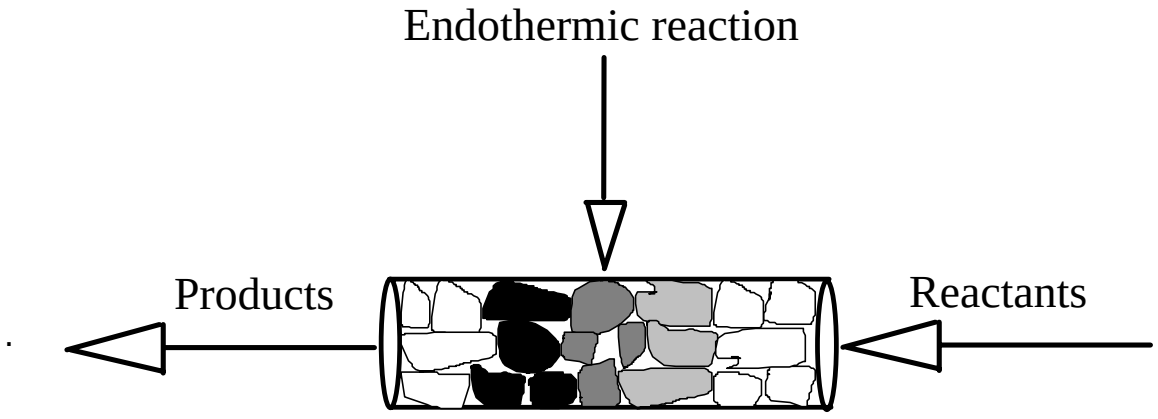

An endothermic reaction occurs from opposite direction in an *asymmetric* fixed-bed reactor during an endothermic semi-cycle

Figure 5.1. A typical operation of an *asymmetric* fixed-bed reactor.

Exothermic: $A \rightarrow C$ $\Delta H_{g,A} < 0$.....(Gas Phase)

Endothermic: $B \rightarrow D$ $\Delta H_{g,B} > 0$.....(Gas Phase)

In the simulation of a RE-GAS type process involving gas phase reactions only, reaction A→C occurs in the gas space of the bed during an exothermic semi-cycle and only reaction $B \rightarrow D$ takes place during an endothermic semi-cycle. Combustion of methane followed by steam reforming of natural gas is a potential example of this type of operation. The solids play the role of a heat reservoir. The heats of exothermic and endothermic reactions are set to be different (Table 5.1) to allow for different front speeds during the exothermic and endothermic semi-cycles. For the details of the model the reader is referred to Chapter 4.

5.3 Differential Creep Velocity and Energy Efficiency

5.3.1 Differential Creep Velocity

The velocity with which the temperature front creeps in a fixed-bed reactor is approximately given by (Rhee et al., 1973)

$$\omega_r = \frac{u\rho_g C_{p,g}}{(1-\varepsilon)\rho_s C_{p,s}}\left(1-\frac{\Delta T_{ad}}{\Delta T_{mx}}\right) = \omega\left(1-\frac{\Delta T_{ad}}{\Delta T_{mx}}\right) \qquad (5.1)$$

Since in the case of an asymmetric fixed-bed reactor $\omega_{r,odd}$ is different from $\omega_{r,even}$ the temperature front experiences a finite displacement between two consecutive cycles. Even if the velocity and physical properties of the reaction mixture for the exothermic and endothermic reactions are approximately the same (i.e. ω—the front velocity that would be observed in a heat regenerator is constant) the front velocity for the

exothermic reaction, $\omega_{r,odd}$, will be different than the front speed for the endothermic reaction, $\omega_{r,even}$, as the adiabatic temperature rise (fall) ΔT_{ad} is different for the two reactions. Moreover, the creeping of the temperature front occurs only for feed temperatures below the initial bed temperature when the maximum transient temperature rise (ΔT_{mx}) exceeds the adiabatic temperature rise for the exothermic reaction (Pinjala et al., 1988; Chapter 4). Approximate expressions for estimation of ΔT_{mx} are provided by Pinjala et al (1988) and Matros (1989). In our study we have used numerically estimated ΔT_{mx} for more accurate estimation of the front velocity ω_r. As the ratio $\Delta T_{ad}/\Delta T_{mx}$ is different for the odd (exothermic) and even (endothermic) semi-cycles a differential creep velocity can be estimated by the following expression (Chapter 4).

$$\omega_{r,diff} = \frac{\omega_{r,odd} \times t^*_{odd} - \omega_{r,even} \times t^*_{even}}{t^*_{odd} + t^*_{even}} \qquad (5.2)$$

For the temperature fronts to remain well within the fixed-bed reactor and not be allowed to escape, the differential creep velocity should be equal to zero. This requirement, based on equation (5.2), results in the following equation:

$$\frac{\omega_{r,odd}}{\omega_{r,even}} = \frac{t^*_{even}}{t^*_{odd}} \qquad (5.3)$$

We will examine in this study whether this criterion must be satisfied for steady periodic operation of an asymmetric fixed-bed reactor.

5.3.2 Energy Efficiency

For a heat regenerator operating in a periodic steady state which involves a heating (odd) semi-cycle and cooling (even) semi-cycle, the energy efficiency is

defined as the ratio of the energy (heat) gained by the cold gases during an even semi-cycle in the bed to the energy (heat) released by the hot gases in an odd semi-cycle i.e.,

$$\eta = \frac{H_{g,even,in} - H_{g,even,out}}{H_{g,odd,in} - H_{g,odd,out}} \tag{5.4a}$$

The purpose of a heat regenerator is to transfer the energy from the hot gases to the cold gases. However, the purpose of the asymmetric operation of a fixed-bed reactor is to utilize the energy provided by the gases during the exothermic semi-cycles to drive the endothermic reaction without allowing the temperature of the exit gases to increase. The energy lost by the hotter exit gases either during the exothermic semi-cycles or during the endothermic semi-cycles indicates the energy that was not utilized to drive the endothermic reaction during the endothermic semi-cycles. This energy which is lost by the hot exit gases decreases the efficiency of an asymmetric fixed-bed reactor. Hence, the efficiency of an asymmetric fixed-bed reactor is defined as

$$\eta = \frac{Q_{endo}}{\left[Q_{exo} + Q_{sn,odd,in}\right]_{T_{ref} = T_{g,in,even}}} \tag{5.4b}$$

This is the generic definition of energy efficiency for an asymmetric fixed-bed reactor. In the case of a heat regenerator, the incoming hot gases have a positive enthalpy (sensible heat only) which is transferred from the hot gases to the cold gases via the inert bed. However, in the case of an asymmetric fixed-bed reactor, we are interested in the in-situ production of heat inside the bed during the exothermic semi-cycle, which is used later to drive the endothermic reaction during the next endothermic semi-cycle. This has an added advantage because, preheating of the incoming gases is

completely eliminated. Hence, to study these effects in the asymmetric fixed-bed-reactor considered in this work, incoming gases are assumed to be cold and are allowed to enter the bed at the same temperature for both semi-cycles. Under these conditions, the energy efficiency depends only on the 'reaction heat' effects rather than on 'non-reactive' sensible heat effects:

$$\eta = \frac{Q_{endo}}{Q_{exo}} \tag{5.4c}$$

At 100% efficiency, which seems like a desirable but elusive goal, the heat of reaction used during an endothermic semi-cycle is equal to that generated in an exothermic semi-cycle i.e.,

$$Q_{exo} = Q_{endo} \tag{5.5}$$

$$\Rightarrow \left[u_{in}\rho_{gm,in}y_{A,in}X_A \Delta H_{g,A} t^*_{odd}\right]_{exo} = \left[u_{in}\rho_{gm,in}y_{B,in}X_B \Delta H_{g,B} t^*_{even}\right]_{endo} \tag{5.6}$$

where $u_{in}\rho_{gm,in}y_{in}$ is the inlet reactant molar flow rate (subscripts and superscripts define the type of reaction and the type of semi-cycle), X is the time averaged conversion during a semi-cycle, ΔH_g is the heat of reaction, and t^*_{odd} and t^*_{even} are the exothermic and the endothermic semi-cycle periods, respectively. Hence, the quantity on the left hand side of equation (5.6) is the total heat released during an exothermic semi-cycle while the quantity on the right hand side of equation (5.6) is the total heat used during an endothermic semi-cycle. The requirement for 100% energy efficiency then results in the need for the following equation to be satisfied:

$$\frac{\left[u_{in}\rho_{gm,in}y_{B,in}X_B \Delta H_{g,B}\right]_{endo}}{\left[u_{in}\rho_{gm,in}y_{A,in}X_A \Delta H_{g,A}\right]_{exo}} = \frac{t^*_{odd}}{t^*_{even}} \tag{5.7}$$

It seems, therefore, that for steady state periodic operation at high conversion and 100% energy efficiency two requirements must be met. First, equation (5.3) has to be satisfied to maintain the temperature front well within the bed. Then, equation (5.7) has to be satisfied to achieve 100% energy utilization. The combination of equations (5.3) and (5.7) results in a single criterion given below:

$$\frac{\left[u_{in}\rho_{gm,in}y_{B,in}X_B(-\Delta H_{g,B})\right]_{endo}}{\left[u_{in}\rho_{gm,in}y_{A,in}X_A(-\Delta H_{g,A})\right]_{exo}} = \frac{\omega_{r,even}}{\omega_{r,odd}} = \frac{t^*_{odd}}{t^*_{even}} \qquad (5.8)$$

It is evident that this equality (equation (5.8)) cannot always be satisfied which leads to less than 100% energy efficiency. For example, if other parameters for two semi-cycles are comparable (inlet molar densities, $\left[\rho_{gm}\right]_{exo}$ and $\left[\rho_{gm}\right]_{endo}$, velocities, $\left[u_{in}\right]_{exo}$ and $\left[u_{in}\right]_{endo}$, mole fractions, $y_{A,in}$ and $y_{B,in}$, and semi-cycle averaged conversions, X_A and X_B), i.e. if $\frac{\left[u_{in}\rho_{gm,in}y_{B,in}X_B\right]_{endo}}{\left[u_{in}\rho_{gm,in}y_{A,in}X_A\right]_{exo}} \approx 1$, then for $\left|\frac{\Delta H_{g,B}}{-\Delta H_{g,A}}\right| < 1$ in order to satisfy equation (5.8) we must have $\frac{\omega_{r,even}}{\omega_{r,odd}} < 1$. This is physically impossible since the expression for the front velocity given by equation (5.1) requires a larger front velocity for the system with the smaller absolute value of the heat of reaction. In the example cited above equation (5.1) requires $\frac{\omega_{r,even}}{\omega_{r,odd}} > 1$ and equation (5.8) cannot be satisfied. Hence, the conditions, $\frac{\left[u_{in}\rho_{gm,in}y_{B,in}X_B(-\Delta H_{g,B})\right]_{endo}}{\left[u_{in}\rho_{gm,in}y_{A,in}X_A(-\Delta H_{g,A})\right]_{exo}} < 1$ and $\frac{\omega_{r,even}}{\omega_{r,odd}} > 1$ lead to the inequality $\frac{\left[u_{in}\rho_{gm,in}y_{B,in}X_B(-\Delta H_{g,B})\right]_{endo}}{\left[u_{in}\rho_{gm,in}y_{A,in}X_A(-\Delta H_{g,A})\right]_{exo}} \neq \frac{\omega_{r,even}}{\omega_{r,odd}}$ and equation (5.8) is not satisfied. The ratio of the semi-cycle periods, $\frac{t^*_{odd}}{t^*_{even}}$ cannot be manipulated arbitrarily

either because it is restricted by the zero differential creep velocity requirement, equation (5.3). Thus, in general, in order to strive for 100% efficiency, the inequality between the ratio of the heat of endothermic and exothermic reaction and the ratio of the front velocities during the endothermic and exothermic part of the cycle has to be compensated by the reactant feed concentrations and conversions during the exothermic and endothermic semi-cycles in order to satisfy equation (5.8). Since conversion in a fixed-bed reactor is a function of the temperature in the bed, which in turn affects the front velocities, it is not easy to find a single manipulated variable to control conversions and efficiency and to satisfy both the 100% energy efficiency criterion (equation (5.7)) and the requirement for zero differential creep velocity (equation (5.3)), i.e., the combination of the two which is equation (5.8). However, we were unable to show that in general equation (5.8) cannot be approached in the limit.

In addition, it should be noted that the assumption of the existence of an unchanging traveling temperature front and constant front velocity is valid only for an infinitely long fixed-bed reactor where end effects are not observed. In a fixed-bed of finite length, a periodic steady state can still be established even when equation (5.3), i.e., the criterion for zero differential creep velocity, is not satisfied. Under these conditions, the temperature front moves to and stays at the feed entrance for all exothermic semi-cycles of the fixed- bed reactor and, hence, the conversion of the endothermic reaction, for which the reactant is introduced from the opposite end, is drastically reduced (Chapter 4).

Many variables such as the ratio of heats of exothermic and endothermic reactions, inlet gas flux and inlet temperature, exothermic and endothermic semi-cycle periods etc. affect the conversions and efficiency in an asymmetric operation of a fixed-bed reactor. Nevertheless, all combinations of these variables lead to only three

sets of conditions that affect reactor performance: i)$Q_{exo} > Q_{endo}$, ii) $Q_{exo} = Q_{endo}$ and iii) $Q_{exo} < Q_{endo}$. These three cases are discussed below.

5.4 Results of Simulation

5.4.1 Case I ($Q_{exo} > Q_{endo}$)

This operation leads to theoretical efficiencies below 100% but it is of interest to examine what can be achieved since this situation is most likely to arise in practice. In the next set of simulations the heat produced in the exothermic semi-cycle is maintained higher than the heat used in the endothermic semi-cycle by satisfying the following constraint:

$$\frac{\left[u_{in}\rho_{gm,in}y_{A,in}X_A(-\Delta H_{g,A})t^*_{odd}\right]_{exo}}{\left[u_{in}\rho_{gm,in}y_{B,in}X_B(-\Delta H_{g,B})t^*_{even}\right]_{endo}} = \frac{Q_{exo}}{Q_{endo}} > 1 \qquad (5.9a)$$

$$\Rightarrow \frac{\left[u_{in}\rho_{gm,in}y_{A,in}X_A(-\Delta H_{g,A})\right]_{exo}}{\left[u_{in}\rho_{gm,in}y_{B,in}X_B(-\Delta H_{g,B})\right]_{endo}} > \frac{t^*_{even}}{t^*_{odd}} \qquad (5.9b)$$

Three subcases can arise in this situation and are discussed below.

5.4.1.1 $\omega_{r,even} \times t^*_{even} = \omega_{r,odd} \times t^*_{odd}$ ($\omega_{r,diff} = 0$)

In Chapter 4, we developed an expression for the zero differential creep velocity ($\omega_{r,diff} = 0$) and showed that for $\omega_{r,diff} = 0$ the temperature front stays well inside the bed at pseudo steady state, using t^*_{odd} = 1000 s (Figure 5.2a). In this work, we study the effect of different semi-cycle periods (t^*_{odd} and t^*_{even}) on the energy efficiency and conversion. For $-\Delta H_{g,A}/\Delta H_{g,B} > 1$, and for comparable mass fluxes and heat capacities of the gases during the exothermic and endothermic semi-cycles ($\left[\rho_{g,in}\right]_{exo} \approx \left[\rho_{g,in}\right]_{endo}$, $\left[u_{in}\right]_{exo} \approx \left[u_{in}\right]_{endo}$ and $\left[C_{p,g}\right]_{exo} \approx \left[C_{p,g}\right]_{endo}$) the zero differential

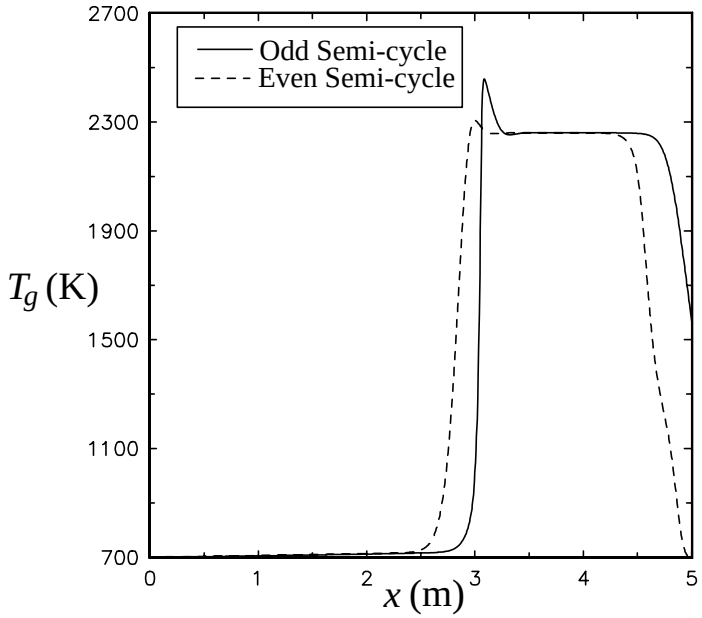

Figure 5.2a. The temperature profiles at the pseudo steady state at the end of exothermic and endothermic semi-cycles for $\omega_{r,odd} \times t^*_{odd} = \omega_{r,even} \times t^*_{even}$ $(\omega_{r,diff} = 0)$.

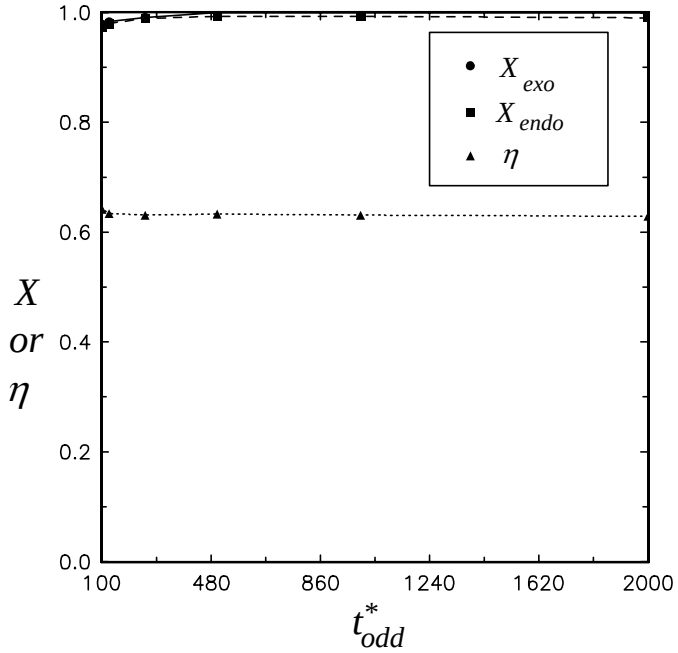

Figure 5.2b. Effect of semi-cycle period on the conversion and energy efficiency at pseudo steady states for $-\Delta H_{g,A} = 2 \times 10^5$ J / mol ; $\Delta H_{g,B} = 1.5 \times 10^5$ J / mol and $t^*_{odd} / t^*_{even} = 1.183$ ($\omega_{r,odd} \times t^*_{odd} = \omega_{r,even} \times t^*_{even}$ $(\omega_{r,diff} = 0)$).

creep velocity criterion can be satisfied only for $t^*_{odd}/t^*_{even} > 1$ (equations (5.1) and (5.3)). This basically means that in spite of the higher heat of the exothermic reaction, which occurs during an exothermic (odd) semi-cycle, the odd semi-cycle period is longer than the even (endothermic) semi-cycle period. This, of course, satisfies the energy constraint, $\frac{Q_{exo}}{Q_{endo}} > 1$ (i.e., equation (5.9)) but causes considerable heat loss during an exothermic semi-cycle. The excess heat is carried out by the hot exiting gases. Since the temperature front stays well within the bed (Figure 5.2a), because equation (5.3) is satisfied ($\omega_{r,diff} = 0$), and more heat is produced during the exothermic semi-cycles than used in the endothermic one, conversions in both reactions are high (nearly unity). Under these conditions, where conversions of both reactions are almost complete, the energy efficiency of the asymmetric process is given by $\eta = \frac{\left[u_{in}\rho_{gm,in}y_{B,in}X_B \Delta H_{g,B} \times t^*_{even}\right]_{endo}}{\left[u_{in}\rho_{gm,in}y_{A,in}X_A \Delta H_{g,A} \times t^*_{odd}\right]_{exo}} = \frac{Q_{endo}}{Q_{exo}}$, and is a constant for a given ratio t^*_{even}/t^*_{odd}. The semi-cycle period has no effect on energy efficiency for a constant t^*_{even}/t^*_{odd} and when conversions in both reactions are almost complete. The results for the conversion in both reactions and for the energy efficiency are presented in Figure 5.2b.

5.4.1.2 $\omega_{r,odd} \times t^*_{odd} > \omega_{r,even} \times t^*_{even} (\omega_{r,diff} > 0)$

We continue considering the case with $\frac{\Delta H_{g,A}}{\Delta H_{g,B}} < 1$ (for example, the heat for the exothermic reaction was -2×10^5 J/mol and the heat of the endothermic reaction was 1.5×10^5 J/mol) and similar physical parameters, $\left[\rho_{g,in}\right]_{exo} \approx \left[\rho_{g,in}\right]_{endo}$, $\left[u_{in}\right]_{exo} \approx \left[u_{in}\right]_{endo}$ and $\left[C_{p,g}\right]_{exo} \approx \left[C_{p,g}\right]_{endo}$ as we did above. In the case considered, $\frac{\omega_{r,odd}}{\omega_{r,even}} \approx 0.85$ which means that the requirement of zero differential creep velocity,

$\omega_{r,diff} = 0$ based on equation (5.3) results in $\frac{t^*_{odd}}{t^*_{even}} \approx 1.18$ which would render this case the same as the one considered above. Here we will consider what happens when differential creep velocity is non zero and positive ($\omega_{r,diff} > 0$) and this also allows us to look at the effect of the ratio of semi-cycle periods on the operation. Here, we set $\frac{t^*_{odd}}{t^*_{even}}$ greater than 1.18 ($\frac{t^*_{odd}}{t^*_{even}} = 1.25 \text{ to } 2.00$). These values of $\frac{t^*_{odd}}{t^*_{even}}$, of course, satisfy $\frac{Q_{exo}}{Q_{endo}} > 1$ (equation (5.9)). Now, because, $\omega_{r,odd} \times t^*_{odd} > \omega_{r,even} \times t^*_{even}$ ($\frac{t^*_{odd}}{t^*_{even}} = 1.25 \text{ to } 2.00$ and $\frac{\omega_{r,odd}}{\omega_{r,even}} \approx 0.85$), during an exothermic semi-cycle the temperature front traverses more distance towards the reactor end which is the exit for the exothermic semi-cycles than the distance it traverses towards the feed entrance for the exothermic semi-cycles during an endothermic semi-cycle (Figure 5.3a). The movement of the front towards the feed entrance for the endothermic semi-cycle (or the exit for the exothermic semi-cycle) is assigned the positive sign. Hence, in this case, after each cycle, the front creeps a distance of $\omega_{r,diff}(t^*_{odd} + t^*_{even})$. This means that after each cycle the front moves a finite distance towards the exit of the exothermic semi-cycles and eventually exits the bed as shown in Figure 5.3a. Hence, even though the energy constraint ($\frac{Q_{exo}}{Q_{endo}} > 1$) is satisfied, periodic operation of the asymmetric fixed-bed reactor is not possible for $\omega_{r,odd} \times t^*_{odd} > \omega_{r,even} \times t^*_{even}$. The bed completely cools down during the periodic steady state under the above mentioned conditions and no reaction can occur in the bed. Figure 5.3b demonstrates this phenomenon. Since the bed is cold and no reaction occurs in the bed, the periodic steady state that is established is trivial and is of no interest.

We have already discussed that for a periodic operation of an asymmetric fixed-bed reactor the energy balance requires that the heat generated during the exothermic

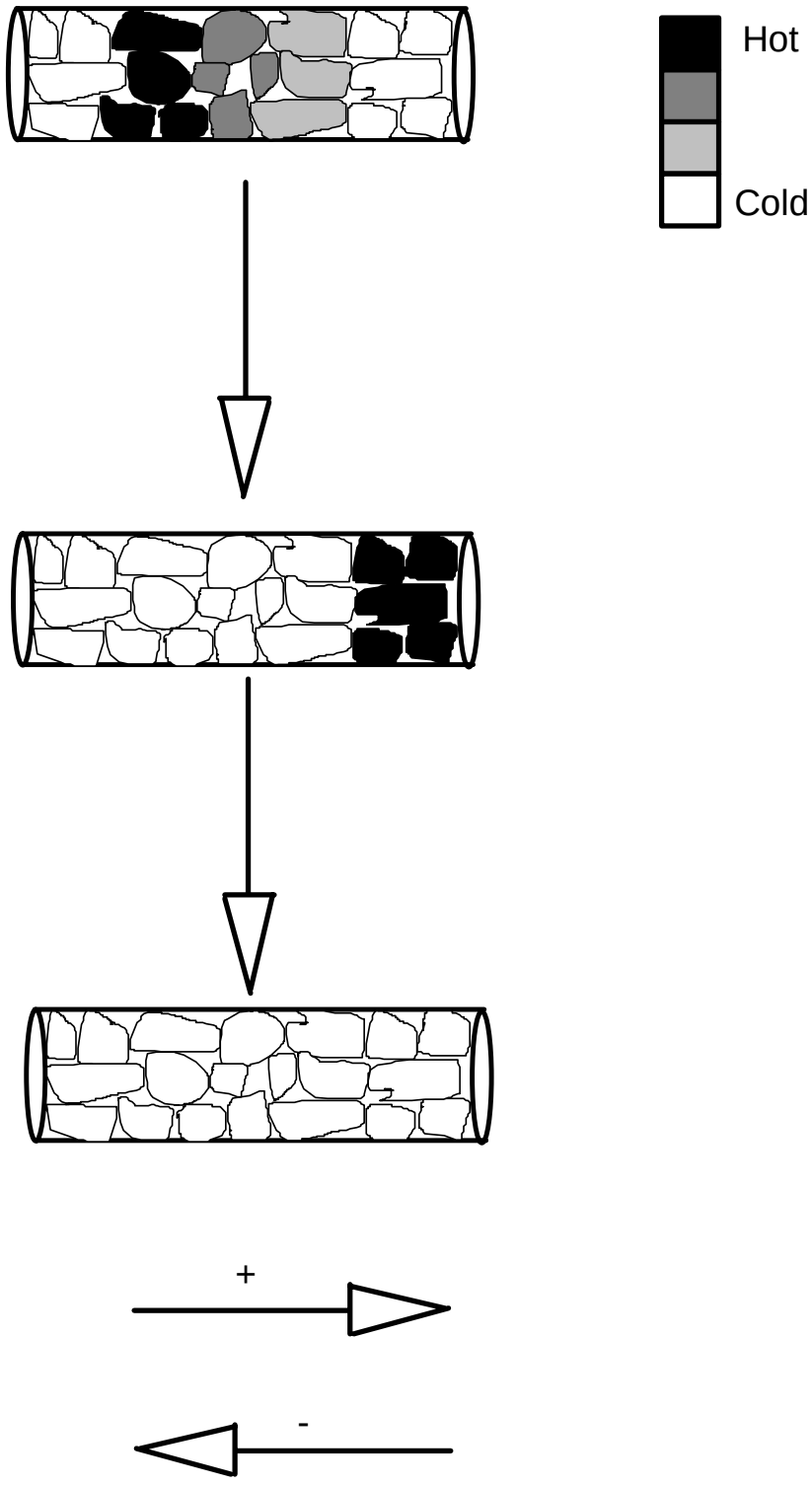

Figure 5.3a. A schematic of the movement of the temperature front in an asymmetric fixed-bed reactor, from the first semi-cycle to the last semi-cycle when the

front exits the bed for $\omega_{r,odd} \times t^*_{odd} > \omega_{r,even} \times t^*_{even} (\omega_{r,diff} > 0)$.

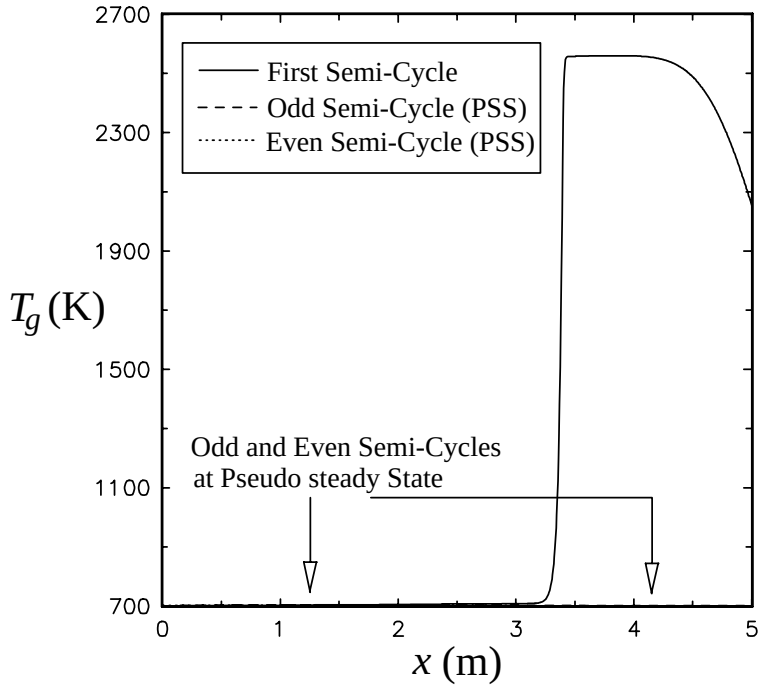

Figure 5.3b. The temperature profiles at the beginning and at the pseudo steady state for $\omega_{r,odd} \times t^*_{odd} > \omega_{r,even} \times t^*_{even} (\omega_{r,diff} > 0)$ (cold bed at pseudo steady state).

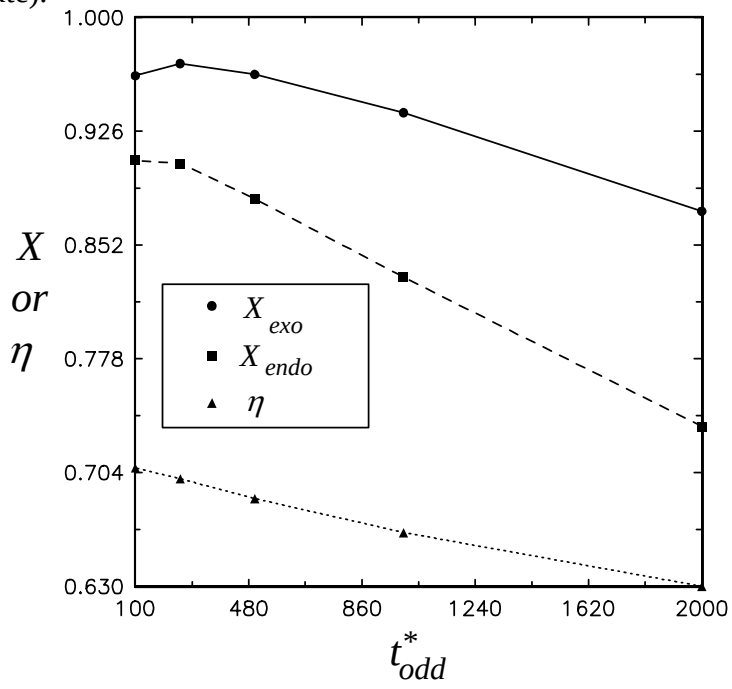

Figure 5.4. Effect of semi-cycle period on the conversion and energy efficiency at pseudo steady states for $-\Delta H_{g,A} = 2 \times 10^5$ J / mol; $\Delta H_{g,B} = 1.5 \times 10^5$ J / mol

and $t^*_{odd}/t^*_{even} = 1.00$ ($\omega_{r,even} \times t^*_{even} > \omega_{r,odd} \times t^*_{odd} (\omega_{r,diff} < 0)$).

semi-cycles should be equal to or greater than the heat utilized during the endothermic semi-cycles ($\frac{Q_{exo}}{Q_{endo}} \geq 1$) i.e., either equation (5.7) or equation (5.9) has to be satisfied.

This leads to the following conclusion. When the heat of the exothermic reaction is smaller than the heat of the endothermic reaction ($\frac{\left(-\Delta H_{g,A}\right)}{\left(\Delta H_{g,B}\right)} < 1$), in order to satisfy the energy criterion, $\frac{Q_{exo}}{Q_{endo}} \geq 1$, the ratio of the semi-cycle periods, $\frac{t^*_{odd}}{t^*_{even}}$ should be greater than one (equation (5.9)) and from equation (5.1), it follows that $\frac{\omega_{r,odd}}{\omega_{r,even}} > 1$ under these conditions. Hence, to satisfy the energy criterion it is required that in general $\omega_{r,odd} \times t^*_{odd} > \omega_{r,even} \times t^*_{even}$. We have just illustrated that for $\omega_{r,diff} > 0$, a periodic operation of asymmetric fixed-bed reactor is not possible and this implies that whenever the heat of the exothermic reaction is smaller than the heat of the endothermic reaction, a trivial periodic steady state exists where bed becomes completely cold and no reaction can occur in the bed. A series of simulations were performed for $\frac{\left(-\Delta H_{g,A}\right)}{\left(\Delta H_{g,B}\right)} < 1$ and of course only trivial periodic steady states could be reached.

5.4.1.3 $\omega_{r,even} \times t^*_{even} > \omega_{r,odd} \times t^*_{odd} (\omega_{r,diff} < 0)$

We examine now the situation for the negative differential creep velocity and of course still must maintain $\frac{\left(-\Delta H_{g,A}\right)}{\left(\Delta H_{g,B}\right)} > 1$ so that we choose $\Delta H_{g,A} = -2.0 \times 10^5$ J / mol and $\Delta H_{g,B} = 1.5 \times 10^5$ J / mol. Then $\frac{t^*_{odd}}{t^*_{even}}$ was chosen such that $\omega_{r,even} \times t^*_{even} > \omega_{r,odd} \times t^*_{odd}$. Since $\frac{\omega_{r,odd}}{\omega_{r,even}} \approx 0.85$, this can be accomplished for any

$\frac{t^*_{odd}}{t^*_{even}} < 1.18$. A series of simulations for $\frac{t^*_{odd}}{t^*_{even}} = 1.00$ were performed and the results are shown in Figure 5.4 for the dependence of conversions and energy efficiency on the duration of semi-cycle periods at fixed $t^*_{odd} / t^*_{even} = 1$. It can be observed that conversions for both the exothermic and the endothermic reaction, as well as the energy efficiency, increase with decreasing semi-cycle periods. For short switching periods the energy loss via exiting gases is low which increases the energy efficiency and conversions for both reactions. Since the endothermic reaction can occur only at high temperatures, and now does not go to completion, heat is lost through the outgoing gases which are hot enough to carry the energy from the bed but not hot enough to complete the reaction. Thus, the shorter the semi-cycle period, the smaller is the heat loss and the higher is the energy efficiency.

This illustrates that it is possible to operate at periodic steady state even when the zero differential creep velocity criterion is not satisfied. That is because, in this case $\omega_{r,even} \times t^*_{even} > \omega_{r,odd} \times t^*_{odd}$.(i.e., $\omega_{r,diff} < 0$), which means that during an endothermic semi-cycle the front traverses more distance towards the feed entrance for the exothermic semi-cycles than the distance it traverses towards the exit for the exothermic semi-cycles during an exothermic semi-cycle. If this phenomenon continued through repeated cycles, the front would escape from the feed entrance for the exothermic semi-cycles. However, for endothermic semi-cycle periods that are not excessively long, not all of the high temperature front escapes, and a substantial portion of the temperature front persists at the feed entrance for the exothermic semi-cycles. A schematic of the temperature front movement in the bed is shown in Figure 5.5. The actual temperature profiles at the pseudo steady state for one such operation where $\omega_{r,even} \times t^*_{even} > \omega_{r,even} \times t^*_{odd}$ are shown in Figure 5.6. The pseudo steady state temperature profile at the end of the exothermic semi-cycle is given by the dashed line

and the pseudo steady state temperature profile at the end of the endothermic semi-cycle is given by the dotted line. The distance between these two temperature fronts is

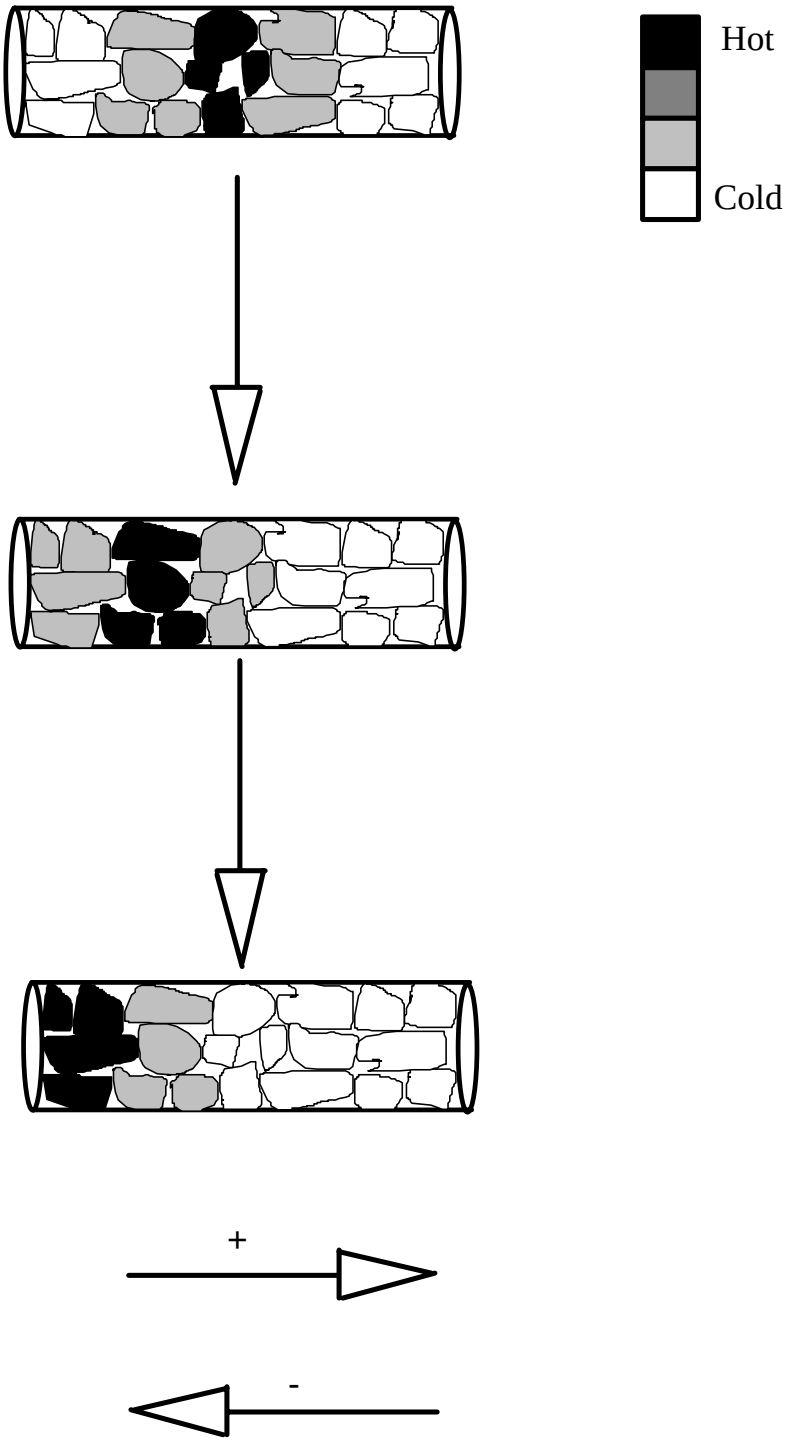

Figure 5.5. A schematic of the movement of the temperature front in an asymmetric fixed-bed reactor, from the first semi-cycle to a pseudo steady state when

the front persists at the entrance of the bed for $\omega_{r,even} \times t^*_{even} > \omega_{r,odd} \times t^*_{odd} (\omega_{r,diff} < 0)$.

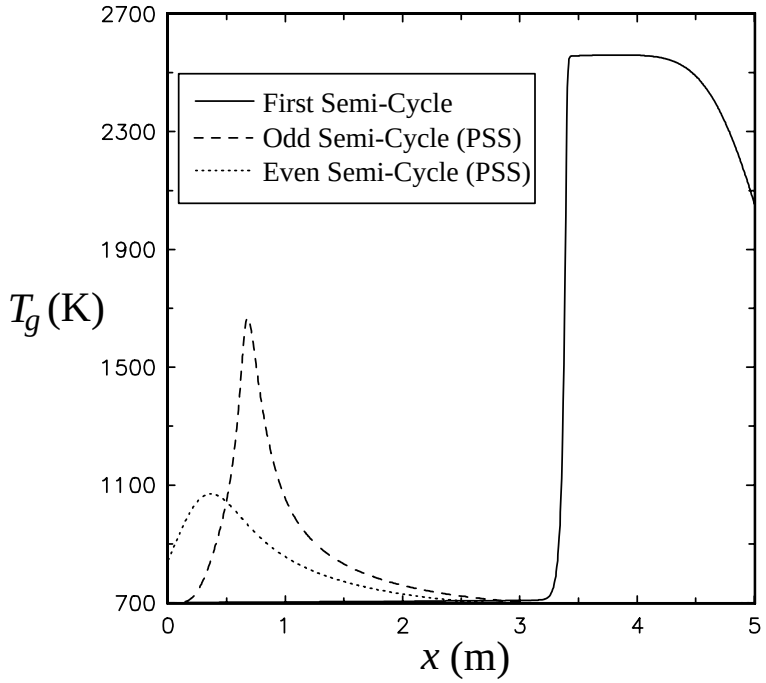

Figure 5.6. The temperature profiles in the beginning and at the pseudo steady state at the end of exothermic and endothermic semi-cycles for $\omega_{r,even} \times t^*_{even} > \omega_{r,odd} \times t^*_{odd} (\omega_{r,diff} < 0)$ (PSS: Pseudo steady state).

equal to the distance traveled by the front in one semi-cycle ($\omega_r \times t^*$). The existence of periodic steady state was tested by comparing the temperature and concentration profiles at the end of two subsequent exothermic and endothermic semi-cycles. The exothermic reaction, which follows the endothermic reaction, can still be ignited and occurs in the bed to heat up the bed. This allows the endothermic reaction to occur again in the next semi-cycle. Conversion for both reactions varied from 0.5 to 0.85 depending upon the semi-cycle periods.

5.4.1.4 Effect of the Bed Length

The model was solved using $-\Delta H_{g,A} = \Delta H_{g,B} = 2 \times 10^5$ J / mol and $t^*_{odd} / t^*_{even} = 1$ for different values of t^*_{odd}, t^*_{even} and reactor lengths. Thus, in both cases (L =5 m and

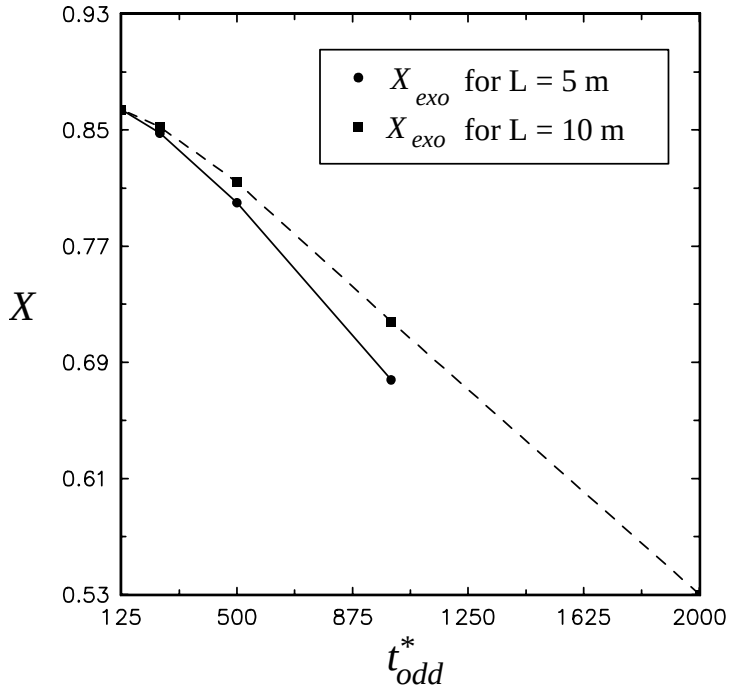

Figure 5.7a. Effect of semi-cycle period and reactor length on the conversion of exothermic reaction for $-\Delta H_g = \Delta H_g^{'} = 2 \times 10^5$ J / mol and $t^*_{odd} / t^*_{even} = 1$ (pseudo steady states).

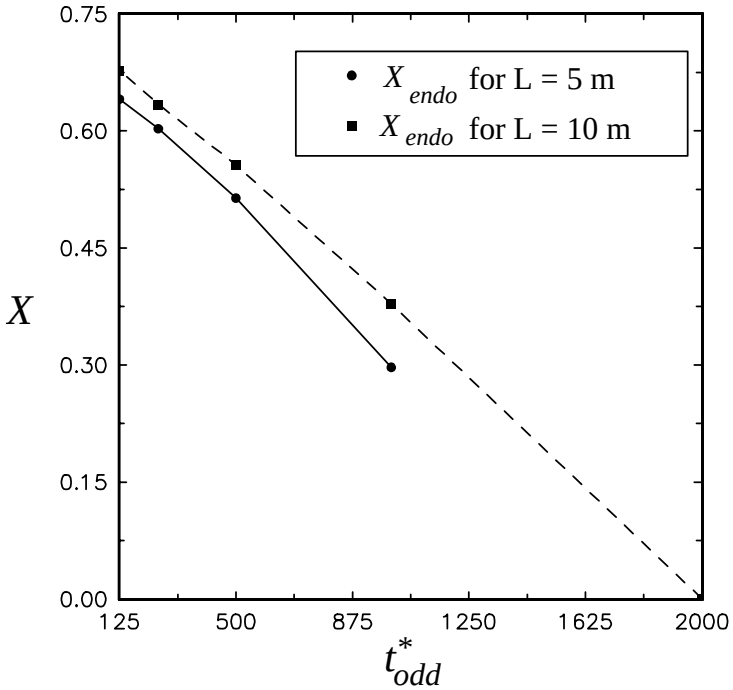

Figure 5.7b. Effect of semi-cycle period and reactor length on the conversion of endothermic reaction for $-\Delta H_g = \Delta H_g^{'} = 2 \times 10^5$ J / mol and $t^*_{odd} / t^*_{even} = 1$ (pseudo steady states).

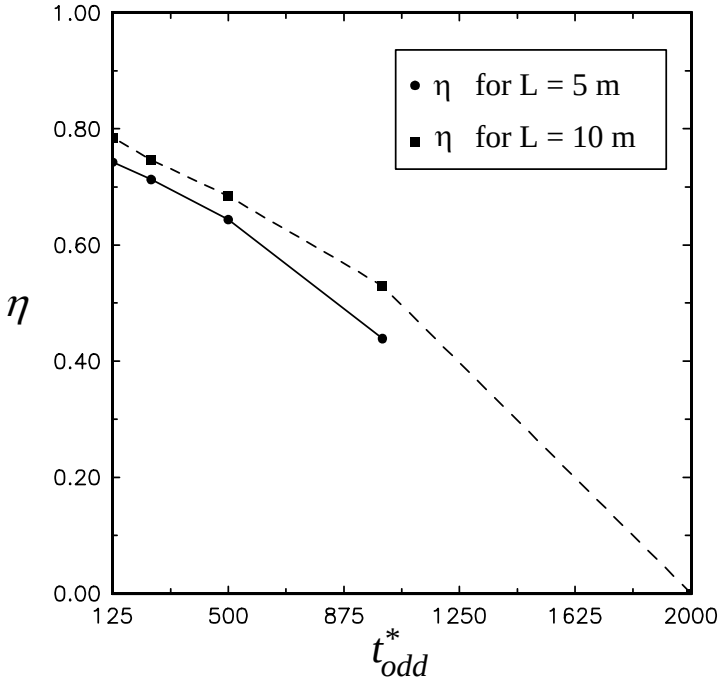

Figure 5.7c. Effect of semi-cycle period and reactor length on the energy efficiency for $-\Delta H_g = \Delta H_g^{'} = 2\times10^5$ J / mol and $t^*_{odd} \big/ t^*_{even} = 1$ (pseudo steady states).

10 m) the criterion for zero differential creep velocity is satisfied. Energy efficiency was below 100% because conversion for the exothermic reaction was greater than the conversion for the endothermic reaction ($X_A > X_B$). The results are presented in Figures 5.7a, 5.7b and 5.7c. As expected, conversions and energy efficiency increase with decreasing semi-cycle periods. However, both conversions and energy efficiency are higher for the longer reactor because of the longer residence time. Since conversions are below unity, reaction is not instantaneous and higher residence time increases the conversion.

5.4.2 Case II ($Q_{exo} = Q_{endo}$)

Theoretically this situation would lead to 100% energy efficiency and we want to examine to what extent can this limit be approached. For a given exothermic and

endothermic reactions, to achieve this case, one would have to operate both exothermic and endothermic semi-cycles at identical conditions. Hence, the above discussed model was solved for the values of parameters shown in Table 1, which are identical for both exothermic and endothermic semi-cycles except for the heats of reactions ($-\Delta H_{g,A} = \Delta H_{g,B} = 2 \times 10^5$ J / mol) using $t^*_{odd} / t^*_{even} = 1$ for different values of the semi-cycle periods, t^*_{odd} and t^*_{even}. If the average conversions over the semi-cycle periods of the exothermic and endothermic reactions are equal ($X_A = X_B$), then the criterion for 100% energy efficiency (equation (5.7)) is satisfied. At the same time the zero differential creep velocity criterion (equation (5.3)) is satisfied and, hence, equation (5.8) holds. However, because of the difference in kinetic parameters of the two reactions (it is practically impossible that two different reactions have equal rates at all temperatures), the average rates of the endothermic and the exothermic reaction are different, which results in unequal average conversions for the exothermic and endothermic reactions ($X_A > X_B$) and, hence, equations (5.7) and (5.8) are not satisfied and the process is less than 100% energy efficient. One way to compensate for the difference in conversions is to manipulate the semi-cycle periods. However, as mentioned before, the ratio $\frac{t^*_{odd}}{t^*_{even}}$ is determined by equation (5.3) to satisfy $\omega_{r,diff} = 0$ and, cannot be varied arbitrarily in order to satisfy the 100% energy efficiency criterion, equation (5.7). Therefore, it can be seen that unless the reactions are nearly identical in nature, which is not the case here, it is not possible to satisfy equation (5.7) (i.e., $Q_{exo} = Q_{endo}$) in order to reach 100% energy efficiency.

5.4.3 Case III ($Q_{exo} < Q_{endo}$)

For $Q_{exo} < Q_{endo}$ energy efficiency exceeds 100% and the first law of thermodynamics is violated. Clearly, a steady state periodic operation of an

asymmetric fixed-bed reactor cannot exist under such conditions. Hence, we simply illustrate the physical situations that unfortunately may lead to this case.

Generally, when the heat of exothermic reaction is smaller than the heat of endothermic reaction (i.e. $\frac{-\Delta H_{g,A}}{\Delta H_{g,B}} < 1$), one gets $Q_{exo} < Q_{endo}$ i.e. $\frac{\left[u_{in}\rho_{gm,in}y_{A,in}\left(-\Delta H_{g,A}\right)\right]_{exo}}{\left[u_{in}\rho_{gm,in}y_{B,in}\left(\Delta H_{g,B}\right)\right]_{endo}} < 1$. An asymmetric process was simulated at such conditions and for different semi-cycle periods all of which satisfy the criterion for zero differential creep velocity (equation (5.3)). Based on the expressions for front velocity and zero differential creep velocity, equations (5.1) and (5.3) respectively, for $-\Delta H_{g,A}/\Delta H_{g,B} < 1$, $\omega_{r,odd}/\omega_{r,even} > 1$ we must maintain $t^*_{odd}/t^*_{even} < 1$ provided other parameters such as heat capacities ($\left[C_{p,g}\right]_{exo}$ and $\left[C_{p,g}\right]_{endo}$) and inlet mass fluxes ($\left[u_{in}\rho_{g,in}\right]_{exo}$ and $\left[u_{in}\rho_{g,in}\right]_{endo}$) are comparable for both the exothermic and endothermic semi-cycles, as is the case here. Under such conditions, generally, $\frac{\left[u_{in}\rho_{gm,in}y_{A,in}X_A\left(-\Delta H_{g,A}\right)\times t^*_{odd}\right]_{exo}}{\left[u_{in}\rho_{gm,in}y_{B,in}X_B\left(\Delta H_{g,B}\right)\times t^*_{even}\right]_{endo}} = \frac{Q_{exo}}{Q_{endo}} < 1$, provided X_A does not exceed X_B greatly. The only situation when X_A may far exceed X_B is if we are conducting a very slow and temperature insensitive endothermic reaction, in which case reaction coupling in this type of operation would be extremely inefficient and ill advised. Hence, in realistic situations the above choice of parameter values leads to $\frac{Q_{exo}}{Q_{endo}} < 1$.

Since more heat is removed in an endothermic semi-cycle than what is produced in an exothermic semi-cycle, the bed cools down in subsequent semi-cycles and ultimately no reaction occurs. This illustrates that an exothermic and endothermic reaction cannot be coupled by manipulating the semi-cycle periods if $-\Delta H_{g,A}/\Delta H_{g,B} < 1$ which was also shown in sub case 2 of case I.

5.4.4 A Necessary Condition for Periodic Operation

Finally, the asymmetric process was simulated using $\frac{\left[u_{in}\rho_{gm,in}y_{A,in}X_A(-\Delta H_{g,A})\right]_{exo}}{\left[u_{in}\rho_{gm,in}y_{B,in}X_B(-\Delta H_{g,B})\right]_{endo}} > 1$ for different t^*_{even}/t^*_{odd}. The range of operability is shown in Figure 5.8. When $t^*_{odd}/t^*_{even} << 1$, the energy constraint, $\frac{Q_{exo}}{Q_{endo}} \geq 1$ (equation (5.9) or equation (5.7)) is not satisfied because energy requirement of the endothermic semi-cycle is greater than the energy supply from the exothermic semi-cycle. Hence, eventually bed cools down and no reaction can occur in the bed (region I). For $t^*_{odd}/t^*_{even} >> 1$, although the energy constraint ($\frac{Q_{exo}}{Q_{endo}} > 1$) is met because the exothermic semi-cycles are longer than the endothermic semi-cycles, the criterion for zero creep velocity, $\omega_{r,diff} = 0$ (equation 3) is not satisfied and the front gradually creeps towards the exit for the exothermic semi-cycles when $\omega_{r,diff} > 0$, i.e., $\omega_{r,odd} \times t^*_{odd} > \omega_{r,even} \times t^*_{even}$ and escapes from the bed (region III). Hence, at the trivial periodic steady state, no reaction occurs in the bed and the bed becomes completely cold. Simulation results for this case are shown in Figure 5.3b which demonstrates this phenomenon. However, when t^*_{even}/t^*_{odd} is such that $\omega_{r,even} \times t^*_{even} > \omega_{r,odd} \times t^*_{odd}$ and $\frac{Q_{exo}}{Q_{endo}} \geq 1$ i.e. when the differential creep velocity is either negative or zero and, heat generated during the exothermic semi-cycle is greater than the heat requirement of the endothermic semi-cycle (region II), the front would have moved towards the feed entrance for the exothermic semi-cycles (Figure 5.6), and extinction can occur only for very long endothermic semi-cycle periods. This is because during an endothermic semi-cycle a significant portion of the high temperature front persists for a long time at the feed entrance for the exothermic semi-cycle, and the exothermic reaction can ignite to heat

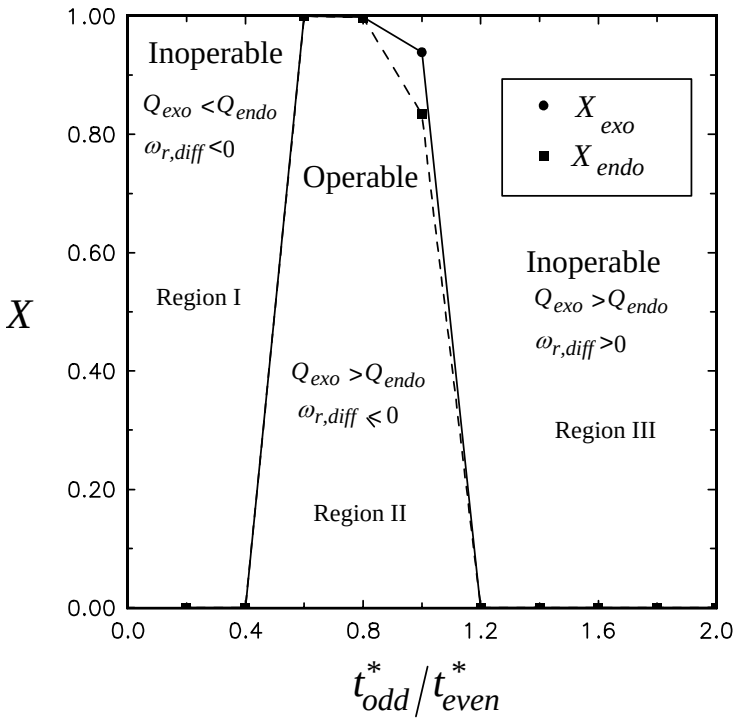

Figure 5.8. Effect of t^*_{odd}/t^*_{even} on the conversion at pseudo steady states for $-\Delta H_g = 2\times10^5$ J / mol; $\Delta H_g^{'} = 1.5$ J / mol and $t^*_{odd} = 1000$ s.

up the bed again during the next exothermic semi-cycle. Also the front speed is defined only in the asymptotic sense, when the bed is infinitely long, and, hence, expressions for the front velocity are not valid at the either end of the bed. However, if the front escapes out of the exit for the exothermic semi-cycle, i.e., when $\omega_{r,even} \times t^*_{even} < \omega_{r,odd} \times t^*_{odd}$, eventually both reactions go to extinction because the endothermic reaction, which starts at that particular end of the reactor, cannot increase the temperature in the bed. It can be seen that in every case an asymmetric process can be successfully operated only when the energy constraint, $\frac{Q_{exo}}{Q_{endo}} \geq 1$ (equation (5.9) or equation (5.7)) is satisfied.

Based on the above observations it can be concluded that for an asymmetric process to operate in a periodic steady state the necessary conditions to be satisfied are:

$$\frac{\left[u_{in}\rho_{gm,in}y_{A,in}X_A(-\Delta H_{g,A})(t^*_{odd})\right]_{exo}}{\left[u_{in}\rho_{gm,in}y_{B,in}X_B(-\Delta H_{g,B})(t^*_{even})\right]_{endo}} = \frac{Q_{exo}}{Q_{endo}} \geq 1$$

and

$$\frac{\omega_{r,odd}}{\omega_{r,even}} \leq \frac{t^*_{even}}{t^*_{odd}} \qquad (5.10)$$

5.5 Conclusions

In a periodically operated asymmetric fixed-bed reactor, conversions for the exothermic and endothermic reactions, each taking place during a semi-cycle, and the energy efficiency increase with decreasing semi-cycle periods until complete conversions are reached. Conversions in both reactions and energy efficiency increase with increasing bed length. It is not always possible to satisfy both the criterion for zero creep velocity (equation(3)) and the energy criterion ($Q_{exo}/Q_{endo} \geq 1$) which requires that the inequality of the ratio of heats of reactions be compensated by adjusting the duration of semi-cycle periods based on equation (5.10). Obviously, the energy criterion has to be satisfied for any asymmetric process to operate in a periodic steady state. Under certain circumstances, when $\omega_{r,even} \times t^*_{even} > \omega_{r,odd} \times t^*_{odd}$ ($\omega_{r,diff} < 0$) and the reaction front moves towards the feed entrance for the exothermic semi-cycles, an asymmetric process can be operated at periodic steady state even when differential creep velocity is finite ($\omega_{r,diff} < 0$). However, for $\omega_{r,diff} > 0$ the temperature front escapes the bed from the exit for the endothermic semi-cycle and no reaction can occur in the bed. The necessary condition for periodic operation of an asymmetric fixed-bed reactor requires that the distance traversed by the front during the endothermic semi-cycle must be equal to or greater than the distance traversed by the front during the exothermic semi-cycle, i.e., for a non trivial periodic steady state to

exist, the differential creep velocity should be zero or negative. When $\omega_{r,diff} = 0$ the hot front and the high temperature zone stay well within the bed allowing higher conversions during the periodic steady state. When conversions for both exothermic and endothermic reactions are complete, the energy efficiency is a constant which is affected only by the ratio of the exothermic and endothermic semi-cycle periods and not by the magnitude of the individual semi-cycle periods. When $\omega_{r,diff} < 0$, the front gradually moves towards the entrance for the exothermic reaction and establishes itself at the edge of the bed during the periodic steady state. Hence, during the endothermic semi-cycle, the hot zone quickly moves out of the bed leading to a decrease in the conversion for the endothermic reaction.

Table 5.1: Parameters Used for Simulation.

Parameter	Value
$T_{g,in}$ (K)	700
$T_{g,0}$ (K)	1000
$T_{s,0}$ (K)	1000
y_{in}	0.1
y,	variable
k_0 (s^{-1})	1.0×10^5
Ea (J/mol)	1.0×10^5
ΔH_A(J/mol)	Reported in the paper
ΔH_B (J/mol)	Reported in the paper
h ($J/m^2.K.s$)	100
C_p (J/kg.K)	1000
ρ_S (kg/m^3)	3000
a_p (m^2/m^3)	300
u_{in} (m/s)	1
P (Pa)	1.013×10^5
L (m)	5
ε	0.5
M_w	28

6. PRODUCTION OF SYNTHESIS GAS IN AN ASYMMETRIC BED—THE RE-GAS PROCESS

The production of synthesis gas by the reaction between methane and steam is an endothermic reaction. An approach to produce synthesis gas by coupling the endothermic steam reforming reaction with exothermic methane combustion in an asymmetric fixed-bed reactor is discussed. Exothermic methane combustion takes place in the bed during an *exothermic (odd) semi-cycle* when a mixture of methane and air is fed into the hot bed. The heat generated by the exothermic reaction is then utilized to drive the endothermic steam reforming reaction which occurs during the next *endothermic (even) semi-cycle* when a mixture of steam and methane is fed into the bed from the other end of the reactor. The maximum transient temperature rise is greater than the adiabatic temperature rise in the bed for the feed gas temperature below the initial bed temperature and a periodic process involving this *wrong-way behavior* is called the *wrong-way process* (Chapter 3). Theoretically this phenomenon is always observed when the rate of heat generation due to reaction is much lower than the rate of heat transfer between gases and solids i.e. when the gases are heated by the solids before the reaction goes to completion. However, practically this is possible only when the inlet gas temperature is below the ignition temperature. The maximum temperature for the steam reforming processes discussed in the literature is around 1500 K (Blanks et al., 1990; Ferreira, et al., 1992; Wagner and Froment, 1992). Hence we set 1500 K as the maximum allowable temperature for our simulations. Therefore it is required to use a low concentration of the fuel to control the maximum temperature around 1500 K. However, for very low fuel concentrations the heat generated by the exothermic reaction is lower than the heat requirement of the endothermic reaction and hence no reaction can occur in the bed. In *the normal process*, the feed gas temperature for the exothermic semi-cycle is maintained equal to

or above the initial bed temperature (at the beginning of the process) where the reaction can self sustain, for accurate temperature control and sufficient production of heat. During the first semi-cycle the maximum temperature rise in the bed is equal to the adiabatic temperature rise. However, during the subsequent semi-cycles the maximum temperature rise in the bed increases beyond the adiabatic temperature rise because, during endothermic semi-cycles the hot temperature zone is pushed toward the entrance for the exothermic semi-cycles (Chapter 4). During the subsequent exothermic semi-cycles, although the incoming fuel+air mixture is at a temperature where reaction is self sustained, the temperature of the bed near the entrance region is hotter and thus the bed shows the wrong-way behavior. However, the maximum temperature in the bed can be maintained around the adiabatic temperature which is below the maximum allowable temperature, when the heat generation rate due to reaction is much higher than the rate of heat transfer from solids to the gases. This is achieved by manipulating the feed gas temperature such that the reaction rates at the entrance of the bed are much higher than the heat transfer rates. Since the wrong-way process does not alter the energy requirement of the endothermic reaction and increases the temperature rise in the bed beyond a tolerable limit, the advantages of the wrong-way process cannot be utilized in the production of synthesis gas. The energy efficiency of the normal process can be improved by recycling the heat.

6.1 Introduction

Hydrogen and carbon monoxide are extensively used in the production of variety of chemicals. For example, hydrogen is used in the production of ammonia, methanol, and petroleum refining. Production of paints, pesticides, insecticides, plastics, foams and variety of other organic compounds are produced using carbon monoxide. The popular methods of production of CO and H_2 are:

1) Steam reforming (primary and secondary) of hydrocarbons

2) Partial oxidation of hydrocarbons

3) Coal gasification

Reactions that produce CO and H_2 are endothermic in nature and hence all of the above processes require external or auto thermal heat supply. Partial oxidation derives the heat from partial oxidation of hydrocarbon fuel. Coal gasification also derives the required heat from the partial combustion. The primary steam reforming involves the reaction between methane and steam to produce synthesis gas in a shell and tube configuration. The endothermic steam reforming takes place in the tubes while a fossil fuel is combusted outside to supply heat (Wagner and Froment, 1992). However, this process is not very efficient due to low heat transfer rates. Also, there is the additional problem of coke deposition at high concentrations of the hydrocarbon feed. Steam reforming of hydrocarbon fuels has been studied extensively by Mond and Langer (1888), Twigg (1989), Rostrup-Nielsen (1975, 1984) and Van Hook (1980), as mentioned in Wagner and Froment (1992).

Blanks et al. (1990) used an auto thermal reactor in the production of synthesis gas by partial oxidation of methane. The heat required for the production of synthesis gas is provided by the partial oxidation of methane. Thus, endothermic steam reforming and exothermic partial oxidation of methane occur simultaneously in the same space in an a periodically operated auto thermal fixed-bed reactor. They first establish an inverted 'U' shaped temperature profile by introducing and burning methane+air mixture at the center of the initially cold reactor. Then catalytic partial oxidation and synthesis gas production takes place in the bed with the reactants fed from one end of the bed. The reactants get heated as they enter the bed and the reaction occurs at the hot zone and products are cooled before they leave the reactor. After a certain time, the reactants are fed from the other end of the reactor to push the

inverted 'U' shaped temperature profile back into the bed. This process is quite efficient but encounters coke deposition problems.

6.1.1 The *RE-GAS* Process

Levenspiel (1988) proposed the *RE-GAS* process to produce synthesis gas. The process involves coupling of endothermic steam reforming reaction with exothermic combustion reaction using a fixed-bed. During an exothermic semi-cycle exothermic reaction heats the bed. During and endothermic semi-cycles the endothermic steam reforming takes place in the bed with reactants, steam and methane fed from the opposite end. Thus each cycle involves an exothermic and an endothermic semi-cycle (Figure 5.1). After repeated cycles the bed operates in a periodic steady state. The coke that is deposited during the endothermic semi-cycle is completely burnt during the exothermic semi-cycle. Here steam reforming and combustion are indirectly coupled in the sense that they do not occur simultaneously in the same space. There have been no cited studies in the literature to explore the possibilities of producing synthesis gas by the RE-GAS process. Since this process offers unique possibility of auto thermal coupling of steam reforming reaction with hydrocarbon combustion along with possible solution to the coke deposition, a preliminary study of this process is required.

6.2 Reactions, Kinetics, and Physical Parameters

6.2.1 Reactions and Kinetics

Methane is the major constituent of natural gas which is extensively employed in the production of synthesis gas by steam reforming. The main reactions are:

$$CH_4 + H_2O \Leftrightarrow CO + 3H_2 \qquad \Delta H = 2.06 \times 10^5 \text{ J / mol}$$
$$CO + H_2O \Leftrightarrow CO_2 + H_2 \qquad \Delta H = -4.12 \times 10^4 \text{ J / mol}$$

The process is globally endothermic because the endothermicity of the first reaction is larger than the exothermicity of the second reaction. The process involves many elementary steps and the detailed kinetics is very elaborate. The focus of this study is to gain a physical insight in the RE-GAS process by mathematical simulation which involves long and tedious computations. Hence, to gain the fundamental understanding of the process a simple global kinetics suggested by Bodrov et al. (1964, 1967) (as reported in Ferreira et al., 1992) is used. The global kinetics is given by,

$$(-r_{s,CH_4}) = \Psi k_{0,s,CH_4} T_s e^{(Ea_{s,CH_4}/RT_s)} C_{CH_4} \text{ mol / m}^3\text{.s}$$

Where Ψ is the global effectiveness factor.

Methane combustion with air has been extensively studied in the literature. The combustion of methane also involves many elementary reactions. However, a global reaction scheme can be written as

$$CH_4 + 2O_2 \rightarrow 2H_2O + CO_2 \qquad \Delta H = -8.02703 \times 10^5 \text{ J / mol}$$

As mentioned before, the focus of this study is to gain the physical insight into the RE-GAS process and not to simulate the kinetics in great detail. A simple global kinetics which represents the kinetics of the combustion process fairly accurately suffices for our current study. In this study we have used the global kinetic expression for methane combustion given by Mulholland et al. (1993).

$$(-r_{g,CH_4}) = k_{0,g,CH_4} e^{(Ea_{g,CH_4}/RT_g)} C_{CH_4} C_{O_2} \text{ mol / m}^3\text{.s}$$

6.2.2 Physical Parameters

Simulation of the RE-GAS process requires estimation of several physical parameters. Heat transfer coefficients, thermal conductivities, viscosity, mass and heat

dispersion coefficients for the gas and the solid phases and effectiveness factors are required for the simulation of the process. Considering the nature of the simulation most of the properties are estimated at a representative temperature. $C_{p,g}$, $C_{p,s}$, ρ_g, ρ_s were estimated using Perry and Green (1984). The gas density is calculated using the ideal gas law. Thermal conductivity of the gas was estimated using Euken Correlation (Perry and Green, 1984). Physical properties of the alumina support are used as the representative properties of the catalyst. The semi-empirical correlation for heat transfer coefficient proposed by Kunii and Levenspiel (Levenspiel, 1983) is used.

$$Nu = 2.0 + 1.8\,\mathrm{Re}^{0.5}\,\mathrm{Pr}^{0.33}$$

where $Nu = \dfrac{hd_p}{\lambda_g}$; $\mathrm{Re} = \dfrac{d_p u \rho}{\mu}$; $\mathrm{Pr} = \dfrac{C_{p,g}\mu}{\lambda_g}$

Viscosity is calculated using the Chapman-Enskog theory of gases (Reid et al., 1987)

$$\mu = \frac{26.99(M_w T_g)^{0.5}}{\sigma_p{}^2 \Theta_v} \times 10^{-17} \qquad \mathrm{kg/m.s}$$

Effective thermal conductivity or the solid heat dispersion coefficient is estimated using

$$D_{e,s,h} = \varepsilon\lambda_g + (1-\varepsilon)\lambda_s \frac{1}{1+\phi\dfrac{\lambda_s}{\lambda_g}}$$ (Kunii and Smith, 1960; Yakae and Kunii, 1960).

Edwards and Richardson (1968) correlated the mass dispersion coefficient as

$$D_{e,g,ms} = 0.73D_{g,m} + \frac{0.5ud_p}{1+\dfrac{9.7D_{g,m}}{ud_p}} \quad \begin{pmatrix} 0.008 < \mathrm{Re} < 50 \\ 0.0377 < d_p < 0.60 \text{ cm} \end{pmatrix}.$$

For the particle diameter and Reynolds number beyond the range indicated above, the chart given by Levenspiel (1973) is used to estimate the mass dispersion coefficient in the gas phase.

An expression for effective thermal diffusivity for the gas in a heat regenerator was derived by Babcock et al. (1966). The thermal diffusivity is given by

$$TD_{e,g,h} = \frac{D_{g,eddy}\varepsilon + \lambda_g \varepsilon + f_{(ha)} + f_{s(ha)}}{\rho_{g,} C_{p,g}\varepsilon + \rho_s C_{p,s}(1-\varepsilon)} \text{ where}$$

$$f_{s(ha)} = \frac{\left[\rho_s C_{p,s}(1-\varepsilon)\omega d_p\right]^2}{60\lambda_s(1-\varepsilon)}; \quad f_{ha} = \frac{\left[\rho_s C_{p,s}(1-\varepsilon)\omega\right]^2}{ha_p}$$

The above equation shows that effective thermal dispersion coefficient is the algebraic sum of the individual contributions of eddy mixing of the gas ($D_{g,eddy}$), molecular conduction in the gas (λ_g), stagnant film resistance ($f_{(ha)}$), and intraparticle resistance $f_{s(ha)}$. The list of estimated physical parameters is given in Table 6.1.

Finally, the effectiveness factor (Ψ) for the endothermic steam reforming reaction is estimated using the method given by Smith (1981). The effectiveness factor for the first order reaction is given as a function of Thiele-type modulus(Φ), the Arrhenius number (α) and a heat of reaction parameter (β).

$$\Psi = \frac{1}{\Phi} e^{\alpha\lambda/5} \quad \text{for } \Phi > 2.5 \quad \text{where,}$$

$$3\Phi = \frac{d_p}{2}\sqrt{\frac{k_s/\rho_s}{D_{e,pore}}}; \quad \alpha = \frac{Ea_s}{RT_s}; \quad \beta = \frac{(-\Delta H_s)D_{e,pore}C_{p,s}}{\lambda_s T_s}$$

Since the reaction essentially occurs when $\Phi > 2.5$, the effectiveness factor is quite accurately estimated using the equations above. The effectiveness factor is calculated as a function of temperature.

6.3 The Model Equations

The model used for the simulation of the RE-GAS process is essentially similar to the model used for the simulation of the RE-GAS type processes discussed in Chapters 4 and 5. Only exothermic methane combustion takes place in the bed during the exothermic semi-cycle and only endothermic steam reforming reaction takes place during the endothermic semi-cycle. Combustion reaction occurs only in the gas phase and not in the solid phase because concentration of the fuel used is very low. Steam reforming occurs in the solid phase. Global kinetics for both reactions are

employed (section 6.2). The mass and heat dispersion in both gas and solid phase is accounted for by the model. The effect of heat and mass transfer in the catalyst is approximated by an effectiveness factor. Since there is negligible external mass transfer resistance at the high velocities employed, external mass transfer resistance is neglected which is supported by the data in the literature (Ferreira et al., 1992). The gas is assumed to be compressible with total mass flux of gas being constant (Kulkarni, 1992). The reader is referred to Chapters 2, 3, 4 and 5 for further details of the assumptions made.

Methane is represented as component A in the following model equations for convenience. The model equations consist of energy balance for the gas and solid phase, Equations (6.1) and (6.2) respectively; reactant A (methane) mass balance in the gas phase (exothermic semi-cycle) and in the solid phase (endothermic semi-cycle), equations (6.3) and (6.4) respectively; and the overall continuity Equation (6.5);

$$\frac{\partial \theta_g}{\partial \tau} = \frac{1}{Pe_{h,g}} \frac{\partial^2 \theta_g}{\partial z^2} - U \frac{\partial \theta_g}{\partial z} + \tau_{s/r,g,A} TR_{g,A} \gamma_{g,A}^{\left(\frac{1-\theta_g}{\theta_g+\theta_{g,d}}\right)} \Omega_g y_A y_B - St_g \frac{1}{\Omega_g} \left(\theta_g - \theta_s\right) \quad (6.1)$$

$$\frac{\partial \theta_s}{\partial \tau} = \frac{1}{Pe_{h,s}} \frac{\partial^2 \theta_s}{\partial z^2} + \tau_{s/r,s,A} TR_{s,A} \gamma_{s,A}^{\left(\frac{1-\theta_s}{\theta_g+\theta_{g,d}}\right)} y_A + St_s(\theta_g - \theta_s) \quad (6.2)$$

$$\frac{\partial y_A}{\partial \tau} = \frac{1}{Pe_{ms,g}} \frac{\partial^2 y_A}{\partial z^2} - U \frac{\partial y_A}{\partial z} - \tau_{s/r,g,A} \gamma_{g,A}^{\left(\frac{1-\theta_g}{\theta_g+\theta_{g,d}}\right)} \Omega_g y_A y_B \quad (6.3)$$

$$\frac{\partial y_A}{\partial \tau} = \frac{1}{Pe_{ms,g}} \frac{\partial^2 y_A}{\partial z^2} - U \frac{\partial y_A}{\partial z} - \tau_{s/r,s,A} \gamma_{s,A}^{\left(\frac{1-\theta_s}{\theta_g+\theta_{g,d}}\right)} y_A \quad (6.4)$$

$$\frac{\partial \Omega_g}{\partial \tau} = -\frac{\partial \left(\Omega_g U\right)}{\partial z} = 0 \quad (6.5)$$

Boundary conditions:

$@ z = 0$

$$-\frac{1}{Pe_{h,g}} \frac{\partial \theta_g}{\partial z} = \theta_{g,in} - \theta_g; \quad \frac{\partial \theta_s}{\partial z} = 0; \quad -\frac{1}{Pe_{ms,g}} \frac{\partial y_A}{\partial z} = y_{A,in} - y_A; \quad -\frac{1}{Pe_{ms,g}} \frac{\partial y_A}{\partial z} = y_{B,in} - y_B$$

$@z = 1$

$$\frac{\partial \theta_{gs}}{\partial z} = 0; \quad \frac{\partial \theta_s}{\partial z} = 0; \quad \frac{\partial y_A}{\partial z} = 0$$

Initial Conditions:

$@t = 0$ and $0 \le z \le 1$

$$\theta_g = \theta_{g,0}; \quad \theta_s = \theta_{s,0}; \quad y_A = y_{A,0}; \quad \Omega_g = \Omega_{g,0}$$

The dimensionless quantities used above are:

$$\tau = \frac{t}{L/u_{in}}; \quad z = \frac{x}{L}; \quad \theta_g = \frac{T_g - T_{g,in}}{\Delta T_{ad}}; \quad \theta_s = \frac{T_s - T_{g,in}}{\Delta T_{ad}}; \; \theta_{g,d} = \frac{2T_{g,in} - T_{g,in}}{\Delta T_{ad}}$$

$$\Omega_g = \frac{\rho_g}{\rho_{g,in}}; \quad U = \frac{u}{\varepsilon u_{in}}; \quad \gamma_{g,A} = e^{\left(\frac{Ea_{g,A}}{RT_{g,ad}}\right)}; \quad \gamma_{s,A} = e^{\left(\frac{-Ea_{s,A}}{RT_{g,ad}}\right)}$$

$$\tau_{s/r,g,A} = \frac{\tau_s}{\tau_{r,g,A}} = \frac{L/u_{in}}{\frac{1}{k_{0,g,A}\rho_{gm,in}/\varepsilon \; e^{\left(-Ea_{g,A}/RT_{g,ad}\right)}}}; \quad \tau_{s/r,s,A} = \frac{\tau_s}{\tau_{r,s,A}} = \frac{L/u_{in}}{\frac{1}{k_{0,s,A}/\varepsilon \; e^{\left(-Ea_{s,A}/RT_{g,ad}\right)}}}$$

$$TR_{g,A} = \frac{1000\left(-\Delta H_{g,A}\right)}{M_w C_{p,g} \Delta T_{ad}}; \quad TR_{s,A} = \frac{P\left(-\Delta H_{s,A}\right)}{RT_g \rho_s C_{p,s} \Delta T_{ad}}$$

$$St_s = \frac{ha_p L}{(1-\varepsilon)\rho_s u_{in} C_{p,s}}; \quad St_g = \frac{ha_p L}{\varepsilon \rho_{g,in} u_{in} C_{p,g}}$$

$$; \quad Pe_{h,g} = \frac{\varepsilon \rho_g u_{in} C_{p,g} L}{D_{e,g,h}}$$

$$Pe_{h,s} = \frac{(1-\varepsilon)\rho_s u_{in} C_{p,s} L}{D_{e,h,s}}; \quad Pe_{ms,g} = \frac{\varepsilon_s u_{in} L}{D_{e,g,ms}}$$

The equations are derived assuming compressible nature of the gas except for the dispersion terms in the mass balance for the gas phase. However, this assumption does not cause much error because, as shown later in the simulation, the effect of dispersion is negligible and all the dispersion terms can be dropped from the model equations.

The mass Peclet number for the gas phase ($Pe_{ms,g}$) is the ratio of the magnitude of the rate of axial convection to the magnitude of the rate of axial dispersion. When $Pe_{ms,g}$ is very large, convection dominates and the dispersion term can be dropped from the model equations. The heat Peclet number in the gas phase ($Pe_{h,g}$) is the ratio of the magnitude of the rate of heat transfer by axial convection to the magnitude of the heat transfer rate by axial dispersion. For high $Pe_{h,g}$,convection dominates dispersion and the second order heat dispersion term can be dropped from the model. $Pe_{h,s}$, the heat Peclet number for the solid phase is the ratio of axial heat convection (product of the thermal capacity of the solids and the linear velocity) to the thermal diffusion in the solid phase. When thermal dispersion in the solid phase is negligible, this term becomes very high and thus the heat dispersion in the solid phase can be neglected. The physical significance of the rest of the dimensionless parameters is explained in Chapters 2, 3, 4 and 5.

6.4 Effect of Dispersion

Although hyperbolic equations are numerically more challenging to solve than the elliptic equations, hyperbolic differential equations can be solved faster than the elliptic differential equations by applying the numerical approximations suggested in Chapter 2, Section 2.6. . Therefore, before simulating the RE-GAS process using reaction-convection-dispersion model (Equations 6.1-6.5), it was advisable to study the effect of heat and mass dispersion on the system. Using the parameters listed in Table
6.1, first exothermic semi-cycle of a typical periodic operation was simulated using reaction-convection-dispersion model and the model without dispersion terms. A comparison of the results of the simulation is shown in Figure 6.1. As can be observed from the figure dispersion has very negligible effect on the results because the

convection term dominates. Therefore the dispersion terms are dropped from the model equations 6.1-6.5.

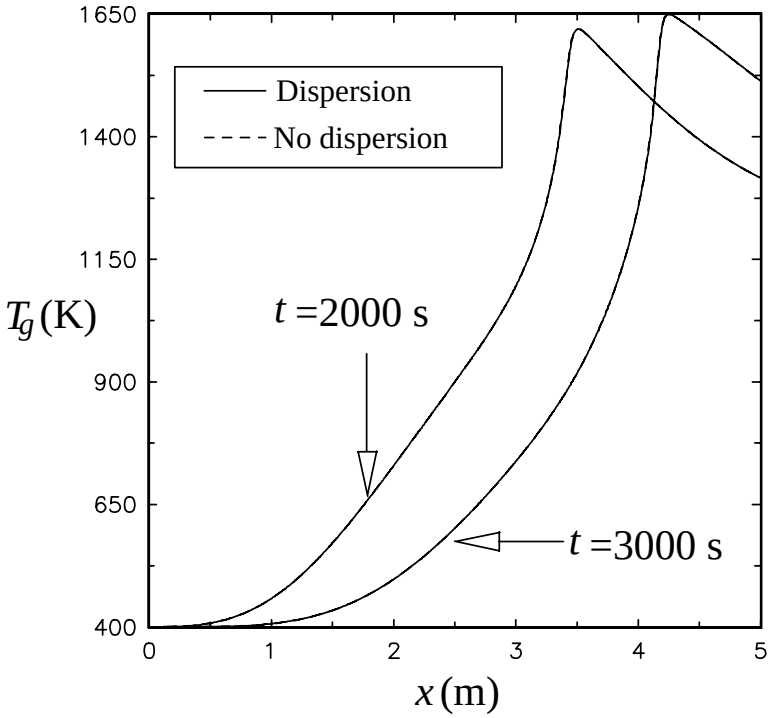

Figure 6.1. A comparison of results obtained using only reaction-convection model with results obtained using reaction-dispersion-convection model.

6.5 Attainability of Periodic Operation

In Chapter 5 we developed the criterion to be satisfied for a periodic operation of asymmetric fixed-bed reactor. The necessary condition to be satisfied was given as

$$\frac{\left[u_{in}\rho_{gm,in}y_{A,in}X_A\left(-\Delta H_{g,A}\right)\times t^*_{odd}\right]_{exo}}{\left[u_{in}\rho_{gm,in}y_{A,in}X_A\left(\Delta H_{s,A}\right)\times t^*_{even}\right]_{endo}} = \frac{Q_{exo}}{Q_{endo}} \geq 1$$

and

$$\frac{\omega_{r,odd}}{\omega_{r,even}} \leq \frac{t^*_{even}}{t^*_{odd}} \qquad (6.6)$$

where front velocity is given by

$$\omega_r = \frac{u\rho_g C_{p,g}}{(1-\varepsilon)\rho_s C_{p,s}}\left(1-\frac{\Delta T_{ad}}{\Delta T_{mx}}\right) = \omega\left(1-\frac{\Delta T_{ad}}{\Delta T_{mx}}\right) \tag{6.7}$$

The above criterion is not a sufficient condition for a periodic steady state. In Chapter 5 we also showed that, for a periodic operation to be possible, heat of exothermic reaction should be greater than the heat of endothermic reaction. For the temperature front and the hot zone to stay well inside the bed, the differential creep velocity should be equal to zero (Chapter 4).

$$\omega_{r,diff} = \frac{\omega_{r,odd} \times t^*_{odd} - \omega_{r,even} \times t^*_{even}}{t^*_{odd} + t^*_{even}} \tag{6.8}$$

The heat of methane combustion is much greater than the heat of steam reforming reaction. For the same inlet conditions for both exothermic and endothermic semi-cycles, it can be shown from equations (6.6)-(6.8) that the period of exothermic semi-cycle must be greater than the period of endothermic semi-cycle. Using the above equations and parameters listed in Table 6.1, it is evident that methane combustion and steam reforming reaction can be coupled in an asymmetric fixed-bed reactor operating in a periodic steady state.

6.6 Physical Restrictions and the Wrong-Way Process

6.6.1 Results of Simulation

The steam reforming operation is carried out at the temperatures below 1500 K (Blanks et al., 1990; Ferreira, et al., 1992; Wagner and Froment, 1992).. The catalyst used for steam reforming is nickel supported on alumina. Therefore, we set the maximum allowable temperature in the bed equal to 1500 K. The ignition temperature for the combustion reaction is reported to be 990 K (Mullholand et al., 1993). This implies that for low fuel concentrations the initial bed temperatures must be higher than 990 K. However, because of the wrong-way behavior, the maximum temperature

rise in the bed can exceed 1500 K. Hence, to maintain the maximum temperature rise in the bed below 1500 K, inlet concentration of the fuel should be very low. This poses an additional problem. If the concentration of the fuel coming in is very low, the total heat released by the combustion reaction during the exothermic semi-cycle is also low. Since the temperature front creeps continuously forward in the axial direction towards the exit, the period of the exothermic semi-cycle cannot be very long. Also, and amount of heat stored in the bed does not increase proportionally with the period of exothermic semi-cycle because of the front movement. Therefore, the heat available for the endothermic semi-cycle is very low as well. This demands that the concentration of methane (the reactant) should be low, or the period of endothermic semi-cycle must be very short. Both of these requirements decrease the output rate of synthesis gas. Therefore, it is suggested that multiple units must operate in parallel to achieve high output rates. Also, as the inlet concentration of methane increases during the endothermic semi-cycles, the front velocity for the endothermic semi-cycle ($\omega_{r,even}$) decreases (equation (6.7), which implies (to satisfy zero differential creep velocity criterion, equation (6.8)) that the endothermic semi-cycle must last for a longer period of time whereas the amount of heat generated during the exothermic semi-cycle remains the same! Thus, the energy criterion (equation (6.6)) is not satisfied unless the concentration of the fuel for the exothermic semi-cycle is increased which allows longer exothermic semi-cycle periods (equations (6.7) and (6.8)). However, at higher concentrations of the fuel, the maximum transient temperature rise is greater than the maximum allowable temperature. Thus, the regenerative production of the synthesis gas by the wrong-way process can be accomplished only in the limited region where concentrations of reactants are very low. The existence of the temperature front during an endothermic semi-cycle is an approximation which is valid only when the maximum temperature in the bed does not decrease considerably.

Figure 6.2a shows the periodic steady state temperature profiles at the end of an exothermic and an endothermic semi-cycle. To maintain the maximum temperature rise in the bed below 1500 K, the inlet mole fraction of the fuel was maintained at 0.008. Since this does not allow very high inlet concentrations of methane during the endothermic semi-cycles, the inlet methane mole fraction was also maintained at 0.008 for the endothermic semi-cycles. For very high concentrations of methane, the bed cools down and no reaction can occur. As can be seen from Figure 6.2b the conversions for both semi-cycles are nearly complete. For the complete conversions as is the case here, the efficiency of the process is given in Chapter 5 as

$$\eta_{cycle} = \frac{\left[\Delta H_{s,A} \times \rho_{gm,in} u_{in} y_{A,in} \times t^*_{even}\right]_{endo}}{\left[\left(-\Delta H_{g,A}\right) \times \rho_{gm,in} u_{in} y_{A,in} \times t^*_{odd}\right]_{exo}} \qquad (6.9a)$$

It is evident from equation (6.9a) that when the heat of reaction and the semi-cycle period for the exothermic semi-cycle are higher than the those for the endothermic semi-cycle, the energy efficiency per cycle is very low. This obviously is the case here, especially because when the heat produced during the exothermic semi-cycle is high, the front velocity is low (equation (6.7)) and the period of the exothermic semi-cycle is required to be greater than that for the endothermic semi-cycle (equations (6.6) and (6.7)). All this indicates that the simulated process is working at an energy efficiency as low as 16%. Therefore it is not a very efficient way to couple these two reactions. The excess heat that leaves the bed should then be used to produce steam. Since the outlet temperature of the gases for the exothermic semi-cycle is always greater than the gas inlet temperature for the endothermic semi-cycle some of the heat leaving the bed can be used in the production of steam and to heat methane. Thus, the overall efficiency of the process, defined as the ratio of the rate of total heat requirement to the rate of total heat supply, i.e., $\eta_{overall} = \frac{Q_{total}}{Q_{r,exo} + Q_{utility}}$ can be much higher. However, in this study we

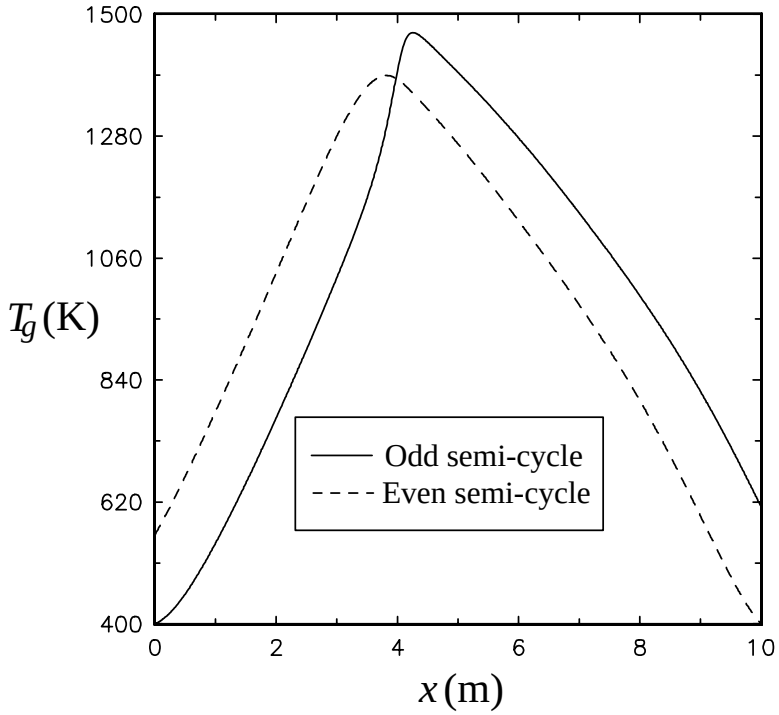

Figure 6.2a. The temperature profiles at periodic steady state for the wrong-way RE-GAS process ($y_{A,in} = 0.008$; T_{mx} <1500 K)**.**

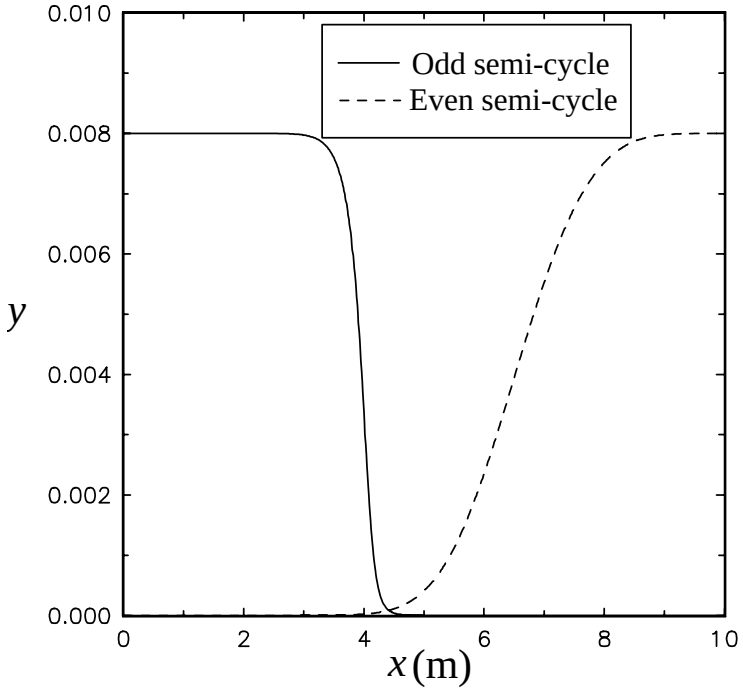

Figure 6.2b. The concentration profiles at periodic steady state for the wrong-way RE-GAS process ($y_{A,in} = 0.008$; T_{mx} <1500 K).

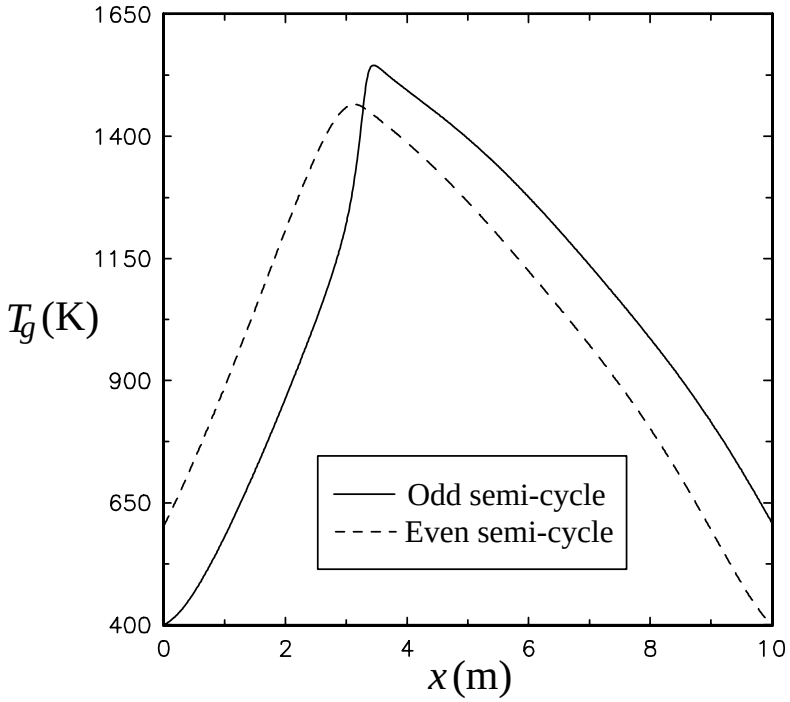

Figure 6.3a. The temperature profiles at periodic steady state for the wrong-way RE-GAS process ($y_{A,in} = 0.01$; $T_{mx} > 1500$ K).

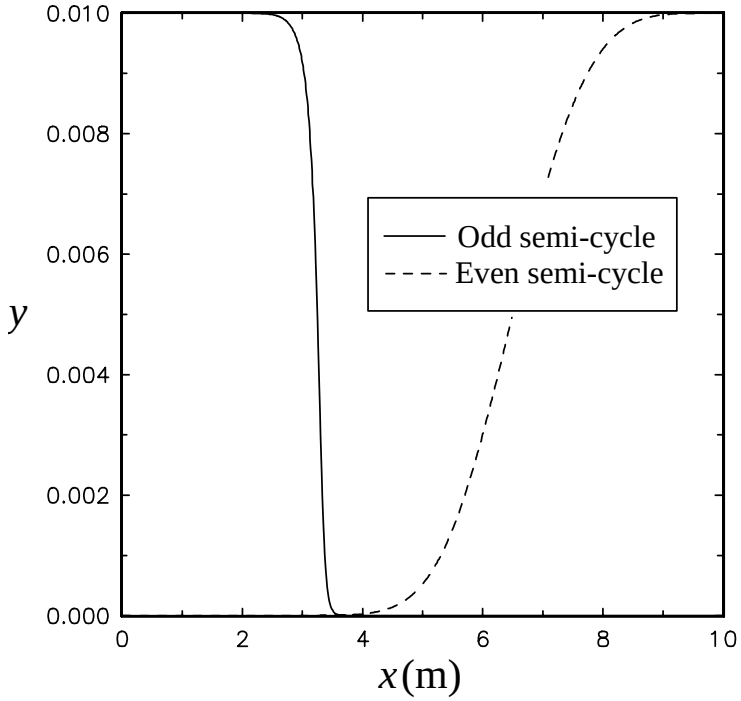

Figure 6.3b. The concentration profiles at periodic steady state for the wrong-way RE-GAS process ($y_{A,in} = 0.01$; $T_{mx} > 1500$ K).

do not concern ourselves with design of the whole plant; but we would like to point out that although the overall energy efficiency of the plant can be higher, the efficiency of the auto thermal fixed-bed reactor itself is very low.

An additional problem is posed by the limit on the maximum temperature in the bed. A small fluctuation in the feed concentration can result in a large and undesirable increase in the catalyst temperature. Figure 6.3a shows how the maximum temperature in the bed increases beyond 1500 K for a small increase in the inlet fuel concentration from 0.008 to 0.01. Figures 6.3b displays the concentration profiles. Therefore the wrong-way process must be operated with extreme caution.

6.6.2 A Final Note on the Wrong-Way Process

It is important to note that under practically all conditions, wrong-way operation of a fixed-bed reactor involving combustion of a fuel during exothermic semi-cycles poses problems resulting from high temperature rise. Since the temperature front creeps towards the exit of the bed which involves taking the heat from the bed as the front traverses through it, the heat stored in the bed during the exothermic semi-cycle does not increase proportionally with the period of the exothermic semi-cycle. Thus, the heat available for the endothermic reaction in the subsequent endothermic semi-cycle is not sufficient for feed having high reactant concentration. Hence, to increase the heat input during the exothermic semi-cycle the inlet concentration of the fuel must be high. This is not practical because the temperature rise in the bed can be very high for high fuel concentration. For example the adiabatic temperature rise for a methane air mixture having methane concentration as low as 10% is around 3300 K. It is impractical to operate a process which requires equipment that can withstand repeated temperature swings from 400K to 3700 K. In the case of wrong-way processes, the maximum temperature rise is more than two

times the adiabatic temperature rise and, hence, the range of the temperature swing is much greater. Thus, from practical point of view, with refractive high temperature materials available today, or perhaps in the near future, any type of wrong-way process involving pure combustion during the exothermic semi-cycles may not be feasible. Also, as explained in this chapter, when heat of the exothermic reaction is very high compared to the heat of the endothermic reaction, the efficiency of the wrong-way process is very low. Therefore, it is advisable to couple only exothermic and endothermic reactions of comparable heat of reactions.

6.7 The Normal Process

The wrong-way process was found unattractive to couple exothermic and endothermic reactions in the RE-GAS process for synthesis gas production because of low energy efficiency and very high temperatures reached in the fixed-bed reactor which cannot be tolerated by the presently available catalyst. Thus, for strict temperature control, the fixed-bed should be operated in the thermodynamic regime where the maximum temperature rise in the bed reaches its minimum possible value, the adiabatic temperature rise.

6.7.1 Simulation of the Normal Process

A comparison of a normal process and a wrong-way process was presented in Chapter 4. In the normal process, the inlet temperature of the feed gas for the exothermic semi-cycle is equal to the initial bed temperature which is above the extinction temperature. As discussed in Chapter 5, for the first exothermic semi-cycle, the maximum temperature rise in the bed is at its minimum and is equal to the adiabatic temperature rise and, hence, the front velocity is equal to zero (equation

(6.7)). There is a monotonic temperature rise from the entrance for the exothermic semi-cycle.

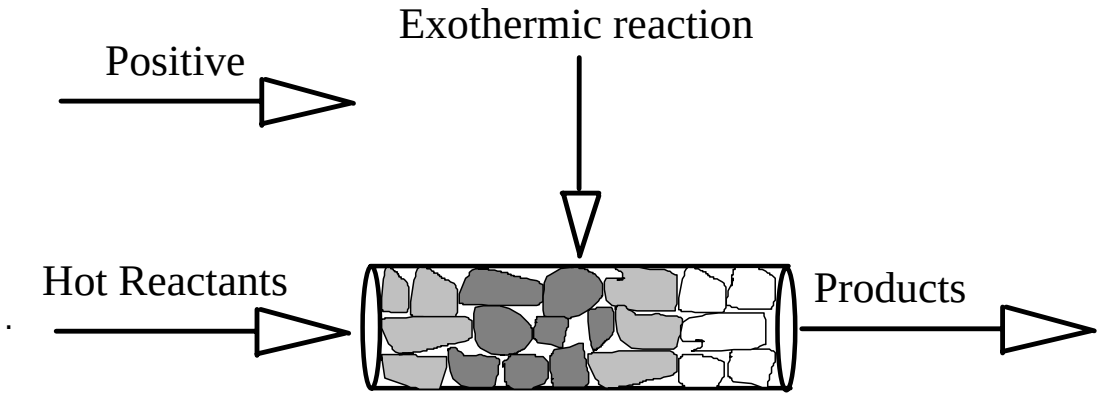

First semi-cycle: hot reactants heat up the bed ($T_{g,in} = T_{s,0}$; $\Delta T_{mx} = \Delta T_{ad}$)

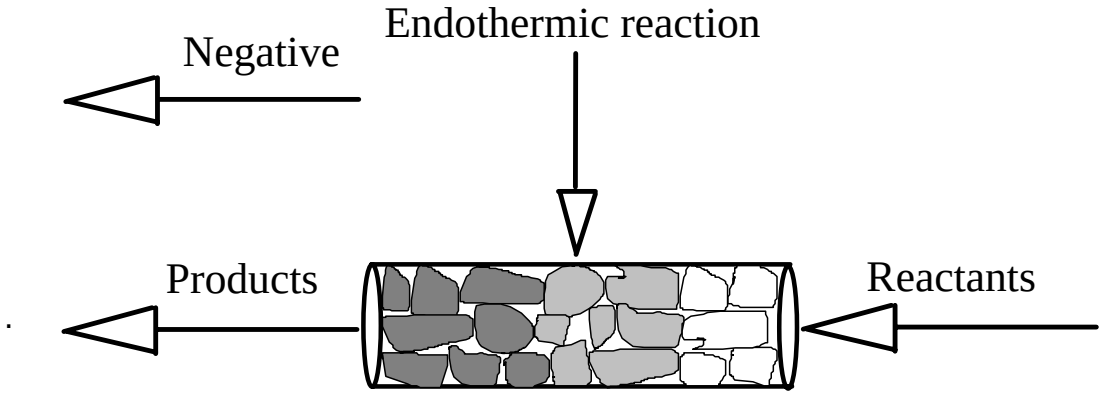

Second semi-cycle: Endothermic Reaction pushes the hotter zone towards the entrance for the exothermic semi-cycle

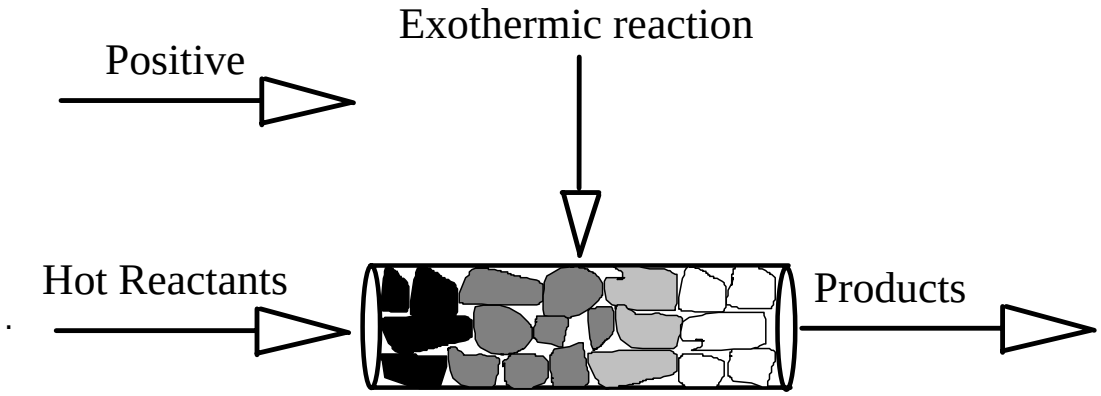

Third semi-cycle: the bed shows the wrong-way behavior ($T_{g,in} < T_{s,0}$; $\Delta T_{mx} > \Delta T_{ad}$)

Figure 6.4. A schematic to explain the wrong-way behavior of a normal process.

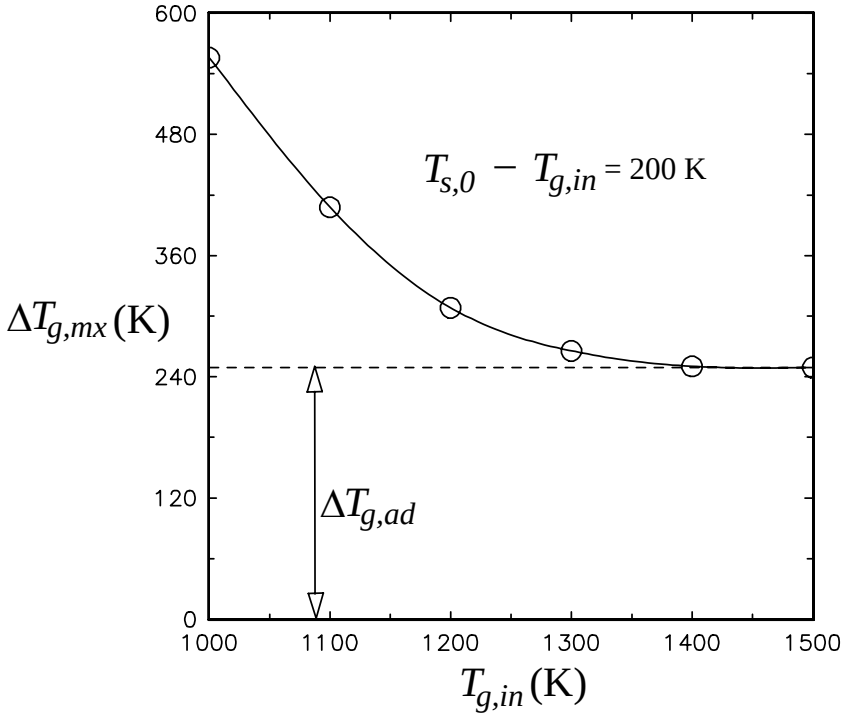

Figure 6.5. The effect for increasing inlet gas temperatures on ΔT_{mx} for the same difference between initial bed temperature and the inlet gas temperature.

However, during the next endothermic semi-cycle, the front exhibits a finite velocity in the negative direction (Figures 5.3a and 5.5) which results in the finite displacement of the front towards the entrance for the exothermic semi-cycle (Figure 6.4). Since there is a monotonic increase in the temperature from the entrance for the exothermic semi-cycle, the movement of the front towards the entrance for the exothermic semi-cycle (in the negative direction) increases the bed temperature at the entrance for the exothermic semi-cycle (Figure 6.4). We showed in Chapter 4 that under these conditions the bed exhibits the wrong-way behavior and the maximum temperature rise in the bed is again greater than the initial bed temperature (Figure 4.4b).

The subsequent wrong-way behavior of the fixed-bed can be minimized in the normal process by manipulating the duration of semi-cycle periods and heat transfer

rates. When the reaction rates are higher compared to the heat transfer rates, the 'intensity' of the wrong-way behavior is decreased. This can be accomplished by setting the inlet gas temperature such that reaction occurs very fast compared to the heat transfer rates. Thus, even when the temperature of the bed at the entrance for the exothermic semi-cycle is higher than the inlet gas temperature, the bed exhibits negligible wrong-way behavior at higher reaction rates. Figure 6.5 shows the effect of increasing the inlet gas temperatures on the maximum temperature rise in the bed for the same difference between the initial bed temperature and the inlet gas temperature (200 K). It is evident that at higher temperatures the reaction rates dominate heat transfer rates and the maximum temperature rise in the bed decreases with increasing inlet gas temperature even for a constant difference in the inlet gas temperature and the initial bed temperature.

The ignition temperature for the gas phase combustion reaction is reported as equal to 990 K (Mulholland, 1993). Since the concentration of the fuel required is very low to maintain the maximum temperature below 1500 K, and higher inlet gas temperatures are required to minimize the wrong-way behavior, the inlet fuel+air temperature is set at 1100 K. Fuel and air can be heated separately in heat regenerators and are mixed at the entrance of the fixed-bed. The combustion reaction heats the bed. During the endothermic semi-cycle a mixture of steam+methane at 400 K is introduced into the bed from the opposite direction. The mixture is heated in the fixed-bed before the endothermic reaction occurs by the heat stored in the bed. There is a finite movement of the temperature front in the negative direction, which as explained before, increases the bed temperature at the entrance for the exothermic semi-cycle (Figure 6.6a). However, as can be observed from the figure, the maximum temperature rise in the bed stays below 1500 K because the reaction rates are too high for a significant wrong-way behavior. Figure 6.6b displays the concentration profiles at a

periodic steady state. The results were obtained using $y_{A,exo}$=0.01, $y_{A,endo} = 0.5$, t^*_{odd}=500 s,

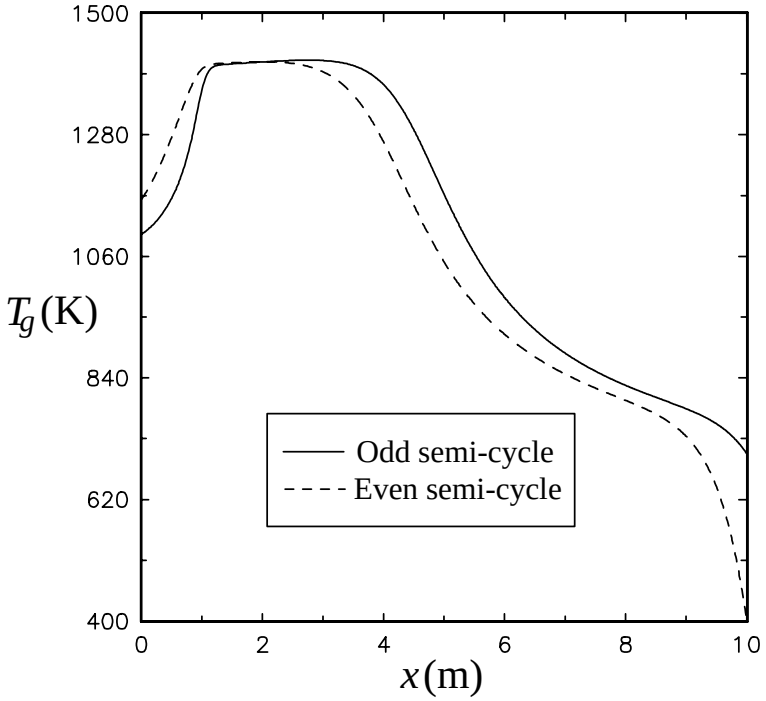

Figure 6.6a. The periodic steady state temperature profiles for the normal RE-GAS process ($y_{A,in,exo} = 0.01$; $y_{A,in,endo} = 0.5$; T_{mx} <1500 K).

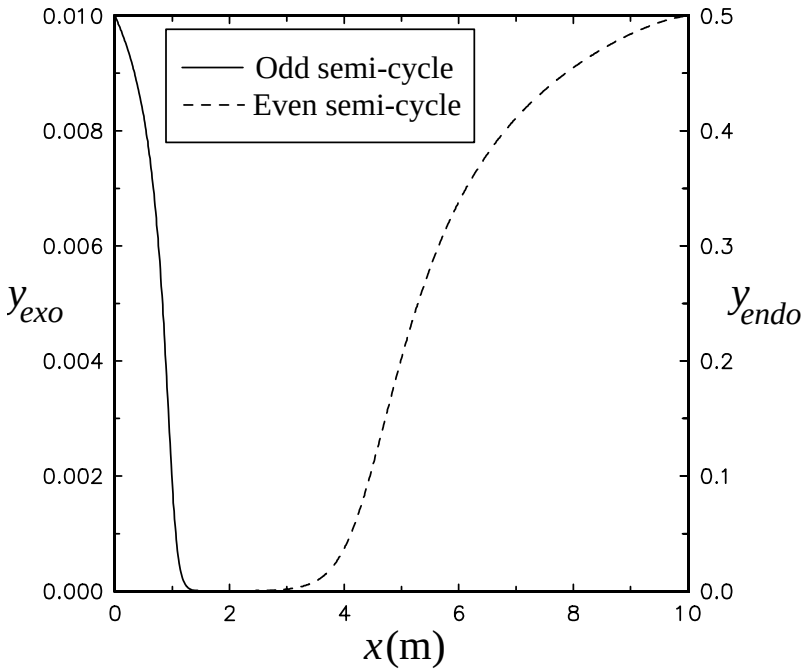

Figure 6.6b. The periodic steady state concentration profiles for the normal RE-GAS process ($y_{A,in,exo} = 0.01$; $y_{A,in,endo} = 0.5$; T_{mx} <1500 K).

$t^*_{even} = 30$ s. Since the inlet gas temperature for the endothermic semi-cycle is nearly three times lower than that for the exothermic semi-cycle, the inlet gas density for the endothermic semi-cycle is nearly three times greater than that for the exothermic semi-cycle. Hence, even for shorter endothermic semi-cycle periods, the output of the process is still high.

The normal process has another advantage over the wrong-way process. The temperature front does not creep during an exothermic semi-cycle. Hence, as the period of exothermic semi-cycle increases more heat is stored in the bed which is available for the endothermic semi-cycle unlike in the wrong-way process where because of the front movement less heat is stored in the bed. As can be seen from Figure 6.6a, the temperature profile monotonically increase from the entrance for the exothermic semi-cycle. For higher exothermic semi-cycle periods this temperature profiles spreads in the bed without creeping i.e., more heat is stored in the bed which

allows longer endothermic semi-cycle periods. Since the temperatures in the bed is always high, and more heat is available for the endothermic semi-cycle, the conversion for the endothermic reaction during the endothermic semi-cycle is nearly complete (Figure 6.6b). Energy efficiency of this process is discussed in the next section.

6.7.2 Criterion for Periodic Operation

In the normal process, the front velocity for the exothermic semi-cycle is equal to zero in the sense the temperature rises monotonically from the entrance and does not escape out of the bed. The temperature of the bed increases until it reaches the adiabatic temperature rise and then the heat of the gas is transferred only regeneratively (since no reaction occurs at this point) to the cooler solids (Figure 6.6a). Thus the bed accumulates more heat with the passing of time and the temperature front spreads with the speed of the front velocity given for heat regenerator without reaction $\left(\omega = \rho_g C_{p,g} u \Big/ \left[\rho_s C_{p,s}(1-\varepsilon)\right]\right)$. This spreading of the temperature front as opposed to the complete displacement increases the energy stored in the bed proportionally to the duration of the odd semi-cycle period. Hence, the front does not move in the positive direction (from entrance of exothermic semi-cycle to the exit of endothermic semi-cycle) but spreads in the positive direction. However, during the endothermic semi-cycles the front shows a finite movement in the negative direction which is compensated by the 'front spreading' during the exothermic semi-cycle. As the period of exothermic semi-cycle increases, larger sections of the bed are heated with the position of the front stagnant at the entrance for the exothermic semi-cycle. As the period of the endothermic semi-cycle increases, more heat is used from the bed. At high endothermic semi-cycle periods, when the heat provided by the exothermic semi-cycle is less than the heat requirement of the endothermic semi-cycle the bed

cools down and no reaction can occur at periodic steady state. Since the front does not physically move during the exothermic semi-cycle, it cannot escape from the exit for the exothermic semi-cycle. Thus, a necessary condition for a periodic operation for the normal process is the trivial energy balance i.e., the total (reactive+sensible) energy provided by exothermic semi-cycle must be equal to the total energy utilized (reactive+sensible) of the endothermic semi-cycle and the conversion for the endothermic reaction must be finite. Thus, the necessary condition to reach periodic steady state is given by

$$Q_{sn,exo} + Q_{r,exo} = Q_{sn,endo} + Q_{r,endo} \quad \text{and} \quad Q_{r,exo} > 0 \quad Q_{r,endo} > 0 \quad \text{i.e.,}$$

$$\left[\rho_{g,in} u_{in} C_{p,g} t^*_{odd}\left(T_{g,in} - T_{g,out}\right) + \rho_{gm,in} u_{in} y_{A,in} X_A t^*_{odd}\left(-\Delta H_{g,A}\right)\right]_{exo}$$

$$= \left[\rho_{g,in} u_{in} C_{p,g} t^*_{even}\left(T_{g,in} - T_{g,out}\right) + \rho_{gm,in} u_{in} y_{A,in} X_A t^*_{even}\left(\Delta H_{s,A}\right)\right]_{endo}$$

$$\Rightarrow \frac{t^*_{odd}}{t^*_{even}} = \frac{\left[\rho_{g,in} u_{in} C_{p,g}\left(T_{g,in} - T_{g,out}\right) + \rho_{gm,in} u_{in} y_{A,in} X_A\left(\Delta H_{s,A}\right)\right]_{endo}}{\left[\rho_{g,in} u_{in} C_{p,g}\left(T_{g,in} - T_{g,out}\right) + \rho_{gm,in} u_{in} y_{A,in} X_A\left(-\Delta H_{g,A}\right)\right]_{exo}} \quad \text{and} \quad (6.10)$$

$$X_{A,exo} > 0 \quad \text{and} \quad X_{A,endo} > 0$$

6.7.3 Energy Efficiency

As discussed in Chapter 5, the purpose of the asymmetric operation of a fixed-bed reactor is to utilize the energy provided by the gases during the exothermic semi-cycles to drive the endothermic reaction without allowing the temperature of the exit gases to increase. The energy lost by the hotter exit gases either during the exothermic semi-cycles or during the endothermic semi-cycles indicates the energy that was not utilized to drive the endothermic reaction during the endothermic semi-cycles. This energy which is lost by the hot exit gases decreases the efficiency of an asymmetric fixed-bed reactor. Hence, the efficiency of an asymmetric fixed-bed reactor is defined as

$$\eta = \frac{Q_{endo}}{\left[Q_{exo} + Q_{sn,odd,in}\right]_{T_{ref}=T_{g,in,even}}} \tag{6.11a}$$

A cycle of the normal process involves heating of the fuel and air mixture from the reference temperature to the inlet temperature, a cycle of exothermic and endothermic reactions in the fixed-bed. Since the gases bring the sensible heat into the bed which is also used to drive the endothermic semi-cycle the energy efficiency of the normal process is defined as,

$$\eta_{cycle} = \frac{Q_{endo}}{Q_{exo} + Q_{preheat}}$$

$$\Rightarrow \eta_{cycle} = \frac{\left[\rho_{gm,in} u_{in} y_{A,in} X_A t^*_{even} \left(\Delta H_{s,A}\right)\right]_{endo}}{\left[\rho_{gm,in} u_{in} y_{A,in} X_A t^*_{odd} \left(-\Delta H_{g,A}\right)\right]_{exo} + \left[\rho_{g,in} u_{in} C_{p,g} t^*_{odd} \left(T_{g,in} - T_{g,out}\right)\right]_{exo}} \tag{6.11b}$$

For simplicity, it is assumed that both gas streams (for exothermic as well endothermic semi-cycle) are available at 400 K because at the operating pressure (2 atm) steam

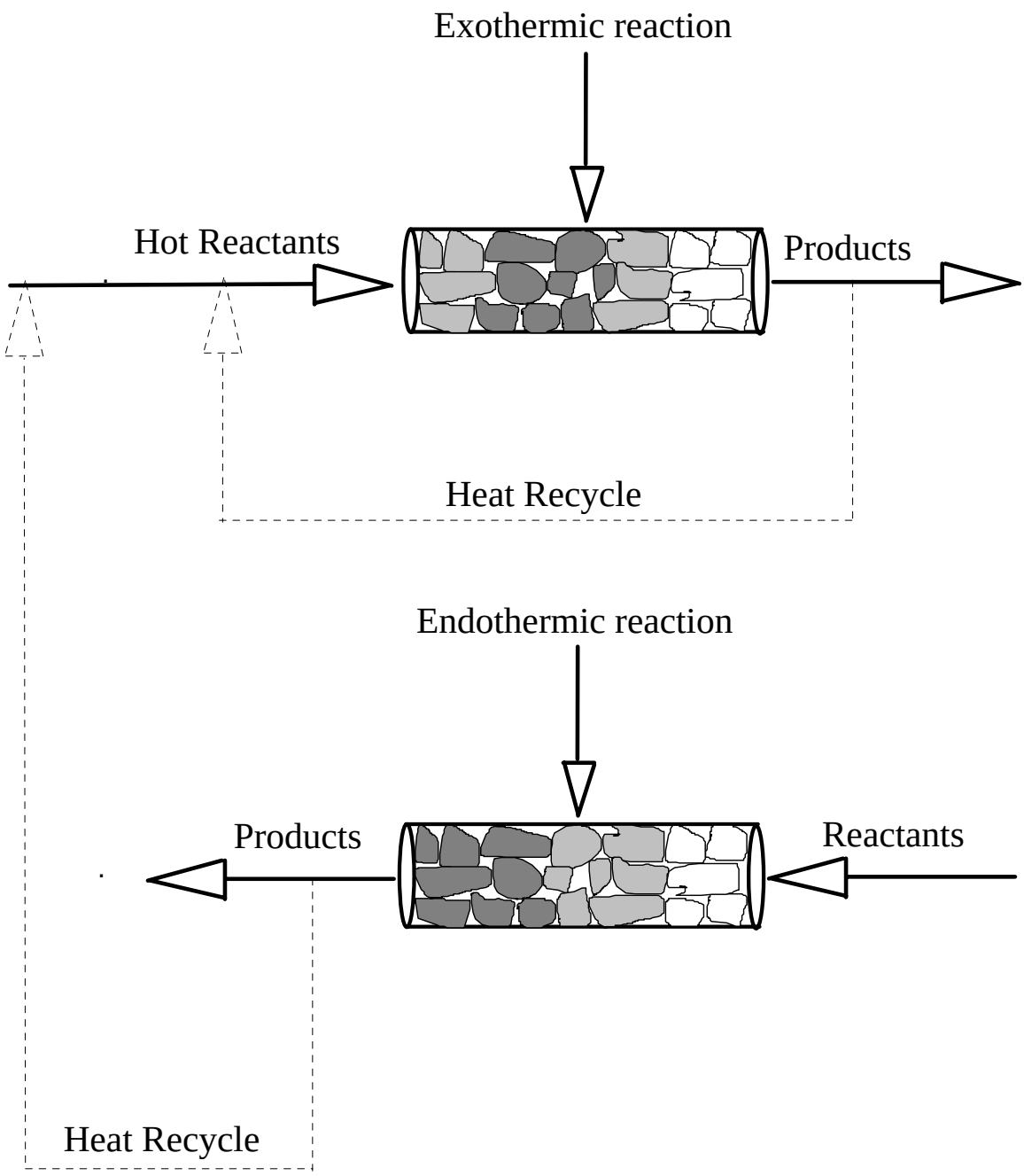

Figure 6.7. A schematic of the normal process with energy recycle.

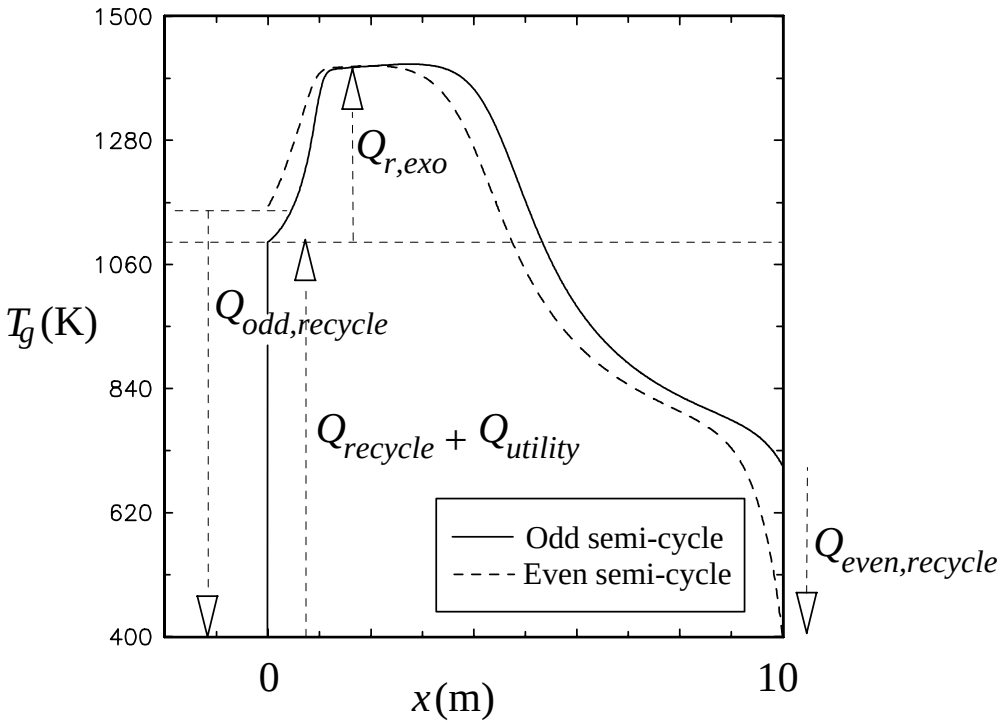

Figure 6.8. The temperature profiles for the normal process with energy recycle.

condenses at lower temperatures. For the case presented in Figure 6.6, the energy efficiency is 46% which is nearly three times higher than that for the wrong-way process.

The normal process, involves preheating the reactants for the combustion reaction from available temperature of 400 K to the inlet temperature of 1100 K. Hence, the sensible heat that is carried out of the bed during both semi-cycles can be recycled to heat the fuel and air to further increase the overall efficiency. If it is possible to recycle all the heat, theoretically the efficiency of this process can rise to 100%. A schematic of the normal process with recycle is shown in Figure 6.7. The temperature profiles for such a process using the reference temperature of 400 K are shown in Figure 6.8. The heat carried out of the bed by the hot exit gases during the endothermic semi-cycle ($Q_{even,recycle}$) and the heat carried out of the bed by the exit gases during the exothermic semi-cycle ($Q_{odd,recycle}$) are used to preheat the inlet gas

stream for the exothermic semi-cycle. The additional preheat is provided by $Q_{utility}$. As $Q_{utility}$ tends to zero the energy efficiency tends to 100%.

The results shown for the normal process are obtained using the inlet fuel mole fraction equal to 0.01, t^*_{odd} = 500 s, and t^*_{even} = 30 s. For this concentration of the fuel, the maximum transient temperature was greater than 1500 K for the wrong-way process. Thus, the normal process offers accurate temperature control and higher energy efficiency. Also, it can be operated at lower concentrations of fuel by proportionately increasing the period of exothermic semi-cycle or decreasing the period of endothermic semi-cycle without having to worry about satisfying the zero differential velocity criterion. For example, Figures 6.9a and 6.9b display the periodic steady state temperature and concentration profiles, respectively, for the normal operation for the inlet fuel mole fraction equal to 0.005, t^*_{odd} = 500 s and t^*_{even} = 15 s. The complete conversion of methane in the steam reforming reaction is achieved under controlled temperature conditions.

6.8 A Note on Thermodynamic Limitations

In this thesis we used the kinetic expression for the steam reforming reaction based on the assumption that the reaction is irreversible. To verify the validity of this assumption, the equilibrium conversions were calculated and compared with the simulated conversions for both the wrong-way and the normal processes. Table 6.2 compares the conversions computed using the global kinetic expression (Ferreira et al., 1992) for the steam reforming reaction for the wrong-way process and for the normal process with the equilibrium conversions for a wide range of temperatures. It can be

observed from the table that the simulated conversions based on the kinetics for the steam reforming reaction are always less than the equilibrium conversions except

when conversions are very close to unity where both the conversion based on the kinetics and

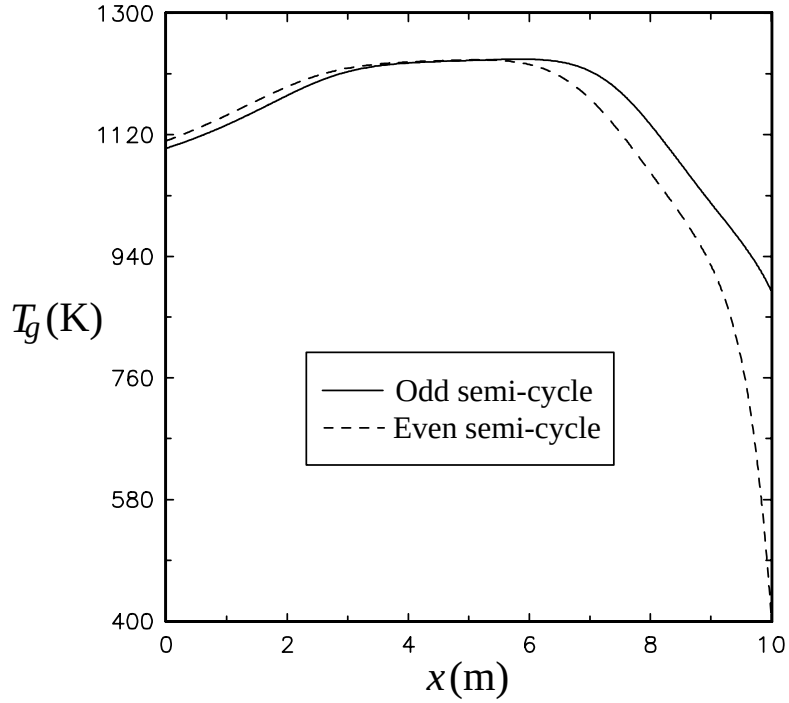

Figure 6.9a. The periodic steady state temperature profiles for the normal RE-GAS process ($y_{A,in,exo} = 0.005$; $y_{A,in,endo} = 0.5$; T_{mx} <1500 K).

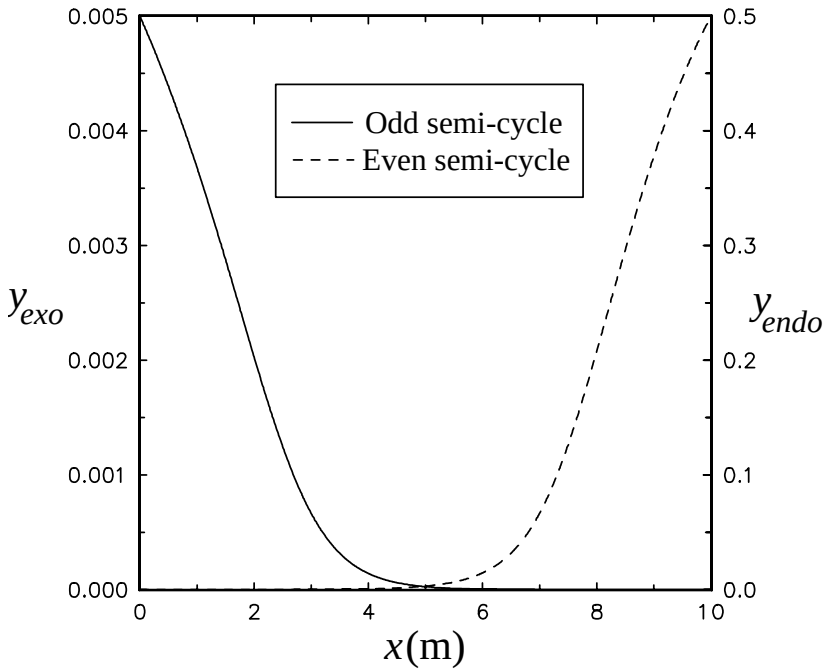

6.9b. The periodic steady state concentration profiles for the normal RE-GAS process

($y_{A,in,exo} = 0.005$; $y_{A,in,endo} = 0.5$; T_{mx} <1500 K).

the thermodynamic conversion converge to unity. Even then, there is negligible difference between the kinetically computed conversion and the thermodynamic conversion. Hence, the assumption that the steam reforming reaction is irreversible is valid in the range of the temperatures encountered in the simulated fixed-bed reactor. However, thermodynamic limitations can be violated for lower gas velocities. Hence, care must be exercised when the steam reforming of methane is assumed to be irreversible. The goal of this research was to gain physical insight into new processes and to explore the feasibility of their operation and not a detailed design of the plant. Hence, a simplified global kinetics for steam reforming reaction was adequate. However, for a more detailed simulation for design of a plant that can operate under wide range of feed rates, thermodynamic limitations must be incorporated.

6.9 Conclusions

Coupling of the catalyzed endothermic steam reforming reaction to produce synthesis gas with methane combustion in an asymmetric a fixed-bed reactor operating in a periodic steady state is feasible. A cycle of operation involves first heating the bed by combustion reaction in the exothermic semi-cycle and then driving the endothermic steam reforming reaction with reactants fed from the opposite end during an endothermic semi-cycle. The wrong-way process involves feeding the reactants at temperature below the bed temperature, which leads to the maximum transient temperature rise well above the maximum allowable temperature. Hence, in the wrong-way process, the fuel concentration must be maintained very low to avoid temperature overshoots. Also, only a small fraction of heat produced during the exothermic semi-cycle is stored in the bed because of the finite movement of the

temperature fronts. Under these conditions, achieving a stable periodic operation demands that the period of the exothermic semi-cycle be greater than the period of the endothermic semi-cycle and this requires that the concentration of the reactants for the endothermic semi-cycles must be low. Although the efficiency/cycle for the wrong-way process is very low, the overall efficiency can be improved by recycling the heat.

In the normal process the inlet gas temperature is maintained above a temperature such that the reaction rate dominates the heat transfer rate to decrease the wrong-way behavior. The maximum temperature rise is then around the adiabatic temperature rise and accurate temperature control is possible. Since the temperature front does not creep but only spreads during the exothermic semi-cycle, most of the heat produced by combustion is stored in the bed and is available for the next endothermic semi-cycle. Since more heat is available, the period of the endothermic semi-cycle can be increased or the concentration of the reactants for the endothermic reaction can be increased to improve the production rate of the process. Process efficiency per cycle is 46% but with efficient heat regeneration with the inlet streams 100% efficiency can be set as the goal.

Table 6.1. Parameters Used in the Simulation of Methane Reforming and Combustion.

Parameter	Wrong-way Process	Normal Process
$T_{g,in}$ (K)	400	1100
$T_{g,0}$ (K)	1100-1300	1100
$T_{s,0}$ (K)	1100-1300	1100
$y_{A,in,exo}$	0.008-0.01	0.005-0.01
$y_{A,in,endo}$	0.008-0.01	0.5
$k_{0,g,A}$ (m^3/mol.s)	1.7×10^8	1.7×10^8
$k_{0,s,A}$ (s^{-1})	11396.5	11396.5
$Ea_{g,A}$ (J/mol)	200928	200928
$Ea_{s,A}$ (J/mol)	129704	129704
$\Delta H_{g,A}$ (J/mol)	-802703.17	-802703.17
$\Delta H_{s,A}$ (J/mol)	2.06×10^5	2.06×10^5
h (J/m^2.K.s)	13.77	13.77
$C_{p,g,exo}$ (J/kg.K)	1150	1150
$C_{p,g,endo}$ (J/kg.K)	2600	2600
ρ_s (kg/m^3)	2704.276	2704.276
a_p (m^2/m^3)	600	600
u_{in} (m/s)	1	1
P (Pa)	2.026×10^5	2.026×10^5
L (m)	10	10
ε	0.5	0.5
$M_{w,exo}$	28	28
$M_{w,endo}$	17	17
d_p	0.005	0.005
λ_s (J/m.K)	4.673	4.673
$D_{e,g,pore}$ (m^2/s)	7.5×10^{-7}	7.5×10^{-7}
$D_{e,g,ms}$ (m^2/s)	0.0025	0.0025
$D_{e,h,g}$ (J/m.K)	0.01463	0.01463
$D_{e,h,s}$ (J/m.K)	0.3347	0.3347

Table 6.2. Comparison of Simulated Conversions with Thermodynamic Conversions.

T_s (K)	X_{eq}	X (Normal)	X (Wrong-Way)
400	0	0	0
500	0	0	0
600	0.009	0.006	(Not computed)
700	0.039	0.0051	0.0042
800	0.12	0.0259	0.0684
900	0.27	0.093	0.24
1000	0.48	0.25	0.41
1100	0.7	0.50	0.58
1200	0.84	0.77	0.74
1300	0.92	0.93	0.88
1500	0.98	0.99	0.99

7. CONCLUSIONS AND RECOMMENDATIONS

7.1 Dynamics of the Fixed-Bed Reactor

The dynamic response of a fixed-bed reactor is a strong function of the initial conditions of the bed, the inlet conditions of the reactive gases and the phase in which the reaction occurs. In the dynamic regime where the inlet gas temperature is lower than the initial bed temperature in presence of an exothermic reaction the maximum temperature rise exceeds the adiabatic temperature rise. The maximum transient temperature reached for an exothermic reaction in a fixed-bed reactor is higher for a gas phase reaction than that for a solid phase reaction due to higher thermal capacity of the solids which leads to sluggish response. Also, the maximum temperature rise in the bed increases with decreasing inlet temperature and increasing volumetric heat transfer coefficient. In the dynamic region, the rate of heat transfer, the rate of reaction and the phase in which reaction occurs all affect the maximum temperature rise in the bed.

7.2 Asymmetric Fixed-Bed Reactor

An asymmetric fixed-bed reactor operating under the forced unsteady state conditions can be efficiently employed to couple exothermic and endothermic reactions. Exothermic reaction occurs during odd semi-cycles with the feed entering from one end, endothermic reaction occurs during even semi-cycles with the feed entering from the other end. The maximum temperature rise and conversion are higher for the wrong-way process (where the inlet gas temperature for the exothermic reaction is below the initial bed temperature), than that for the normal process (where the inlet gas temperature is equal to or greater than the initial bed temperature). The

temperature fronts during the odd and even semi-cycles exhibit different front velocities due to different reactions taking place during the two semi-cycles. This leads to a net displacement of the inverted U shaped temperature front after two successive even or odd semi-cycles. The rate of displacement is given by the differential creep velocity (Equation (4.8)). To establish a periodically moving temperature front at the pseudo-steady state, unequal switching periods given by equation (4.7) should be used. Initially, the normal process does not exhibit a finite front velocity during the heating period whereas during the cooling period a finite front velocity is displayed. Also, the temperature in the bed monotonically increases during the odd semi-cycles. During the even semi-cycles this leads to the quick departure of the high temperature region from the original feed end of the reactor (i.e., feed end for odd semi-cycles) which in turn leads to lower conversions for the endothermic reaction during even semi-cycles.

The maximum energy efficiency is achieved only when total heat generated by the exothermic reaction is equal to the total heat absorbed by the endothermic reaction. The RE-GAS type process can operate at 100% efficiency only when the differential creep velocity is equal to zero.

The gas phase reactions result in steeper profiles compared to the solid phase reactions. Also, the maximum temperature rise for the gas phase reactions is higher than that for the solid phase reactions. The difference is observed in the dynamic regime and is explained by the higher thermal inertia of the solids compared to that of the gases.

In a periodically operated asymmetric fixed-bed reactor, conversions for the exothermic and endothermic reactions, each taking place during a semi-cycle, and the energy efficiency increase with decreasing semi-cycle periods until complete conversions are reached. Conversions in both reactions and energy efficiency increase

with increasing bed length. It is not always possible to satisfy both the criterion for zero creep velocity (equation(5.3)) and the energy criterion ($Q_{exo}/Q_{endo} \geq 1$) which requires that the inequality of the ratio of heats of reactions be compensated by adjusting the duration of semi-cycle periods based on equation (5.10). Obviously, the energy criterion has to be satisfied for any asymmetric process to operate in a periodic steady state. Under certain circumstances, when $\omega_{r,even} \times t^*_{even} > \omega_{r,odd} \times t^*_{odd}$ ($\omega_{r,diff} < 0$) and the reaction front moves towards the feed entrance for the exothermic semi-cycles, an asymmetric process can be operated at periodic steady state even when differential creep velocity is finite ($\omega_{r,diff} < 0$). However, for $\omega_{r,diff} > 0$ the temperature front escapes the bed from the exit for the exothermic semi-cycle and no reaction can occur in the bed. The necessary condition for periodic operation of an asymmetric fixed-bed reactor requires that the distance traversed by the front during the endothermic semi-cycle must be equal to or greater than the distance traversed by the front during the exothermic semi-cycle, i.e., for a non trivial periodic steady state to exist, the differential creep velocity should be zero or negative. When $\omega_{r,diff} = 0$ the hot front and the high temperature zone stay well within the bed allowing higher conversions during the periodic steady state. When conversions for both exothermic and endothermic reactions are complete, the energy efficiency is a constant which is affected only by the ratio of the exothermic and endothermic semi-cycle periods and not by the magnitude of the individual semi-cycle periods. When $\omega_{r,diff} < 0$, the front gradually moves towards the entrance for the exothermic reaction and establishes itself at the edge of the bed during the periodic steady state. Hence, during the endothermic semi-cycle, the hot zone quickly moves out of the bed leading to a decrease in the conversion for the endothermic reaction.

7.3 The RE-GAS Process for Synthesis Gas Production

Coupling of endothermic steam reforming reaction to produce synthesis gas with methane combustion via an asymmetric fixed-bed reactor operating in a periodic steady state and subject to not exceeding the maximum allowable temperature is feasible. A cycle of operation involves first heating the bed by methane combustion with air in the exothermic semi-cycle and then driving the endothermic methane steam reforming reaction with reactants fed from the opposite end during an endothermic semi-cycle. The wrong-way process involves feeding the reactants at the temperature below the bed temperature which can lead to the maximum transient temperature rise well above the catalyst deactivation temperature. In the wrong-way process, fuel concentration must be maintained very low to avoid temperature overshoots. Also, only a small fraction of the heat produced during the exothermic semi-cycle is stored in the bed because of the finite movement of the temperature front. A stable periodic operation demands that the period of the exothermic semi-cycle must be greater than the period of the endothermic semi-cycle and dictates that the concentration of the reactant (methane) for the endothermic semi-cycle be low. Although efficiency/cycle for the wrong-way process is very low, the overall efficiency can be improved by recycling the heat.

In the normal process the inlet gas temperature is maintained above a temperature such that the reaction rates dominate heat transfer rates to decrease the wrong-way behavior. The maximum temperature rise is around the adiabatic temperature rise and accurate temperature control is possible. Since the temperature front does not creep during the exothermic semi-cycle, most of the heat produced by combustion is stored in the bed, which is available for the next endothermic semi-cycle. Since more heat is available, the period of the endothermic semi-cycle can be increased, or the concentration of the reactants for the endothermic steam reforming reaction can be increased to improve the output rate of the process. Theoretical energy

efficiency of such a process coupled with heat recovery via heat regeneration can approach 100%.

7.4 The Numerical Algorithm

The processes discussed above exhibit very steep temperature and concentration fronts. A robust numerical algorithm based on the implicit finite difference approximations was developed to accurately capture such steep fronts. The developed completely implicit temporally and spatially adaptive algorithm works better than the algorithms based on the polynomial approximation on finite elements for fixed-bed reactors involving reaction, heat transfer and steep moving fronts. Linear approximation works better than higher order polynomial approximations for steep fronts having high second order derivatives. Finite difference approximations of first order are more robust and accurate than higher order polynomial or higher order finite difference approximations especially in the region of high second derivatives where higher order differences are not very accurate. Although the steepness of the front is measured by the magnitude of the first derivative, to capture the front accurately, the greatest number of nodes must be placed in the region of the highest magnitude of the second derivatives. By placing a greater number of nodes in the region of high second derivatives, the second derivative control minimizes the numerical dispersion and, hence, captures the steepness of the front better than the first derivative control which places the nodes in the steeper regions of the front where the front can be approximated by linear functions. For grid adaptation linear interpolation is preferred over higher order interpolation. The physics of the problem is incorporated in the algorithm by employing the chosen characteristic-time limited time step control along with the first derivative control for the time step management. The temporal and spatial adaptation are coupled to give more accurate results. An optional intelligent

trade off between accuracy and computer time is achieved by a variable space and time tolerance scheme which automatically varies the spatial and temporal tolerances if the finite difference system becomes too big for the computer to handle in a reasonable amount of time.

For a system of equations involving only convective terms, an implicit discretization using backward differences (section 2.6) can lead to a system of unconditionally stable explicit equations which allows explicit marching in spatial as well as temporal directions. A combination of explicit-implicit discretization for the diffusion-convection equations results in a conditionally stable system of explicit equations which can allow larger time steps than only the explicit discretization can allow.

The developed adaptive algorithm is applicable to various types of linear and nonlinear problems for the fixed-bed reactor involving steep and steep moving fronts as illustrated by examples presented above.

7.5 Recommendations for Future Work

1) The stability of the asymmetric fixed-bed reactor subject to periodic swings should be explored.

2) There was negligible dispersion in the processes discussed in this thesis. A process where dispersion effects are significant must be studied to explore the existence of multiple steady states. Convective model cannot predict multiple steady states.

3) A two dimensional model incorporating the momentum equation can simulate flow maldistributions and distributed hot spots. For a closer look at reality, a 2-D model should be used. However, with current computational facilities it is not possible to simulate processes involving fast gas phase combustion reactions and very steep fronts

in a reasonable amount of time. However, the processes involving solid phase reactions can be simulated within a reasonable amount of time.

4) Asymmetric fixed-bed reactor can potentially be employed in numerous processes. the possibility of coupling some of the endothermic reactions with exothermic reactions should be explored. For example, coupling of dehydrogenation of hydrocarbons with methane or residual coke combustion should be investigated.

REFERENCES

Agar, D. W., and W. Ruppel, "Extended Reactor Concept for Dynamic DeNOx Design," *Chem. Eng. Sci*., **43**, 2073-2078 (1988).

Babcock, R. E., D. W. Green, and R. H. Perry, "Longitudinal Dispersion Mechanisms in Packed Beds," *AIChE J.*, **12**, 922-927 (1966).

Blanks, R. F., T. S. Wittrig, and D. A. Peterson, "Bi-directional Adiabatic Synthesis Gas Generator," *Chem. Eng. Sci*. **45**, 2407-2413 (1990).

Bunimovich, G., A., N. V. Vernikovskaya, V. O. Strots, B. S Balzhinimaev, and Yu. Sh. Matros, "SO_2 Oxidation in a Reverse-Flow Reactor: Influence of a Vanadium Catalyst Dynamic Properties," *Chem. Eng. Sci.*, **50**, 565-580 (1995).

Carey, G. F., "Adaptive Refinement and Nonlinear Fluid Problems," *Comp. Methods Appl. Mech. Eng.*, **17/18**, 541-560 (1979).

Chen, Y. C., and D. Luss, "Wrong -Way Behavior of Packed-Bed Reactors: Influence of Interphase Transport," *AIChE J*., **35**, 1148 (1989).

Crider, J. E., and A. S. Foss, "Computational Studies of Transients in Packed Bed Tubular Chemical Reactors," *AIChE J*., **12**, 514 (1966).

Dudukovic′, M. P., and P. A. Ramachandran, "A Moving Finite Element Collocation Method for Transient Problems with Steep Gradients," *Chem. Eng. Sci*. **39**, 1321 (1984).

Edwards, M. F., and J. F. Richardson, "Gas Dispersion in Packed Beds," *Chem. Eng. Sci.*, **23**, 109-123 (1968).

Eigenberger, G., and J. B. Butt, "A Modified Crank-Nicolson Technique with Non-equidistant Space Steps," *Chem. Eng. Sci.*, **31**, 681-691 (1976).

Eigenberger, G. and U. Nieken, "Catalytic Combustion with Periodic Flow Reversal," *Chem. Eng. Sci.*, **43**, 2109-2159 (1988).

Ermenc, E. D., "Wisconsin Process: Pebble Furnace Fixes Atmospheric Nitrogen," *Chemical Engineering Progress*, **52**, No. 4, 149-153 (1956a).

Ermenc, E. D., "Wisconsin Process System for Recovery of Dilute Oxides of Nitrogen," *Chemical Engineering Progress*, **52**, No. 11, 488-492 (1956b).

Ferreira, R. M. Q., M. M. Marques, M. F. Babo, and A. E. Rodrigues, "Modelling of the Methane Steam Reforming Reactor with Large Pore Catalysts," *Chem. Eng. Sci.*, **47**, 11, 2909-2914 (1992).

Finlayson, B. A., *Nonlinear Analysis in Chemical Engineering*, McGraw Hill Book Co. (1980)

Finlayson, B. A., *Numerical Methods for Problems with Moving Fronts*, Ravenna Park Publishing Inc., Seattle, Washington (1992).

Fletcher, C. A. J., *Computational Techniques for Fluid Mechanics* Vol 1, second ed, Springer-Verlog (1991).

Gawdzik, A., and L. Rakowski, "Dynamic Properties of the Adiabatic Tubular Reactor with Switch Flow," *Chem. Eng. Sci.*, **43**, 3023-3030 (1988).

Gawdzik, A., and L. Rakowski, "The Methods of Analysis of Dynamic Properties of the Adiabatic Tubular Reactor with Switch Flow," *Computers Chem. Engng.*, **13**, 1165-1173 (1989).

Gupta, V. K., and S. K. Bhatia, "Solution of Cyclic Profiles in Catalytic Reactor Operation with Periodic Flow Reversal," *Computers Chem. Engng.*, **15**, 229-237 (1991).

Il'in, A., and D. Luss, "Wrong-Way Behavior of Packed-Bed Reactors: Influence of Reactant Adsorption on Support," *AIChE J.*, **38**, 10, 1609-1617 (1992).

Jakob, L. M., *Heat Transfer*, John Wiley & Sons (1957).

Jiang, B. N., and G. F. Carey, "A Stable Least-squares Finite Element Method for Non- linear Hyperbolic Problems," *Int. J. Num. methods Fluids.*, **8**, 933-942 (1988).

Kulkarni, M. S., *Modeling a Heat Regenerator-Reactor with Temperature Dependent Gas Properties*, Master's Thesis, Oregon State University, Corvallis (1992).

Kunii, D., and J. M. Smith, "Heat Transfer Characteristics of Porous Rocks," *AIChE J*., **6**, 71 (1960).

Yakae, S., and D. Kunii, "Heat Transfer in Fixed-Beds near the Walls," *AIChE J.*, **6**, 97 (1960)

Levenspiel, O., "Chemical Engineering's Grand Adventure," *Chem. Eng. Sci.*, **43**, 1427, (1988).

Levenspiel, O., *Chemical Reaction Engineering*, Wiley Eastern Limited (1972).

Levenspiel, O., *Engineering Flow and Heat Exchange*, Plenum Publishing Co. (1984).

Matros, Yu. Sh., *Catalytic Processes Under Unsteady-State Conditions*, Elsevier (1989).

Mehta, P. S., W. N. Sams, and D. Luss, "Wrong-Way Behavior of Packed-Bed Reactors: I. The Pseudo-Homogeneous Model," *AIChE J.*, **27**, 234 (1981).

Mulholland, J. A., A. F. Sarofim, and J. M. Beer, "On the Derivation of Global Ignition Kinetics from a Detailed Mechanism for Simple Hydrocarbon Oxidation," *Comb. Sci. & Tech.*, **87**, 139-156 (1993).

Nieken, U., G. Kolios, and G. Eigenberger, "Limiting Cases and Approximate solutions for Fixed-Bed Recators with Periodic Flow Reversal," *AIChE J.*, **41**, 1915- 1925.

Perry, R. H., and D, Green, *Perry's Chemical Engineers' Handbook*, McGraw Hill Book Co. (1984).

Press, W. H., B. P. Flannery, S. A. Teukolsky, and W. T. Vetterling, *Numerical Recipes*, Cambridge University Press (1986).

Pinjala, V., Y. C. Chen, and D. Luss, "Wrong-Way Behavior of Packed-Bed Reactors: II. Impact of Thermal Diffusion," *AIChE J.*, **34**, 1663 (1988).

Poulain, C. A., and B. A. Finlayson, "A Comparison of Numerical Methods Applied to Non Linear Adsorption Columns," *Int. J. Num. Methods Fluids*, Vol. **17**, 080-089 (1993).

Ramachandran, P. A., and M. P. Dudukovic′, "Solution by Triple Collocation for Periodic Operation of Heat Regenerators," *Computers & Chemical Engineering*, **8**, 377-388 (1984).

Reid, R. C., J. M. Prausnitz, and B. E. Poling, *Properties of Gases and Liquids*, McGraw Hill Inc. (1987).

Rhee, H. K., D. Foley, and N. R. Amundson, "Creeping Reaction Zone in a Catalytic Fixed-Bed Reactor: A Cell Model Approach," *Chem. Eng. Sci*., **28**, 607-615 (1973).

Sharma, C. S., and R. Hughes, "The Behavior of an Adiabatic Fixed-Bed Reactor for the Oxidation of carbon Monoxide: II Effect of Perturbations," *Chem. Eng. Sci.*, **34**, 625 (1976).

Schmidt, F. W., and A. J. Willmott, *Thermal Energy Storage and Regeneration*, McGraw Hill Book Co. (1981).

Smith, J. M., *Chemical Engineering Kinetics*, Mc Graw Hill Book Co. (1981).

Snyder, J. D., and B. Subramaniam, "Numerical Simulation of a periodic Flow Reversal Reactor for Sulfur Dioxide Oxidation," *Chem. Eng. Sci.*, **48**, 4051-4064 (1993).

Van Doesburg, H., and W. A. DeJong, "Transient Behavior of an Adiabatic Fixed-Bed Methanator: I Experiments with Binary Feeds of CO and CO_2 in Hydrogen," *Chem. Eng. Sci.*, **31**, 45 (1976a).

Van Doesburg, H., and W. A. DeJong, "Transient Behavior of an Adiabatic Fixed-Bed Methanator: II Methanation of Mixtures of Carbon Monoxide and Carbon Dioxide," *Chem. Eng. Sci.*, **31**, 53 (1976b).

Villadsen, J. V. and M. L. Michelsen, *Solution of Differential Equation Models by Polynomial Approximation*, Prentice Hall Inc. (1978).

Wagner, E. S., and G. F. Froment, "Steam Reforming Analyzed,"Hydrocarbon Processing," 69-77 (1992).

Wallace, K., and H. J. Viljoen, "Modeling of a Monolithic Catalyst with Reciprocating Flow," *AIChE J.*, **41**, 1229-1234 (1995).

VITA

Date and Place of Birth: 14 May, 1967
Undergraduate Study: University Department of Chemical Technology
University of Bombay, India, July 1989

Graduate Study: M.S. (ChE), Oregon State University, Corvallis, Oregon, July 1992
D.Sc. (ChE) Washington University, St. Louis, Misouri, December 1996.

Publications:

- Kulkarni, M. S., and M. P. Dudukoviḉ, "A Robust Algorithm for Fixed-Bed Reactors with Steep Moving Temperature and Reaction Fronts," *Chem. Eng. Sci.*, **51**, 4, 571-585 (1996).

- Kulkarni, M. S., and M. P. Dudukoviḉ, "Dynamics of Gas Phase and Solid Phase Reactions in Fixed-Bed Reactors," *Chem. Eng. Sci.*, **51,** 11, 3083-3088 (1996).

- Kulkarni, M. S., and M. P. Dudukoviḉ, "A Bi-Directional Fixed-Bed Reactor for Coupling of Exothermic and Endothermic Reactions," *AIChE J.* (accepted for publication) (1996).

- Kulkarni, M. S., and M. P. Dudukoviḉ, "Periodic Operation of Asymmetric Bi-Directional Fixed-Bed Reactors: Energy Efficiency", As Submitted in *Chem. Eng. Sci.*, (1996).

- Kulkarni, M. S., *Modeling a Heat Regenerator-Reactor with Temperature Dependent Gas Properties*, Master's Thesis, Oregon State University, Corvallis, (1992).

Papers Under Developement

- Kulkarni, M.S., and M. P. Dudukoviḉ, "Production of Synthesis Gas in an Asymmetric Bed—The REGAS Process."

Presentations

- Kulkarni, M. S., and M. P. Dudukoviḉ, "A New Robust Algorithm for the study of Gas Phase Incineration of Hydrocarbons by Forced Flow Reversal in a Regenerative Bed", Paper 60f, *Summer AIChE Meeting*, Boston, July 31 (1995).

- Kulkarni, M. S., and M. P. Dudukoviḉ, "An Adaptive Algorithm for Processes Involving Fast Reactions in Packed-Bed Reactors Subject to Forced Flow Reversal", Paper 171g, *AIChE Meeting*, Miami, Nov. 14 (1995).

- Kulkarni, M. S., and M. P. Dudukoviḉ, "A Study of Dynamics of Gas Phase and Solid Phase Reactions in Asymmetric Fixed-Bed Reactors", Paper 79e, *AIChE Meeting*, Miami, Nov. 13 (1995).

- Kulkarni, M. S., and M. P. Dudukoviḉ, "Periodic Operation of Asymmetric Bi-Directional Fixed-Bed Reactors: Energy Efficiency", To be presented, *AIChE Meeting*, Chicago, (1996).